Development of Self-regulatory Gene Circuits for Cartilage Tissue Engineering

by

Biming Wu

A dissertation submitted in partial fulfillment
of the requirements for the degree of
Doctor of Philosophy
(Biomedical Engineering)
in the University of Michigan
2018

Doctoral Committee:

Assistant Professor Rhima M. Coleman, Chair
Professor Renny T. Franceschi
Assistant Research Scientist Thomas M. Lanigan
Professor Jan P. Stegemann

Biming Wu

bimwu@umich.edu

ORCID iD: 0000-0002-3147-2057

DEDICATION

To my family: Ang Yao, Gaoshu Wu, Huizhen Ding, Zuqiu Yao, Guifang Huang, and Wenxia Wu

For all their love and support

致 父亲母亲；外公外婆；爷爷奶奶

ACKNOWLEDGEMENTS

I would like to first express my deepest gratitude towards to my thesis advisor, Professor Rhima M. Coleman. Thank you for giving me the opportunity to be your first student and providing me the support and guidance in the past six years. Starting a new laboratory is hard. Despite all the challenges and limitations, you have always encouraged me to pursue my passion and trusted me with the freedom in both science and personal development. At the same time, you are always there when I needed your guidance. More importantly, you showed me how to be confident when tomorrow is uncertain and how to be optimistic when the situation is not. As you often say, it does not matter where we come from and where we are now as long as we keep moving forward. I would not have been able to accomplish this chapter of my journey without you and thank you!

I would also like to thank the rest of committee, Drs, Thomas M. Lanigan, Renny T. Franceschi, and Jan P. Stegemann, for providing advice to guide my work, supporting my research with both scientific insights and laboratory resources, and giving me constructive feedback. Their support has not only strengthened my dissertation and but also motivated me to continue my scientific training.

Besides my dissertation committee, I am also extremely grateful to have many amazing colleagues and collaborators: Sanjana Murali, Megan Burns, Evran Ural, Dr. Kevin Miles, Dr. Bita Carrion, Dr. Mohammad Souzanchi, Sunny Karnan, Victor Wang, Leora Goldbloomhelzner, Tiana Wong, Chelsea Stephens, Hannah Floyd, Samad Emory, Kathleen McCrumb, Maria Steele, Chuck Nicholas, Dana Jackson, Karen Gates, Katie Stoll, Monica Rondeau, Tareta Johnson, Dr.

Lonnie Shea, Dr. Joe Decker, Dr. Xudong Fan, Dr. Qiushu Chen, Xiaotian Tan, Xuzhou Li, Dr. Paul Krebsbach, Dr. Luis Villa, Dr. Ariella Shikanov, Dr. Jiwon Kim, Dr. Zhou Hong, Dr. Yen Kong. It was my great pleasure to work with all of you and thank you for generously sharing your knowledge and experiences.

To all my friends, especially Neha Kaushal, Sibu Kuruvilla, Jiwon Kim, Brandan Walters, Cameron Yamanishi, Sarah Deslate, Kunal Rambhia, Xiuyuna Yang, Yu-chen Cheng, Xi Chen, Jingtong Du, Jonathan Lundt, Joseph Labuz, Ana Rioja, Adeline Hong, David Lai, Brandon Bruhn, and Jeremy Holzwarth, I am grateful to have all of you during this chapter of life. Thank you for the positive energy and fun memories.

To my best friend, Emily Durisin, thank you for being such as an amazing partner – your encouragement, support, and love. I am fortunate to have you in my life. Finally, to my parents, each of you has given me half of my DNA; together, you deserve all my accomplishments.

TABLE OF CONTENTS

LIST OF FIGURES

LIST OF TABLES

ABSTRACT

Articular (hyaline) cartilage protects the subchondral bone from the high mechanical load during joint movement. This mechanical function of articular cartilage largely relies on the specialized composition and organization of the extracellular matrix deposited by chondrocytes, specifically, aggrecan, type II collagen, and sulfated glycosaminoglycans. The avascular nature of articular cartilage prevents access to progenitor cells and factors that mediate the endogenous healing response inherent in many other tissues. Thus, focal defects that result from traumatic injuries in articular cartilage do not heal and the intense biomechanical loading environment of the tissue leads to the painful and debilitating joint disease osteoarthritis.

Efforts to develop mesenchymal stem cell (MSC)-based functional cartilage regeneration are hindered by the unstable phenotype that chondrocytes derived from these cells adopt using common cartilage tissue engineering strategies. Typically, MSC-derived chondrocytes (MdChs) express a transient articular phenotype before further differentiating through the stages of endochondral ossification, leading to the hypertrophic phenotype. Hypertrophic chondrocytes, driven by the transcription factor RUNX2 (Runt-related transcription factor 2), stop producing and start degrading the structural matrix macromolecules aggrecan and type II collagen, compromising the mechanical integrity of the overall tissue. Therefore, biological interventions that suppress chondrocyte maturation and encourage matrix retention can improve the functional outcome of MSC-derived cartilage tissues.

This thesis focuses on developing a self-regulatory RUNX2 silencing gene circuit to

improve accrual of articular cartilage-specific matrix by MSC-derived chondrocytes via tunable negative-feedback regulation of RUNX2 activity. Specifically, we engineered a synthetic *cis* promoter to initiate RNA interference of *Runx2* exclusively during chondrocyte hypertrophy. To induce chondrocyte-specific RUNX2 silencing, synthetic *cis* promoters were engineered with a single or multiple copies of *cis*-enhancers upstream of the *Col10a1* basal promoter. We showed that these promoters can direct transcription exclusively in pre-hypertrophic and hypertrophic chondrocytes with minimum activity in undifferentiated progenitor cells. Integrating the *cis* promoter and RNAi of *Runx2* into a gene circuit, we further demonstrated that the *cis*-RUNX2 silencing circuit can: 1) induce loss of RUNX2 function specifically during chondrocyte hypertrophy, 2) resist elevation of intracellular RUNX2 activity via negative-feedback regulation, and 3) provide adjustable levels of RUNX2 suppression.

With these gene circuits, we observed improved matrix accumulation and downregulation of hypertrophy markers during chondrogenesis of a murine chondrogenic cell line and primary MSCs. The successful engineering of this gene circuit highlights the potential to introduce artificial regulatory machinery into mammalian cells to modulate their behavior and optimize tissue engineering outcomes.

Chapter 1 Introduction

1.1 Background and Motivation: Articular Cartilage and Its Injuries

Articular (hyaline) cartilage covers the ends of long bones with a low-friction gliding surface[1]. It also protects the subchondral bone from the high mechanical load during joint movement by redistributing the impact[2–5]. This unique mechanical function of articular cartilage largely relies on the specialized composition and organization of the extracellular matrix (ECM) deposited by chondrocytes[6], which reside within the dense network of their secretion (**Figure 1-1**). Among the matrix molecules, type II collagen, aggrecan, and sulfated glycosaminoglycans (sGAGs) are the major contributors to the mechanical integrity. sGAGs are negatively-charged side chain molecules of aggrecan that attract water from the aqueous synovial environment into cartilage tissue. This generates a hydrostatic swelling pressure that resists the compressive loads exerted on cartilage[7,8]. Type II collagen forms fibrils that provide the tensile strength needed in articular cartilage to resist the swelling pressure due to aggrecan and tensile loads that arise throughout the tissue during daily activities[9].

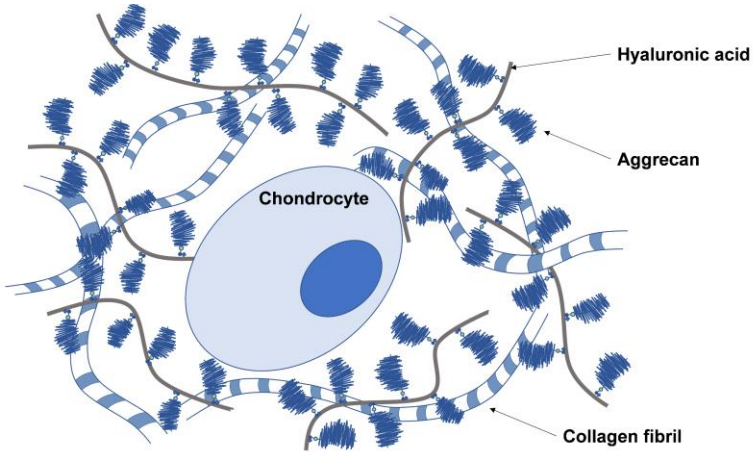

Figure 1-1. Schematic of articular cartilage matrix regions.

Traumatic joint injuries occur frequently, especially among young and active populations[10]. These traumas often result in either partial- or full-thickness cartilage defects that can penetrate down to the subchondral bone[11,12]. The lack of blood vessels in articular cartilage prevents the injury sites from accessing progenitor cells and nutrients, therefore hampering the potential of spontaneous repair of the defect[13,14]. When these defects are left untreated, the disrupted tissue integrity leads to abnormally high loads on the remaining healthy cartilage[15,16]. Under excessive mechanical stress, chondrocytes produce inflammatory cytokines, such as IL-1β (interleukin-1 beta)[17,18] and TNFα (Tumor necrosis factor-alpha) [19,20], which further induce the expression of matrix-degrading enzymes[21–24] and suppress the synthesis of aggrecan or type II collagen[25,26]. Such long-term overload and injury/stress-induced inflammatory responses accelerate the deterioration of the remaining healthy cartilage, eventually leading to posttraumatic osteoarthritis (PTOA, **Figure 1-2**)[27]. Therefore, various clinical repair strategies have been developed with the goal of repairing the damaged cartilage and preventing further loss of cartilage.

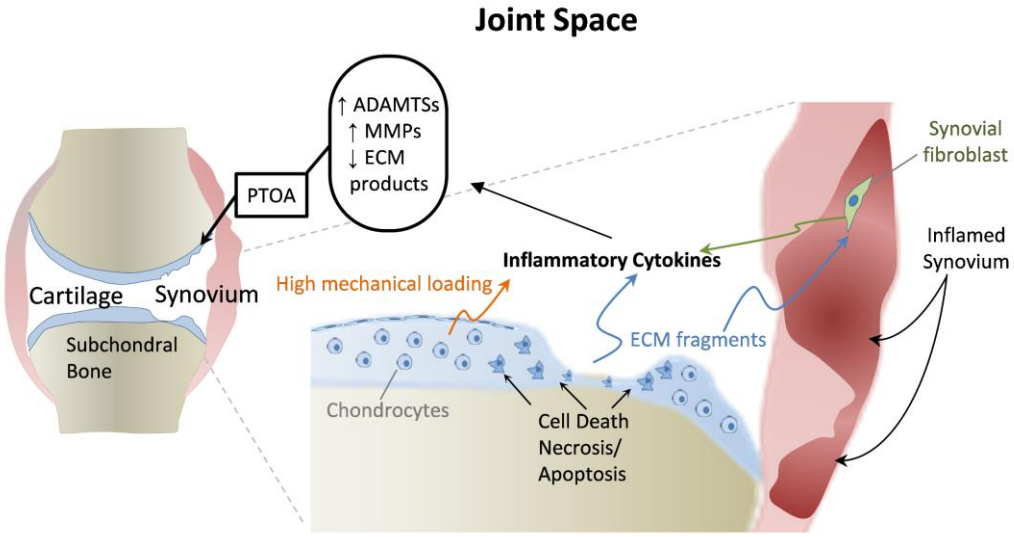

Figure 1-2. Injury/stress-induced inflammatory responses in articular cartilage.

1.2 Current Clinical Repair Strategies for Articular Cartilage Traumatic Injuries

Three surgical procedures are commonly used to clinically repair articular cartilage traumatic focal defects: microfracture, osteochondral transplantation[28], and autologous

chondrocyte implantation. Each has advantages and disadvantages that drive the clinical decision-making process, but none fully restore cartilage function.

Microfracture is one of the most frequently performed techniques to stimulate the spontaneous repair of full-thickness cartilage defects[29]. As a relatively simple procedure, the repair process involves debridement of the defects, removal of calcified cartilage, and perforation of the subchondral bone plate underneath the injury sites to allow bone marrow and blood to be released into injury sites. The arrival of bone marrow mesenchymal stem cells (MSCs) initiates the repair process and eventually forms cartilaginous tissues. As an inexpensive and minimally invasive procedure with short recovery time and low morbidity[30,31,32,33], microfracture is generally prescribed for repairing small defects (e.g., $<2cm^2$) in younger patients[34]. However, in many cases, fibrocartilage forms within the repair site that is not as stiff as hyaline cartilage[35–37]; therefore, this tissue cannot adequately support the physiologic loading conditions in the knee and hip joints. The inferior mechanical properties of the fibrocartilage consequently affects the long-term effectiveness of the microfracture procedure, typically resulting in degeneration of the repair tissue and early onset of PTOA[34,38].

Osteochondral transplantation provides rapid restoration of joint mobility by replacing focal defects with hyaline cartilage[39]. Depending on the actual size of the defect, either autografts or allografts can be used. For autograft transplantation, single or multiple cartilage plugs, including the subchondral bone tissue, are harvested from the low weight-bearing area of the patient's knee before being implanted into the injury sites. Although this method immediately restores most of the mechanical function at the defect sites, problems such as insufficient donor tissues, donor site morbidity, and damages to the harvested autografts often challenge its clinical outcome[40]. To eliminate these problems, allografts are also used in this type of repair, especially for larger lesions

(e.g., >3cm^2)[39]. Allografts are associated with other risks, such as disease transmission and immune responses by the host system. In addition, donor grafts from the tissue banks are not freshly harvested and the processing procedures often induce some cell death as well as reduces the mechanical strength of the tissues[41,42].

Autologous chondrocyte implantation (ACI) is also performed to repair large cartilage lesions (e.g., 2-12cm^2)[43,44]. ACI is a two-step surgical procedure that starts with harvesting a piece of healthy tissue from the low weight-bearing region of the patient's cartilage. Following the first surgery, chondrocytes within the removed cartilage are isolated and expanded *in vitro* before being injected back into the chondral defects beneath a periosteal patch in a second surgery[45]. More recently, **matrix-induced autologous chondrocyte implantation (MACI)** has been adopted to avoid complications associated with the use of periosteum such as hypertrophy and calcification[46,47]. Instead of relying on the sutured periosteal cover to contain the implanted chondrocytes, cells were seeded on a bilayer membrane made of type I/III collagen before being implanted into the defects using fibrin glue[48]. Both ACI and MACI require monolayer expansion of articular chondrocytes to increase the yield of cells so that only a small piece of cartilage is needed to repair a larger defect. However, studies have shown that primary articular chondrocytes have limited potential to proliferate and tend to dedifferentiate during *in vitro* expansion[49]. Among young patients, ACI has demonstrated 60% to 90% good-excellent clinical results after 1 to 11 years; however, aging has shown to decrease not only quantity but also the growing potential of human chondrocytes, further limiting the effectiveness of ACI in certain patient populations[50–52].

1.3 Cartilage Tissue Engineering: from Chondrocytes to MSCs

To overcome the limitations of the current clinical repair options, tissue engineering solutions have been proposed to generate neotissues containing sufficient structural molecules

(aggrecan and type II collagen) to restore mechanical function of the damaged articular cartilage. Cells, scaffolds, and culture conditions are three essential components of tissue engineering, and synergistic interaction among them contribute to the functional success of an engineered cartilage tissue. Primary chondrocytes remain the only type of cells that have been approved by the FDA to repair articular cartilage. Since 1994, articular chondrocyte-based repair strategies have evolved from the scaffold-free implantation in ACI, to collagen membrane-immobilized delivery (MACI, Vericel corporation, MA), and eventually to the chondrocyte-encapsulated 3D scaffolds (e.g., NeoCart by Histogenics corporation, MA, currently in clinical trial). While the development of biomaterial scaffolds and chondro-conductive culture environments has progressed significantly over the past two decades, the problems associated with the availability and expansion of articular chondrocytes still limits the success of tissue-engineered cartilage products. Therefore, different types of cells such as mesenchymal stem cells (MSCs)[53,54], embryonic stem cells[55,56], induced pluripotent stem cells (iPSCs)[57,58], and even dermal fibroblasts[59] have been examined as an alternative to articular chondrocytes for cartilage regeneration.

MSCs have emerged as a promising candidate as these pluripotent stem cells can differentiate into chondrocytes[60,61]and have a high proliferative potential during *in vitro* expansion[61,62,63]. Initially observed at sites of tissue injury by pathologist J. Cohnheim in 1867[64], they were first isolated from the bone marrow of guinea-pigs by A. Friedenstein in 1970[65]. MSCs are typically defined by 1) high clonogenicity; 2) lack of epitopes for hematopoietic cells and presence of keys epitopes associated with non-hematopoietic cells; and 3) ability to differentiate into adipocytes, chondrocytes, and osteoblasts using defined supplements *in vitro* (trilineage differentiation)[66]. Many factors have been investigated to encourage the formation of articular cartilage from MSCs, including growth factors, scaffold designs, oxygen tension and mechanical

cues. A classic chondrogenic induction cocktail contains high-glucose basal medium, dexamethasone, ascorbic acid, and most importantly growth factors such as TGF-βs (transforming growth factors)[67–69], BMPs (bone morphogenetic proteins)[70,71], and IGFs (insulin-like growth factors)[69,72]. Besides these factors that promote the production of aggrecan and type II collagen during differentiation, FGFs (fibroblast growth factors) have also been shown to improve chondrogenesis of MSCs when they are supplemented during the expansion of these cells[73–75]. In addition to the use of growth factors, different types of scaffolds have been developed to support MSC-based cartilage repair. Natural materials (e.g., agarose[76], alginate[77], chitosan[78], collagen[79], and hyaluronic acid[80]) and synthetic polymers (e.g. PCL[81], PEG[82], PGA[83], and PLGA[84]) have all been used individually or combined to support chondrogenesis of MSCs. Moreover, the positive roles of mechanical stimuli, such as shear and dynamic compression, in maintaining of the well-being of chondrocytes have received substantial attention[85,86]. Because of these findings, bioreactors that exert a physiologic level of shear or direct compressive loading to cells have also been developed to improve cartilage tissue engineering and MACI procedures[87,88].

1.4 *In Vitro* Chondrogenesis of MSCs Resembles Endochondral Ossification

Despite all recent advances, cartilage tissues engineered from MSCs still cannot fully recapitulate the composition or mechanical properties of native articular cartilage[89,90,91]. When growth factors such as TGF-β, IGFs, and BMPs are used to induce chondrogenesis of MSCs, they continue to differentiate down the path of endochondral ossification (**Figure 1-3**)[92,93]. During limb development, initial chondrogenesis and subsequent endochondral ossification are a multiple-step process including mesenchymal condensation, early chondrogenesis, proliferation, hypertrophic maturation, calcification, and eventual invasion of blood vessels and bone-forming cells[94]. After committing to the chondrogenic phenotype, characterized by production of aggrecan and type II collagen, MSC-derived chondrocytes (MdChs) also express markers that are indicative of

continuing maturation (chondrocyte hypertrophy)[95]. These maturing chondrocytes stop producing and start degrading aggrecan and type II collagen, disrupting the ECM structure that is needed for the mechanical integrity of newly formed cartilage tissue.

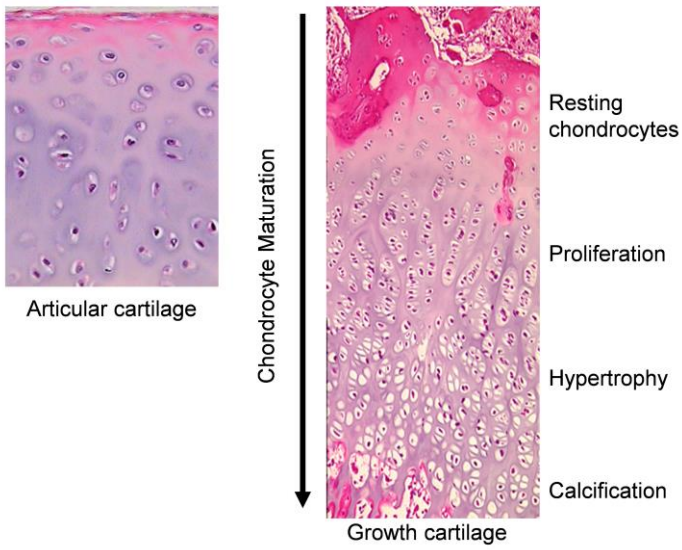

Figure 1-3. H&E staining of articular and growth plate cartilage.

During endochondral ossification, hypertrophy-induced ECM remodeling is a critical step that prepares for the subsequent mineral deposition within cartilaginous matrix[96]. During this process, matrix metalloproteinase-13 (MMP13) is secreted by hypertrophic chondrocytes[97]. As a member of a larger family of MMPs, MMP13 can degrade both aggrecan [98] and type II collagen[99]. Specifically, it cleaves aggrecan at the Asn[341]-Phe[342] bond in the IGD, releasing the domains that were bound by chondroitin-sulfates[100]. The loss of these negatively-charged molecules directly reduces the compressive strength of cartilage tissue[8]. MMP13 also has a high affinity to type II collagen and breaks the molecule into a ¾ and a ¼ fragments[101], disrupting the structure of collagen fibrils that contribute to the tensile strength of articular cartilage. Similarly, hypertrophy of MdChs induces the degradation of aggrecan and type II collagen, compromising the mechanical strengths of engineered cartilage tissues[102,103]. **Therefore, inhibition of hypertrophy in MdChs and the**

maturation-associated matrix degradation associated with this phenotype would significantly improve the application of MSCs in cartilage tissue engineering.

Many molecular and biophysical cues stimulate chondrocyte hypertrophy, including IHH[104], TGF-β[105], Wnt/β-catenin[106], Smad[107], calcium[108], and reactive oxygen species[109]. These stimuli all modulate the activity of master regulator of chondrocyte hypertrophy, the transcription factor RUNX2 (runt-related transcription factor 2) RUNX2[106,110,111]. RUNX2 upregulates COL10a1[112,113], MMP13[114,115], VEGF[116,117] during hypertrophy and terminal differentiation of chondrocytes as endochondral ossification progresses. Transgenic mice expressing conditional knockout of RUNX2 exhibit impaired endochondral ossification, marked by delayed chondrocyte maturation and less absorption of articular cartilage[118–120]. **These findings suggest that targeting RUNX2 in chondrogenic cells can increase long-term matrix accumulation by maintaining aggrecan and collagen II production and preventing their degradation.**

1.5 RNAi-based Treatments in Cartilage Tissue Engineering

Gene silencing via RNA interference (RNAi) can be used to directly target intracellular regulators of chondrocyte phenotype, such as RUNX2. RNAi of a gene induces its loss of function by stimulating targeted degradation or suppressing the translation of its mRNAs[121,122]. Three types of RNA molecules are commonly used to facilitate RNAi; they include the naturally occurring short interfering RNAs (siRNAs), microRNAs (miRNAs), and the artificial short hairpin RNAs (shRNAs). Compared to the forced overexpression of a transgene, the gene silencing approach allows precise targeting of a therapeutic pathway by mimicking regulatory machineries that naturally exist in cells, therefore exerting less stress on cells[123,124,125]. The clinical potential of RNAi techniques has been heavily investigated in many diseases areas, such as cancer, viral infections, inflammatory disorders, and more than 40 RNAi clinical trial programs have been completed or are ongoing (https://www.clinicaltrials.gov)[126].

Combining the power of RNAi with our increasing knowledge of chondrocyte regulation, different research groups have demonstrated the feasibility of silencing key regulators to promote chondrogenesis of MSCs and inhibiting hypertrophy that is undesirable for cartilage tissue engineering. For example, siRNAs targeting ERK5 and ERK1/2 promote chondrogenic differentiation of adult human MSCs[127] while ones against RUNX2 suppress hypertrophy in MdChs[128,129]. Non-viral or viral systems are required to deliver RNAi across the cell membrane as chondrocytes/MSCs do not uptake naked RNA molecules spontaneously. Different non-viral approaches based on lipids[130,131], electroporation[132], nanoparticles[133,129], quantum dots[128,134], and extracellular vesicles[135] have been developed to deliver siRNAs and miRNAs. However, silencing from these non-viral methods tends to be transient and, therefore, achievement of lasting effects requires sustained delivery of new RNA molecules[136]. Continuous delivery of RNA could be challenging if the silencing of a gene is needed during the entire life cycle of the implanted neotissue. In contrast, viral vectors can introduce stable integration of shRNAs and provide long-term inhibition of the targeted genes[137,138]. The recombinant vectors intended for both adeno-associated virus (AAV) and lentiviral virus (LV) can efficiently transduce chondrocytes as well as MSCs[139–142]. LV-delivered shRNAs can also be passed onto daughter cells during mitosis.

1.6 Design of Lentiviral-based shRNA Vector

Commonly used lentiviral vectors are based on the second- or third-generation lentiviral vectors due to safety considerations. To reduce the likelihood of generating replication-competent viruses, current plasmid vectors only contain a promoter, the sequence of interest that needs to be expressed, and essential *cis*-acting elements that are required for viral packaging, reverse transcription, and genome integration (**Figure 1-4a**). Other components required for viral replication are usually delivered to host cells in separate plasmids[143]. For the purpose of this thesis, we will focus on the design of the **promoter** and **shRNA elements** within the vector plasmid.

shRNA is a synthetic RNA molecule that can be transcribed by endogenous machinery. After transcription, the precursor RNA folds into a hairpin structure because the molecule contains a siRNA sequence and its reverse complement sequence, which are separated by a short loop region (**Figure 1-4b**). The formed shRNAs can be further processed into mature siRNAs to induce silencing based on their targeted sequences[144]. This type of shRNAs (referred here as basic shRNAs) are often expressed using Pol III promoter such as U6 and H1[145,146147]. While these strong promoters can generate a large amount of shRNAs to induce a high level of silencing, this type of RNAi has also been reported to cause high cell toxicity and animal death[148]. To improve shRNA-based gene silencing, Zeng and colleagues discovered that precursor miRNAs can be used to process artificial shRNAs from a random long mRNA transcript (**Figure 1-4c**)[149,150]. This finding allows shRNAs to be processed by naturally occurring miRNA pathways, mitigating toxicity induced by basic shRNAs[151]. Moreover, the miRNA-based shRNAs can be expressed by Pol II promoters[152,153], allowing the possibility of using mammalian promoters, especially tissue-specific ones, to control RNAi.

In mammalian cells, the promoter, located at the 5' end of the transcription start site of each gene, directs the initiation of transcription by polymerase. These promoters can be separated into two classes: "broad" and "sharp"[154]. Defined by their patterns of transcription start sites (TSSs), broad promoters can initiate transcription over a dispersed genetic region (~100bp) while sharp promoters maintain their TSSs at a focused, narrow region (less than a few nucleotides)[155]. A recent genome-wide analysis revealed that the CpG-rich broad promoters represent the majority of mammalian promoters[156], controlling the embryonic and housekeeping genes[157,158]. In contrast, the sharp promoters usually contain a highly conserved TATA-box[154]. Although they

only represent less than 12% of mammalian promoters[157], this type of promoter commonly controls the tissue-specific gene expression[156].

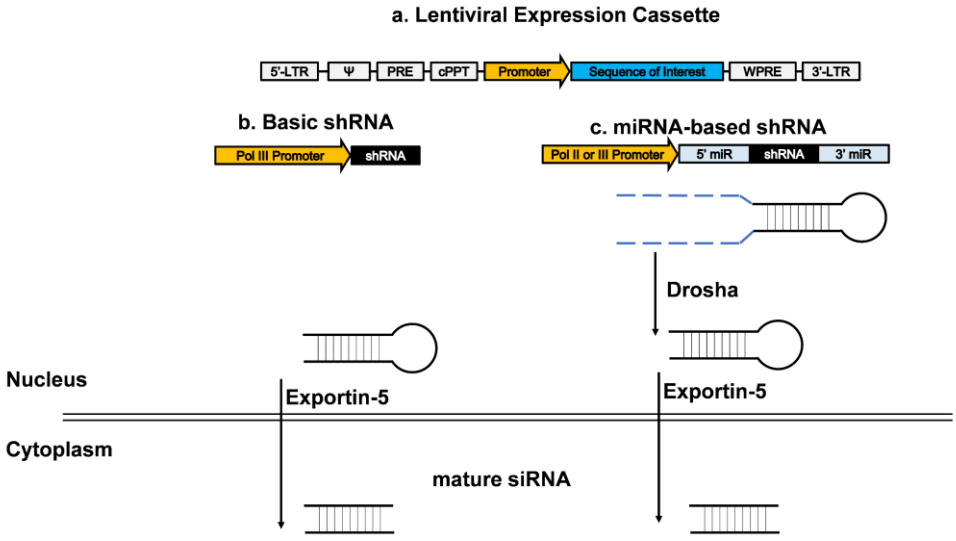

Figure 1-4. Lentiviral-based shRNA system. (a) Diagram of a lentiviral vector. Processing of (b) basic shRNA and (c) microRNA-based shRNA.

Because tissue specific promoters initiate transcription in only certain cell types, they can target miRNA-based shRNA expression in cells of interest while restricting unwanted silencing in non-target cells. These promoters could lead to more confined, persistent silencing, fewer side effects, and a lower chance of causing cancers compared to the nonspecific, constitutively active promoters[159–161].Typically, tissue-specific promoters are derived from marker genes of a certain cell type. For example, promoters of aggrecan and osteocalcin are used to target chondrocytes[120]and osteoblasts[162,163], respectively. The increasing number of available tissue-specific promoters have made it very convenient to induce gene silencing in various types of cells. Furthermore, findings from several bioinformatics studies have predicted that partial promoter sequences can recapitulate tissue specificity even though they do not contain all the regulatory elements that exist within the full-length endogenous promoters[154,164,165]. Therefore, truncated

tissue-specific promoters can be synthesized to reduce the size of viral vectors and improve packaging efficiency[166,167].

1.7 Project Goal and Hypothesis

The overall goal of this project is to develop a gene circuit that can inhibit the maturation of MSC-derived chondrocytes in a self-sufficient manner as they progress to hypertrophy and enhance their accumulation of cartilaginous ECM. We also aim to use the design of such a gene circuit as proof-of-concept to demonstrate the feasibility of integrating artificial regulatory machinery into mammalian cells to modulate their behavior and optimize tissue engineering outcomes. Here, we propose a lentiviral vector that aims to inhibit chondrocyte hypertrophy and increase accrual of cartilage matrix via RNAi of *Runx2* under the control of a synthetic *Col10a1*-like promoter (**Figure 1-5**). By completing the engineering design cycle, we also intend to establish a design-test platform that could help streamline the creation of new gene circuits that employ novel tissue-specific promoters or target other regulatory pathways. **We hypothesize that 1) RNAi of *Runx2* can enhance matrix accumulation by chondroprogenitor cells by inhibiting matrix-degrading enzymes; 2) synthetic *cis* promoters containing single or multiple copies of *cis*-enhancers and the *Col10a1* basal promoter can recapitulate the tissue-specificity of endogenous *Col10a1* promoter and induce RUNX silencing exclusively in hypertrophic chondrocytes; and 3) *cis*-based, RUNX2-silencing gene circuits can improve accrual of articular cartilage-specific matrix by MSC-derived chondrocytes via tunable negative-feedback regulation of intracellular RUNX2 activity.**

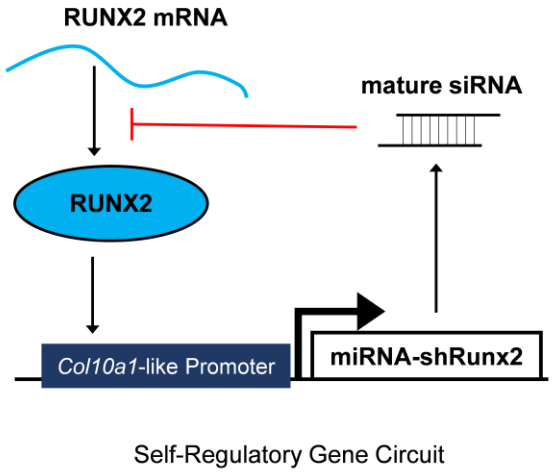

Figure 1-5. Design of self-regulatory *Col10a1*-sh*Runx2* gene circuit.

1.8 Specific Aims

Specific Aim 1: Evaluate the effects of RUNX2 silencing at different stages of chondrocyte maturation using monolayer ATDC5 model.

RUNX2 is suggested to be involved at different stages of chondrocyte development, therefore it is important to understand how loss of its function impacts accumulation of matrix during chondrogenesis. In this aim, we will first characterize sequential progression from early to late chondrogenesis in the monolayer ATDC5 model. Using Tet-on/doxycycline lentiviral system, we will create an inducible ATDC5 model that allows flexible induction of RNA interference of *Runx2*. By suppressing the translation of RUNX2 at different phases of chondrocyte differentiation, we will evaluate cellular responses, the progression of chondrogenesis, as well as the final accrual of sGAG-rich matrix. Results from this aim will be used to validate the potential of RUNX2 silencing to inhibit maturation-associated matrix loss.

Specific Aim 2: Investigate chondrogenic response to phosphate during early and late chondrogenesis in both monolayer (2D) and pellet (3D) ATDC5 models.

This aim will compare chondrogenic differentiation of ATDC5 cells between monolayer (2D) and (3D) cultures. To further understand how these two systems respond to the hypertrophy

stimuli[168], we will perturb differentiation in both models with phosphate at different stages of chondrogenesis, monitor cellular responses, and quantify the accumulation of sGAG-rich matrix and mineral deposits. In addition, we will also investigate if phosphate can be used to expedite chondrogenic maturation in both models

Specific Aim 3: Study the matrix accumulation during chondrogenic differentiation of ATDC5 cells and murine MSCs under the control of the self-regulatory *cis*-RUNX2 silencing gene circuits.

In this specific aim, we will first synthesize *Col10a1*-like *cis* promoters by assembling the *Col10a1* basal promoter and different copies of *cis*-enhancer, and we then will validate the tissue-specificity of these promoters in the 2D ATDC5 model. Using the verified *cis* promoters, we will assemble *cis*-sh*Runx2* gene circuits and characterize their activity during chondrogenic differentiation using a luciferase reporter in the 2D ATDC5 model. Different versions of *cis*-sh*Runx2* gene circuits will be evaluated under the normal chondrogenic condition and phosphate-stimulated environment. Finally, we will examine how different RUNX2 silencing gene circuits affect accumulation of matrix during long-term ATDC5 (5-weeek) and murine MSC (8-weeek) pellet cultures.

1.9 References

1. Forster, H. & Fisher, J. The Influence of Loading Time and Lubricant on the Friction of Articular Cartilage. *Proc. Inst. Mech. Eng. Part H J. Eng. Med.* **210,** 109–119 (1996).
2. Tepic, S., Macirowski, T., Mann, R. W. & Mann, R. W. Mechanical properties of articular cartilage elucidated by osmotic loading and ultrasound. *Proc. Natl. Acad. Sci. U. S. A.* **80,** 3331–3 (1983).
3. Chan, B., Donzelli, P. S. & Spilker, R. L. A mixed-penalty biphasic finite element formulation incorporating viscous fluids and material interfaces. *Ann. Biomed. Eng.* **28,** 589–97 (2000).
4. Wilson, W., van Donkelaar, C. C., van Rietbergen, B., Ito, K. & Huiskes, R. Stresses in the local collagen network of articular cartilage: a poroviscoelastic fibril-reinforced finite element study. *J. Biomech.* **37,** 357–66 (2004).
5. Wilson, W., van Donkelaar, C. C., van Rietbergen, B. & Huiskes, R. A fibril-reinforced poroviscoelastic swelling model for articular cartilage. *J. Biomech.* **38,** 1195–1204 (2005).

6. Quiroga, J. M. P., Wilson, W., Ito, K. & van Donkelaar, C. C. Relative contribution of articular cartilage's constitutive components to load support depending on strain rate. *Biomech. Model. Mechanobiol.* **16,** 151–158 (2017).

7. Roughley, P. J. & Mort, J. S. The role of aggrecan in normal and osteoarthritic cartilage. *J. Exp. Orthop.* **1,** 8 (2014).

8. Han, E., Chen, S. S., Klisch, S. M. & Sah, R. L. Contribution of proteoglycan osmotic swelling pressure to the compressive properties of articular cartilage. *Biophys. J.* **101,** 916–24 (2011).

9. Jones, B., Hung, C. & Ateshian, G. Biphasic Analysis of Cartilage Stresses in the Patellofemoral Joint. *J. Knee Surg.* **29,** 092–098 (2015).

10. Lee, H. H. & Chu, C. R. Clinical and Basic Science of Cartilage Injury and Arthritis in the Football (Soccer) Athlete. *Cartilage* **3,** (2012).

11. Hunziker, E. B. & Rosenberg, L. C. Repair of partial-thickness defects in articular cartilage: cell recruitment from the synovial membrane. *J. Bone Joint Surg. Am.* **78,** 721–33 (1996).

12. Falah, M., Nierenberg, G., Soudry, M., Hayden, M. & Volpin, G. Treatment of articular cartilage lesions of the knee. *Int. Orthop.* **34,** 621–30 (2010).

13. Viswananthan, S., Wolfstadt, J., Chahal, J. & Gomez-Aristizabal, A. *Osteoarthritis: Pathogenesis, Diagnosis, Available Treatments, Drug Safety, Regenerative and Precision Medicine*. (Springer Switzerland, 2015). doi:10.1007/978-3-319-19560-5_12

14. Hunziker, E. B. & Rosenberg, L. C. Repair of partial-thickness defects in articular cartilage: cell recruitment from the synovial membrane. *J. Bone Joint Surg. Am.* **78,** 721–33 (1996).

15. Venäläinen, M. S. *et al.* Quantitative Evaluation of the Mechanical Risks Caused by Focal Cartilage Defects in the Knee. *Sci. Rep.* **6,** 37538 (2016).

16. Milentijevic, D., Rubel, I. F., Liew, A. S. L., Helfet, D. L. & Torzilli, P. A. An in vivo rabbit model for cartilage trauma: a preliminary study of the influence of impact stress magnitude on chondrocyte death and matrix damage. *J. Orthop. Trauma* **19,** 466–73 (2005).

17. Honda, K. *et al.* The effects of high magnitude cyclic tensile load on cartilage matrix metabolism in cultured chondrocytes. *Eur. J. Cell Biol.* **79,** 601–609 (2000).

18. Fujisawa, T. *et al.* Cyclic Mechanical Stress Induces Extracellular Matrix Degradation in Cultured Chondrocytes via Gene Expression of Matrix Metalloproteinases and Interleukin-1. *J. Biochem.* **125,** 966–975 (1999).

19. Ding, L. *et al.* Mechanical impact induces cartilage degradation via mitogen activated protein kinases. *Osteoarthr. Cartil.* **18,** 1509–1517 (2010).

20. Honda, K. *et al.* The effects of high magnitude cyclic tensile load on cartilage matrix metabolism in cultured chondrocytes. *Eur. J. Cell Biol.* **79,** 601–609 (2000).

21. Mengshol, J. A., Vincenti, M. P., Coon, C. I., Barchowsky, A. & Brinckerhoff, C. E. Interleukin-1 induction of collagenase 3 (matrix metalloproteinase 13) gene expression in chondrocytes requires p38, c-jun N-terminal kinase, and nuclear factor κB: Differential

regulation of collagenase 1 and collagenase 3. *Arthritis Rheum.* **43,** 801 (2000).

22. Liacini, A. *et al.* Induction of matrix metalloproteinase-13 gene expression by TNF-alpha is mediated by MAP kinases, AP-1, and NF-kappaB transcription factors in articular chondrocytes. *Exp. Cell Res.* **288,** 208–17 (2003).

23. Raymond, L. *et al.* Interleukin-1 beta induction of matrix metalloproteinase-1 transcription in chondrocytes requires ERK-dependent activation of CCAAT enhancer-binding protein-beta. *J. Cell. Physiol.* **207,** 683–688 (2006).

24. Ding, L. *et al.* Mechanical impact induces cartilage degradation via mitogen activated protein kinases. *Osteoarthr. Cartil.* **18,** 1509–1517 (2010).

25. Taskiran, D., Stefanovicracic, M., Georgescu, H. & Evans, C. Nitric-Oxide Mediates Suppression of Cartilage Proteoglycan Synthesis by Interleukin-1. *Biochem. Biophys. Res. Commun.* **200,** 142–148 (1994).

26. Saklatvala, J. Tumour necrosis factor α stimulates resorption and inhibits synthesis of proteoglycan in cartilage. *Nature* **322,** 547–549 (1986).

27. Buckwalter, J. A., Anderson, D. D., Brown, T. D., Tochigi, Y. & Martin, J. A. The Roles of Mechanical Stresses in the Pathogenesis of Osteoarthritis: Implications for Treatment of Joint Injuries. *Cartilage* **4,** 286–294 (2013).

28. Nikolaou, V. . & Giannoudis, P. . History of osteochondral allograft transplantation. *Injury* **48,** 1283–1286 (2017).

29. Mithoefer, K., McAdams, T., Williams, R. J., Kreuz, P. C. & Mandelbaum, B. R. Clinical Efficacy of the Microfracture Technique for Articular Cartilage Repair in the Knee. *Am. J. Sports Med.* **37,** 2053–2063 (2009).

30. Miller, D. J., Smith, M. V., Matava, M. J., Wright, R. W. & Brophy, R. H. Microfracture and Osteochondral Autograft Transplantation Are Cost-effective Treatments for Articular Cartilage Lesions of the Distal Femur. *Am. J. Sports Med.* **43,** 2175–2181 (2015).

31. Basad, E., Ishaque, B., Bachmann, G., Stürz, H. & Steinmeyer, J. Matrix-induced autologous chondrocyte implantation versus microfracture in the treatment of cartilage defects of the knee: a 2-year randomised study. *Knee Surgery, Sport. Traumatol. Arthrosc.* **18,** 519–527 (2010).

32. Cerynik, D. L., Lewullis, G. E., Joves, B. C., Palmer, M. P. & Tom, J. A. Outcomes of microfracture in professional basketball players. *Knee Surgery, Sport. Traumatol. Arthrosc.* **17,** 1135–1139 (2009).

33. MITHOEFER, KAI MD; WILLIAMS, RILEY J. III MD; WARREN, RUSSELL F. MD; POTTER, HOLLIS G. MD; SPOCK, CHRISTOPHER R. BS; JONES, EDWARD C. MD; WICKIEWICZ, THOMAS L. MD; MARX, ROBERT G. MD, MSC, F. THE MICROFRACTURE TECHNIQUE FOR THE TREATMENT OF ARTICULAR C... : JBJS. *Journal of Bone & Joint Surgery* 1911–1920 (2005).

34. Kreuz, P. C. *et al.* Results after microfracture of full-thickness chondral defects in different compartments in the knee. *Osteoarthr. Cartil.* **14,** 1119–1125 (2006).

35. Mienaltowski, M. J. *et al.* Transcriptional profiling differences for articular cartilage and repair tissue in equine joint surface lesions. *BMC Med. Genomics* **2,** 60 (2009).

36. MIYATA, S., TATEISHI, T., FURUKAWA, K. & USHIDA, T. Influence of Structure and Composition on Dynamic Viscoelastic Property of Cartilaginous Tissue: Criteria for Classification between Hyaline Cartilage and Fibrocartilage Based on Mechanical Function. *JSME Int. J. Ser. C* **48,** 547–554 (2005).

37. Bedi, A., Feeley, B. T. & Williams, R. J. Management of Articular Cartilage Defects of the Knee. *J. Bone Jt. Surgery-American Vol.* **92,** 994–1009 (2010).

38. Solheim, E. *et al.* Results at 10–14 years after microfracture treatment of articular cartilage defects in the knee. *Knee Surgery, Sport. Traumatol. Arthrosc.* **24,** 1587–1593 (2016).

39. Camp, C. L., Stuart, M. J. & Krych, A. J. Current concepts of articular cartilage restoration techniques in the knee. *Sports Health* **6,** 265–73 (2014).

40. Paul, J. *et al.* Donor-Site Morbidity After Osteochondral Autologous Transplantation for Lesions of the Talus. *J. Bone Jt. Surgery-American Vol.* **91,** 1683–1688 (2009).

41. Williams, S. K. *et al.* Prolonged storage effects on the articular cartilage of fresh human osteochondral allografts. *J. Bone Joint Surg. Am.* **85–A,** 2111–20 (2003).

42. Pallante, A. L. *et al.* Treatment of Articular Cartilage Defects in the Goat with Frozen Versus Fresh Osteochondral Allografts. *J. Bone Jt. Surg.* **94,** 1984–1995 (2012).

43. PETERSON, LARS MD, PHD; MINAS, TOM MD; BRITTBERG, MATS MD, PHD; LINDAHL, ANDERS MD, P. TREATMENT OF OSTEOCHONDRITIS DISSECANS OF THE KNEE WITH AUTO... : JBJS. *The Journal of Bone & Joint Surgery* 17–24 (2003).

44. Gobbi, A. & Bathan, L. Biological Approaches for Cartilage Repair. *J. Knee Surg.* **22,** 36–44 (2010).

45. Brittberg, M. *et al.* Treatment of Deep Cartilage Defects in the Knee with Autologous Chondrocyte Transplantation. *N. Engl. J. Med.* **331,** 889–895 (1994).

46. Kreuz, P. C. *et al.* Classification of graft hypertrophy after autologous chondrocyte implantation of full-thickness chondral defects in the knee. *Osteoarthr. Cartil.* **15,** 1339–1347 (2007).

47. Ueno, T. *et al.* Cellular origin of endochondral ossification from grafted periosteum. *Anat. Rec.* **264,** 348–57 (2001).

48. Cherubino, P., Grassi, F., Bulgheroni, P. & Ronga, M. Autologous Chondrocyte Implantation Using a Bilayer Collagen Membrane: A Preliminary Report. *J. Orthop. Surg.* **11,** 10–15 (2003).

49. Lin, Z. *et al.* Gene expression profiles of human chondrocytes during passaged monolayer cultivation. *J. Orthop. Res.* **26,** 1230–1237 (2008).

50. Barbero, A. *et al.* Age related changes in human articular chondrocyte yield, proliferation and post-expansion chondrogenic capacity. *Osteoarthr. Cartil.* **12,** 476–84 (2004).

51. Loeser, R. F. Aging and osteoarthritis: the role of chondrocyte senescence and aging changes in the cartilage matrix. *Osteoarthritis Cartilage* **17,** 971–9 (2009).

52. Dozin, B., Malpeli, M., Camardella, L., Cancedda, R. & Pietrangelo, A. Response of young, aged and osteoarthritic human articular chondrocytes to inflammatory cytokines: molecular and cellular aspects. *Matrix Biol.* **21,** 449–459 (2002).

53. Li, W.-J. *et al.* A three-dimensional nanofibrous scaffold for cartilage tissue engineering using human mesenchymal stem cells. *Biomaterials* **26,** 599–609 (2005).

54. Meinel, L. *et al.* Engineering cartilage-like tissue using human mesenchymal stem cells and silk protein scaffolds. *Biotechnol. Bioeng.* **88,** 379–391 (2004).

55. Kramer, J. *et al.* Embryonic stem cell-derived chondrogenic differentiation in vitro: activation by BMP-2 and BMP-4. *Mech. Dev.* **92,** 193–205 (2000).

56. Toh, W. S. *et al.* Effects of Culture Conditions and Bone Morphogenetic Protein 2 on Extent of Chondrogenesis from Human Embryonic Stem Cells. *Stem Cells* **25,** 950–960 (2007).

57. Wei, Y. *et al.* Chondrogenic differentiation of induced pluripotent stem cells from osteoarthritic chondrocytes in alginate matrix. *Eur. Cell. Mater.* **23,** 1–12 (2012).

58. Diekman, B. O. *et al.* Cartilage tissue engineering using differentiated and purified induced pluripotent stem cells. *Proc. Natl. Acad. Sci. U. S. A.* **109,** 19172–7 (2012).

59. Deng, Y., Hu, J. C. & Athanasiou, K. A. Isolation and chondroinduction of a dermis-isolated, aggrecan-sensitive subpopulation with high chondrogenic potential. *Arthritis Rheum.* **56,** 168–176 (2007).

60. Sudo, K. *et al.* Mesenchymal Progenitors Able to Differentiate into Osteogenic, Chondrogenic, and/or Adipogenic Cells In Vitro Are Present in Most Primary Fibroblast-Like Cell Populations. *Stem Cells* **25,** 1610–1617 (2007).

61. Pittenger, M. F. *et al.* Multilineage potential of adult human mesenchymal stem cells. *Science* **284,** 143–7 (1999).

62. Baksh, D., Yao, R. & Tuan, R. S. Comparison of Proliferative and Multilineage Differentiation Potential of Human Mesenchymal Stem Cells Derived from Umbilical Cord and Bone Marrow. *Stem Cells* **25,** 1384–1392 (2007).

63. Lange, C., Schroeder, J., Lioznov, M. V. & Zander, A. R. High-Potential Human Mesenchymal Stem Cells. *Stem Cells Dev.* **14,** 70–80 (2005).

64. Cohnheim, J. Ueber Entzündung und Eiterung. *Arch. für Pathol. Anat. und Physiol. und für Klin. Med.* **40,** 1–79 (1867).

65. Friedenstein, A. J., Chailakhjan, R. K. & Lalykina, K. S. THE DEVELOPMENT OF FIBROBLAST COLONIES IN MONOLAYER CULTURES OF GUINEA-PIG BONE MARROW AND SPLEEN CELLS. *Cell Prolif.* **3,** 393–403 (1970).

66. Prockop, D. J. & Reger, R. L. Mesenchymal Stromal Cells - Chapter 2. (2013). doi:10.1007/978-1-4614-5711-4

67. Johnstone, B., Hering, T. M., Caplan, a I., Goldberg, V. M. & Yoo, J. U. In vitro chondrogenesis of bone marrow-derived mesenchymal progenitor cells. *Exp. Cell Res.* **238,** 265–72 (1998).

68. Bian, L. *et al.* Enhanced MSC chondrogenesis following delivery of TGF-β3 from alginate microspheres within hyaluronic acid hydrogels in vitro and in vivo. *Biomaterials* **32,** 6425–34 (2011).

69. Worster, A. A. *et al.* Chondrocytic differentiation of mesenchymal stem cells sequentially exposed to transforming growth factor-β1 in monolayer and insulin-like growth factor-I in a three-dimensional matrix. *J. Orthop. Res.* **19,** 738–749 (2001).

70. Schmitt, B. *et al.* BMP2 initiates chondrogenic lineage development of adult human mesenchymal stem cells in high-density culture. *Differentiation* **71,** 567–577 (2003).

71. Sekiya, I., Colter, D. C. & Prockop, D. J. BMP-6 Enhances Chondrogenesis in a Subpopulation of Human Marrow Stromal Cells. *Biochem. Biophys. Res. Commun.* **284,** 411–418 (2001).

72. Longobardi, L. *et al.* Effect of IGF-I in the Chondrogenesis of Bone Marrow Mesenchymal Stem Cells in the Presence or Absence of TGF- □ Signaling. **21,** 626–636 (2006).

73. Ito, T., Sawada, R., Fujiwara, Y. & Tsuchiya, T. FGF-2 increases osteogenic and chondrogenic differentiation potentials of human mesenchymal stem cells by inactivation of TGF-β signaling. *Cytotechnology* **56,** 1–7 (2008).

74. Solchaga, L. A. *et al.* FGF-2 enhances the mitotic and chondrogenic potentials of human adult bone marrow-derived mesenchymal stem cells. *J. Cell. Physiol.* **203,** 398–409 (2005).

75. Shu, C., Smith, S. M., Little, C. B. & Melrose, J. Use of FGF-2 and FGF-18 to direct bone marrow stromal stem cells to chondrogenic and osteogenic lineages. *Futur. Sci. OA* **2,** FSO142 (2016).

76. Charles Huang, C.-Y., Reuben, P. M., D'Ippolito, G., Schiller, P. C. & Cheung, H. S. Chondrogenesis of human bone marrow-derived mesenchymal stem cells in agarose culture. *Anat. Rec.* **278A,** 428–436 (2004).

77. Ma, H.-L., Hung, S.-C., Lin, S.-Y., Chen, Y.-L. & Lo, W.-H. Chondrogenesis of human mesenchymal stem cells encapsulated in alginate beads. *J. Biomed. Mater. Res.* **64A,** 273–281 (2003).

78. Cho, J. H. *et al.* Chondrogenic differentiation of human mesenchymal stem cells using a thermosensitive poly(N-isopropylacrylamide) and water-soluble chitosan copolymer. *Biomaterials* **25,** 5743–5751 (2004).

79. Nöth, U. *et al.* Chondrogenic differentiation of human mesenchymal stem cells in collagen type I hydrogels. *J. Biomed. Mater. Res. Part A* **83A,** 626–635 (2007).

80. Erickson, I. E. *et al.* Macromer density influences mesenchymal stem cell chondrogenesis and maturation in photocrosslinked hyaluronic acid hydrogels. *Osteoarthr. Cartil.* **17,** 1639–48 (2009).

81. Alves da Silva, M. L. *et al.* Cartilage Tissue Engineering Using Electrospun PCL Nanofiber Meshes and MSCs. *Biomacromolecules* **11,** 3228–3236 (2010).

82. Williams, C. G. *et al.* In vitro chondrogenesis of bone marrow-derived mesenchymal stem cells in a photopolymerizing hydrogel. *Tissue Eng.* **9,** 679–88 (2003).

83. Choi, K.-H., Choi, B. H., Park, S. R., Kim, B. J. & Min, B.-H. The chondrogenic differentiation of mesenchymal stem cells on an extracellular matrix scaffold derived from porcine chondrocytes. *Biomaterials* **31,** 5355–5365 (2010).

84. Xin, X., Hussain, M. & Mao, J. J. Continuing differentiation of human mesenchymal stem cells and induced chondrogenic and osteogenic lineages in electrospun PLGA nanofiber scaffold. *Biomaterials* **28,** 316–325 (2007).

85. Jin, M., Frank, E. H., Quinn, T. M., Hunziker, E. B. & Grodzinsky, A. J. Tissue Shear Deformation Stimulates Proteoglycan and Protein Biosynthesis in Bovine Cartilage Explants. *Arch. Biochem. Biophys.* **395,** 41–48 (2001).

86. Davisson, T., Kunig, S., Chen, A., Sah, R. & Ratcliffe, A. Static and dynamic compression modulate matrix metabolism in tissue engineered cartilage. *J. Orthop. Res.* **20,** 842–848 (2002).

87. Saini, S. & Wick, T. M. Concentric Cylinder Bioreactor for Production of Tissue Engineered Cartilage: Effect of Seeding Density and Hydrodynamic Loading on Construct Development. *Biotechnol. Prog.* **19,** 510–521 (2003).

88. Bueno, E. M., Bilgen, B. & Barabino, G. A. Wavy-Walled Bioreactor Supports Increased Cell Proliferation and Matrix Deposition in Engineered Cartilage Constructs. *Tissue Eng.* **11,** 1699–1709 (2005).

89. Murdoch, A. D. *et al.* Chondrogenic Differentiation of Human Bone Marrow Stem Cells in Transwell Cultures: Generation of Scaffold-Free Cartilage. *Stem Cells* **25,** 2786–2796 (2007).

90. Hu, J. C. & Athanasiou, K. A. A Self-Assembling Process in Articular Cartilage Tissue Engineering. *Tissue Eng.* **12,** 969–979 (2006).

91. Nöth, U., Tuli, R., Osyczka, A. M., Danielson, K. G. & Tuan, R. S. In Vitro Engineered Cartilage Constructs Produced by Press-Coating Biodegradable Polymer with Human Mesenchymal Stem Cells. *Tissue Eng.* **8,** 131–144 (2002).

92. Scotti, C. *et al.* Recapitulation of endochondral bone formation using human adult mesenchymal stem cells as a paradigm for developmental engineering. *Proc. Natl. Acad. Sci. U. S. A.* **107,** 7251–6 (2010).

93. Farrell, E. *et al.* In-vivo generation of bone via endochondral ossification by in-vitro chondrogenic priming of adult human and rat mesenchymal stem cells. *BMC Musculoskelet. Disord.* **12,** 31 (2011).

94. Kronenberg, H. M. Developmental regulation of the growth plate. *Nature* **423,** 332–6 (2003).

95. Steinert, A. F. *et al.* Hypertrophy is induced during the in vitro chondrogenic differentiation

of human mesenchymal stem cells by bone morphogenetic protein-2 and bone morphogenetic protein-4 gene transfer. *Arthritis Res. Ther.* **11,** R148 (2009).

96. Alini, M. *et al.* Cellular and matrix changes before and at the time of calcification in the growth plate studied in vitro: Arrest of type X collagen synthesis and net loss of collagen when calcification is initiated. *J. Bone Miner. Res.* **9,** 1077–1087 (2009).

97. D'Angelo, M. *et al.* MMP-13 is induced during chondrocyte hypertrophy. *J. Cell. Biochem.* **77,** 678–693 (2000).

98. Fosang, A. J., Last, K., Knäuper, V., Murphy, G. & Neame, P. J. Degradation of cartilage aggrecan by collagenase-3 (MMP-13). *FEBS Lett.* **380,** 17–20 (1996).

99. Mitchell, P. G. *et al.* Cloning, expression, and type II collagenolytic activity of matrix metalloproteinase-13 from human osteoarthritic cartilage. *J. Clin. Invest.* **97,** 761–768 (1996).

100. Tortorella, M. D. *et al.* Sites of aggrecan cleavage by recombinant human aggrecanase-1 (ADAMTS-4). *J. Biol. Chem.* **275,** 18566–73 (2000).

101. Mitchell, P. G. *et al.* Cloning, expression, and type II collagenolytic activity of matrix metalloproteinase-13 from human osteoarthritic cartilage. *J. Clin. Invest.* **97,** 761–768 (1996).

102. Boeuf, S. *et al.* Regulation of aggrecanases from the ADAMTS family and aggrecan neoepitope formation during in vitro chondrogenesis of human mesenchymal stem cells. *Eur. Cell. Mater.* **23,** 320–32 (2012).

103. Kawaguchi, H. Endochondral ossification signals in cartilage degradation during osteoarthritis progression in experimental mouse models. *Mol. Cells* **25,** 1–6 (2008).

104. Mak, K. K., Kronenberg, H. M., Chuang, P.-T., Mackem, S. & Yang, Y. Indian hedgehog signals independently of PTHrP to promote chondrocyte hypertrophy. *Development* **135,** 1947–56 (2008).

105. Mueller, M. B. *et al.* Hypertrophy in mesenchymal stem cell chondrogenesis: effect of TGF-beta isoforms and chondrogenic conditioning. *Cells. Tissues. Organs* **192,** 158–66 (2010).

106. Dong, Y.-F., Soung, D. Y., Schwarz, E. M., O'Keefe, R. J. & Drissi, H. Wnt induction of chondrocyte hypertrophy through the Runx2 transcription factor. *J. Cell. Physiol.* **208,** 77–86 (2006).

107. Hellingman, C. A. *et al.* Smad Signaling Determines Chondrogenic Differentiation of Bone-Marrow-Derived Mesenchymal Stem Cells: Inhibition of Smad1/5/8P Prevents Terminal Differentiation and Calcification. *Tissue Eng. Part A* **17,** 1157–1167 (2011).

108. Wang, W., Xu, J. & Kirsch, T. Annexin-mediated Ca2+ influx regulates growth plate chondrocyte maturation and apoptosis. *J. Biol. Chem.* **278,** 3762–9 (2003).

109. Morita, K. *et al.* Reactive oxygen species induce chondrocyte hypertrophy in endochondral ossification. *J. Exp. Med.* **204,** 1613–23 (2007).

110. Leboy, P. S., Grasso-Knight, G., D'Angelo, M. & Volk, S. W. Smad-Runx Interactions

During Chondrocyte Maturation. *Journal of Bone and Joint Surgery,* S15-22 (2001).

111. Yoshida, C. A. *et al.* Runx2 and Runx3 are essential for chondrocyte maturation, and Runx2 regulates limb growth through induction of Indian hedgehog. *Genes Dev.* **18,** 952–63 (2004).

112. Zheng, Q. *et al.* Type X collagen gene regulation by Runx2 contributes directly to its hypertrophic chondrocyte-specific expression in vivo. *J. Cell Biol.* **162,** 833–42 (2003).

113. Li, F. *et al.* Runx2 Contributes to Murine Col10a1 Gene Regulation Through Direct Interaction With Its Cis-Enhancer. doi:10.1002/jbmr.504

114. Wang, X. *et al.* Regulation of MMP-13 expression by RUNX2 and FGF2 in osteoarthritic cartilage. *Osteoarthr. Cartil.* **12,** 963–73 (2004).

115. Nishimura, R. *et al.* Osterix regulates calcification and degradation of chondrogenic matrices through matrix metalloproteinase 13 (MMP13) expression in association with transcription factor Runx2 during endochondral ossification. *J. Biol. Chem.* **287,** 33179–90 (2012).

116. Zelzer, E. *et al.* Tissue specific regulation of VEGF expression during bone development requires Cbfa1/Runx2. *Mech. Dev.* **106,** 97–106 (2001).

117. Sun, X., Wei, L., Chen, Q. & Terek, R. M. HDAC4 represses vascular endothelial growth factor expression in chondrosarcoma by modulating RUNX2 activity. *J. Biol. Chem.* **284,** 21881–90 (2009).

118. Lu, Y. *et al.* Col10a1-Runx2 transgenic mice with delayed chondrocyte maturation are less susceptible to developing osteoarthritis. *Am. J. Transl. Res.* **6,** 736–45 (2014).

119. Ding, M. *et al.* Targeting Runx2 expression in hypertrophic chondrocytes impairs endochondral ossification during early skeletal development. *J. Cell. Physiol.* **227,** 3446–56 (2012).

120. Liao, L. *et al.* Deletion of Runx2 in Articular Chondrocytes Decelerates the Progression of DMM-Induced Osteoarthritis in Adult Mice. *Sci. Rep.* **7,** 2371 (2017).

121. Sabariegos, R., Giménez-Barcons, M., Tàpia, N., Clotet, B. & Martínez, M. A. Sequence homology required by human immunodeficiency virus type 1 to escape from short interfering RNAs. *J. Virol.* **80,** 571–7 (2006).

122. Ambesajir, A., Kaushik, A., Kaushik, J. J. & Petros, S. T. RNA interference: A futuristic tool and its therapeutic applications. *Saudi J. Biol. Sci.* **19,** 395–403 (2012).

123. Battistella, M. & Marsden, P. Advances, Nuances, and Potential Pitfalls When Exploiting the Therapeutic Potential of RNA Interference. *Clin. Pharmacol. Ther.* **97,** 79–87 (2015).

124. Borna, H., Imani, S., Iman, M. & Azimzadeh Jamalkandi, S. Therapeutic face of RNAi: in vivo challenges. *Expert Opin. Biol. Ther.* **15,** 269–285 (2015).

125. Gibson, T. J., Seiler, M. & Veitia, R. A. The transience of transient overexpression. *Nat. Methods* **10,** 715–721 (2013).

126. Chakraborty, C., Sharma, A. R., Sharma, G., Doss, C. G. P. & Lee, S.-S. Therapeutic

miRNA and siRNA: Moving from Bench to Clinic as Next Generation Medicine. *Mol. Ther. Nucleic Acids* **8,** 132–143 (2017).

127. Bobick, B. E., Matsche, A. I., Chen, F. H. & Tuan, R. S. The ERK5 and ERK1/2 signaling pathways play opposing regulatory roles during chondrogenesis of adult human bone marrow-derived multipotent progenitor cells. *J. Cell. Physiol.* **224,** n/a-n/a (2010).

128. Xu, J. *et al.* Nanocarrier-Mediated Codelivery of Small Molecular Drugs and siRNA to Enhance Chondrogenic Differentiation and Suppress Hypertrophy of Human Mesenchymal Stem Cells. *Adv. Funct. Mater.* **26,** 2463–2472 (2016).

129. Jeon, S. Y., Park, J. S., Yang, H. N., Woo, D. G. & Park, K.-H. Co-delivery of SOX9 genes and anti-Cbfa-1 siRNA coated onto PLGA nanoparticles for chondrogenesis of human MSCs. *Biomaterials* **33,** 4413–4423 (2012).

130. Ollitrault, D. *et al.* BMP-2, Hypoxia, and *COL1A1* / *HtrA1* siRNAs Favor Neo-Cartilage Hyaline Matrix Formation in Chondrocytes. *Tissue Eng. Part C Methods* **21,** 133–147 (2015).

131. Chang, T. *et al.* MicroRNA-30a promotes extracellular matrix degradation in articular cartilage *via* downregulation of Sox9. *Cell Prolif.* **49,** 207–218 (2016).

132. Koelling, S. *et al.* Migratory Chondrogenic Progenitor Cells from Repair Tissue during the Later Stages of Human Osteoarthritis. *Cell Stem Cell* **4,** 324–335 (2009).

133. Yan, H. *et al.* Suppression of NF-κB activity via nanoparticle-based siRNA delivery alters early cartilage responses to injury. *Proc. Natl. Acad. Sci. U. S. A.* **113,** E6199–E6208 (2016).

134. Wu, Y. *et al.* Functional quantum dot-siRNA nanoplexes to regulate chondrogenic differentiation of mesenchymal stem cells. *Acta Biomater.* **46,** 165–176 (2016).

135. Lamichhane, T. N., Raiker, R. S. & Jay, S. M. Exogenous DNA Loading into Extracellular Vesicles via Electroporation is Size-Dependent and Enables Limited Gene Delivery. *Mol. Pharm.* **12,** 3650–3657 (2015).

136. Ramamoorth, M. & Narvekar, A. Non viral vectors in gene therapy- an overview. *J. Clin. Diagn. Res.* **9,** GE01-6 (2015).

137. Moore, C. B., Guthrie, E. H., Huang, M. T.-H. & Taxman, D. J. Short hairpin RNA (shRNA): design, delivery, and assessment of gene knockdown. *Methods Mol. Biol.* **629,** 141–58 (2010).

138. Cucchiarini, M. & Madry, H. Use of Tissue Engineering Strategies to Repair Joint Tissues in Osteoarthritis: Viral Gene Transfer Approaches. *Curr. Rheumatol. Rep.* **16,** 449 (2014).

139. Arai, Y. *et al.* Gene delivery to human chondrocytes by an adeno associated virus vector. *J. Rheumatol.* **27,** 979–82 (2000).

140. Pagnotto, M. R. *et al.* Adeno-associated viral gene transfer of transforming growth factor-β1 to human mesenchymal stem cells improves cartilage repair. *Gene Ther.* **14,** 804–813 (2007).

141. Li, Y. *et al.* Transduction of Passaged Human Articular Chondrocytes with Adenoviral,

Retroviral, and Lentiviral Vectors and the Effects of Enhanced Expression of SOX9. *Tissue Eng.* **10,** 575–584 (2004).

142. Ricks, D. M., Kutner, R., Zhang, X.-Y., Welsh, D. A. & Reiser, J. Optimized Lentiviral Transduction of Mouse Bone Marrow-Derived Mesenchymal Stem Cells. *Stem Cells Dev.* **17,** 441–450 (2008).

143. Sakuma, T., Barry, M. A. & Ikeda, Y. Lentiviral vectors: basic to translational. *Biochem. J.* **443,** 603–18 (2012).

144. Paddison, P. J., Caudy, A. A., Bernstein, E., Hannon, G. J. & Conklin, D. S. Short hairpin RNAs (shRNAs) induce sequence-specific silencing in mammalian cells. *Genes Dev.* **16,** 948–958 (2002).

145. Lin, X. *et al.* Development of a tightly regulated U6 promoter for shRNA expression. *FEBS Lett.* **577,** 376–380 (2004).

146. Xia, X. G. *et al.* An enhanced U6 promoter for synthesis of short hairpin RNA. *Nucleic Acids Res.* **31,** 100e–100 (2003).

147. Ong, S. T., Li, F., Du, J., Tan, Y. W. & Wang, S. Hybrid Cytomegalovirus Enhancer–H1 Promoter-Based Plasmid and Baculovirus Vectors Mediate Effective RNA Interference. *Hum. Gene Ther.* **16,** 1404–1412 (2005).

148. Grimm, D. *et al.* Fatality in mice due to oversaturation of cellular microRNA/short hairpin RNA pathways. *Nature* **441,** 537–541 (2006).

149. Zeng, Y., Wagner, E. J. & Cullen, B. R. Both natural and designed micro RNAs can inhibit the expression of cognate mRNAs when expressed in human cells. *Mol. Cell* **9,** 1327–33 (2002).

150. Zeng, Y. & Cullen, B. R. Sequence requirements for micro RNA processing and function in human cells. *RNA* **9,** 112–23 (2003).

151. McBride, J. L. *et al.* Artificial miRNAs mitigate shRNA-mediated toxicity in the brain: implications for the therapeutic development of RNAi. *Proc. Natl. Acad. Sci. U. S. A.* **105,** 5868–73 (2008).

152. Stegmeier, F., Hu, G., Rickles, R. J., Hannon, G. J. & Elledge, S. J. A lentiviral microRNA-based system for single-copy polymerase II-regulated RNA interference in mammalian cells. *Proc. Natl. Acad. Sci. U. S. A.* **102,** 13212–7 (2005).

153. Meerbrey, K. L. *et al.* The pINDUCER lentiviral toolkit for inducible RNA interference in vitro and in vivo. *Proc. Natl. Acad. Sci. U. S. A.* **108,** 3665–70 (2011).

154. Carninci, P. *et al.* Genome-wide analysis of mammalian promoter architecture and evolution. *Nat. Genet.* **38,** 626–635 (2006).

155. Sandelin, A. *et al.* Mammalian RNA polymerase II core promoters: insights from genome-wide studies. *Nat. Rev. Genet.* **8,** 424–436 (2007).

156. Smallwood, S. A. & Kelsey, G. Genome-wide analysis of DNA methylation in low cell numbers by reduced representation bisulfite sequencing. *Methods Mol. Biol.* **925,** 187–97

(2012).

157. Schug, J. *et al.* Promoter features related to tissue specificity as measured by Shannon entropy. *Genome Biol.* **6,** R33 (2005).

158. Bird, A. P. DNA methylation versus gene expression. *J. Embryol. Exp. Morphol.* **83 Suppl,** 31–40 (1984).

159. Zheng, C. & Baum, B. J. Evaluation of promoters for use in tissue-specific gene delivery. *Methods Mol. Biol.* **434,** 205–19 (2008).

160. Weeratna, R., Wu, T., Efler, S., Zhang, L. & Davis, H. Designing gene therapy vectors: avoiding immune responses by using tissue-specific promoters. *Gene Ther.* **8,** 1872–1878 (2001).

161. Brenner, S. & Malech, H. L. Current developments in the design of onco-retrovirus and lentivirus vector systems for hematopoietic cell gene therapy. *Biochim. Biophys. Acta - Mol. Cell Res.* **1640,** 1–24 (2003).

162. Clemens, T. L. *et al.* Analysis of Osteocalcin Expression in Transgenic Mice Reveals a Species Difference in Vitamin D Regulation of Mouse and Human Osteocalcin Genes. *J. Bone Miner. Res.* **12,** 1570–1576 (1997).

163. Zhang, M. *et al.* Osteoblast-specific knockout of the insulin-like growth factor (IGF) receptor gene reveals an essential role of IGF signaling in bone matrix mineralization. *J. Biol. Chem.* **277,** 44005–12 (2002).

164. Smith, A. D., Sumazin, P., Xuan, Z. & Zhang, M. Q. DNA motifs in human and mouse proximal promoters predict tissue-specific expression. *Proc. Natl. Acad. Sci. U. S. A.* **103,** 6275–80 (2006).

165. Smith, A. D., Sumazin, P. & Zhang, M. Q. Tissue-specific regulatory elements in mammalian promoters. *Mol. Syst. Biol.* **3,** 73 (2007).

166. Wu, Z., Yang, H. & Colosi, P. Effect of genome size on AAV vector packaging. *Mol. Ther.* **18,** 80–86 (2010).

167. Kumar, M., Keller, B., Makalou, N. & Sutton, R. E. Systematic Determination of the Packaging Limit of Lentiviral Vectors. *Hum. Gene Ther.* **12,** 1893–1905 (2001).

168. Magne, D. *et al.* Phosphate is a specific signal for ATDC5 chondrocyte maturation and apoptosis-associated mineralization: possible implication of apoptosis in the regulation of endochondral ossification. *J. Bone Miner. Res.* **18,** 1430–42 (2003).

Chapter 2 Phenotype-dependent Effects of RUNX2 Silencing During Chondrogenesis

2.1 Introduction

Defects in articular cartilage occur frequently after joint injuries; however, the lack of blood supply hinders the natural healing of these damages due to the limited access to progenitor cells and nutrients[1]. Unrepaired defects lead to abnormal joint loading, which further induces deterioration of remaining cartilage tissues[2–4]. Clinical surgical techniques for cartilage repair, such as microfracture and osteochondral transplantation are not designed to form new hyaline cartilage and therefore do not restore the long-term function of injured tissues[5,6]. Currently, all FDA approved cell-based cartilage products require articular chondrocytes, which have very limited availability and poor capacity to proliferate[7]. Furthermore, repair strategies using autologous articular chondrocytes often cause donor site morbidity and require multiple invasive surgeries[8,9].

Mesenchymal stem cells (MSCs) have been extensively studied as an alternative cell source to regenerate articular cartilage due to the fact that they can be harvested from numerous tissues, have a higher potential for *in vitro* expansion, and can be induced to differentiate into chondrocytes[10,11]. Despite these advantages, chondrogenic induction of MSCs *in vitro* yields a phenotype indicative of the late phases of endochondral ossification found in growth cartilage, which include hypertrophic maturation and matrix calcification[12–14]. Specifically, MSC-derived chondrocytes (MdChs) express hypertrophy markers such as COL10a1 and MMP13[15]. Consequently, existing aggrecan and type II collagen are degraded in the cartilaginous matrix[16,17].

RUNX2 (Runt-related transcription factor 2) has been shown to drive the chondrocytes to the pre-hypertrophic phenotype by directly controlling the transcription of both COL10a1 and MMP13[18–21]. This transcription factor also upregulates several other proteins that modify the existing cartilage ECM and contribute to the progression of endochondral ossification[22–24]. Because of the essential role of RUNX2 in chondrocyte hypertrophy, targeting its activity could be an effective strategy to prevent maturation-associated matrix degradation and improve MSC-based cartilage repair.

To enhance the accumulation of aggrecan and type II collagen in MSC-based cartilage products, growth factors are frequently used to either encourage the production or inhibit the degradation of these structural macromolecules[25–30]. However, the response of the cells to growth factor supplementation is dependent on the expression of specific receptors and the maturation stage of the target cells[31]. For example, TGF-β (transforming growth factor-β), when used to induce early chondrogenesis of MSCs *in vitro*[25,26], upregulates aggrecan and collagen II by binding ALK-5 (activin receptor-like kinase 5)[32]. Nevertheless, TGF-β can also upregulate RUNX2 through binding of the ALK-1 receptor, contributing to chondrocyte hypertrophy[33]. Due to the inherent heterogeneity in stem cell populations, the same medium recipe might induce variable cell responses depending on the maturation stage of chondrogenic cell populations. The dependence on maturation stage has also been demonstrated in recent studies using PTHrP (parathyroid hormone-related peptide) to inhibit hypertrophy of human MdChs. Recently, Li *et al.* have shown that PTHrP can suppress RUNX2 expression in human MSCs at both the mRNA and protein levels[34–36]. However, supplementation of PTHrP to undifferentiated MSC cultures inhibited TGFβ-induced chondrogenesis[36]. These findings suggest that RUNX2 is involved at different stages of chondrocyte development. This has been confirmed in later studies that

demonstrate RUNX2 expression in mesenchymal condensation prior to early chondrogenesis[37–39]. Based on this data, direct manipulation of intracellular pathways that regulate chondrocyte phenotype through the RUNX2 pathway can bypass the need for specific receptor-ligand interactions to control the phenotype of chondrogenic cells and improve accrual of cartilage structural macromolecules in engineered tissues.

To determine if inhibition of RUNX2 can enhance matrix accumulation during chondrogenesis, we created a doxycycline-inducible lentiviral system to induce RNA interference (RNAi) of *Runx2* in the murine pre-chondrogenic cell line ATDC5. ATDC5 cultures are an effective model system to recapitulate the different phases of early and late chondrogenesis[40–42]. At confluence, the addition of insulin breaks contact inhibition and stimulates pre-chondrogenic proliferation, followed by early chondrogenesis and then chondrocyte hypertrophy. Using this model system we investigated the effects of suppression of RUNX2 translation at different stages of chondrocyte maturation. We found that induction of RUNX2 silencing in undifferentiated chondroprogenitors inhibits pre-chondrogenic proliferation that is required for their further differentiation into chondrocytes. After this proliferation phase, RNAi of *Runx2* no longer interferes with early chondrogenesis, instead it downregulates expression of maturation markers (*Col10a1* and *Mmp13*) and improves the accumulation of sGAG-rich matrix.

2.2 Methods

2.2.1 Vector and Virus Production

The Tet-on inducible system was modified from the pINDUCER plasmid originally developed by Meerbrey et al[43]. Different shRNA sequences of Runx2 were selected from the Hannon-Elledge library (RNAi Codex http://cancan.cshl.edu/cgi-bin/Codex/Codex.cgi), and PCR amplified using primers 5'-CAGAAGGCTCGAGAAGGTATATGCTGTTGACAGTGAG-CG and 5'-CTAAAGTAGCCCCTTGAATTCCGAGGCAGTAGGCA. The PCR product was

digested with EcoRI and XhoI, and then ligated to pINDUCER13 vector that was also digested with EcoRI and XhoI. To remove the luciferase cDNA from Tet-on-Luc-mir30-sh*Runx2*, mir30-sh*Runx2* was PCR amplified using primers 5'-GATCCAGCCTACCGGTAAGCCTTGTTAAG-TGCTCGC and 5'-CTAAAGTAGCCCCTTGAATTCCGAGGCAGTAGGCA. The PCR product was digested with EcoRI and AgeI, and then ligated to Tet-on-Luc-mir30-sh*Runx2* that was also digested with EcoRI and AgeI. Correct cloning of Tet-on sh*Runx2* (included mir30) was confirmed by Sanger sequencing at UM Sequencing core, and lentiviral supernatant of the correct plasmid vectors was produced at UM Vector Core. Viruses containing a scrambled sh*Runx2* sequence was synthesized similarly.

2.2.2 Chondrogenic Cell Cultures

ATDC5 cells (Sigma) were maintained in DMEM/F12 (Life Technologies) supplemented with 5% FBS (Life Technologies) and 1% Antibiotic-Antimycotic (Life Technologies). Chondrogenesis of ATDC5 cells was induced with chondrogenic differentiation medium (ITS+) consisting of the growth medium supplemented with 1% ITS+ Premix (Corning) and 50 µg/ml ascorbate acid-2-phosphate (Sigma).

Four days prior to chondrogenic induction, cells were seeded at the density of 10,000 cells/cm^2 in multiple well plates. When cells reached 100% confluence (D0), chondrogenesis was initiated by replacing the growth medium with differentiation medium. Cultures were fed with fresh medium every other day and maintained up to 28 days.

Cell Transduction and Induction of Silencing

Proliferating ATDC5 cells were transduced [multiplicity of infection (MOI) = 1] with lentiviral supernatant of Tet-on sh*Runx2* or scramble vectors. Polyclonal populations of cells stably expressing the inducible sh*Runx2* were obtained by puromycin selection. Transduced cells that

survived puromycin selection were chondrogenically induced in the absence or presence of 0.5 μg/ml doxycycline (Dox) during the selected time periods.

2.2.3 Biochemical Analysis

Cartilage-specific matrix production was measured by the 1,9-dimethylmethylene blue (DMMB) assay as previously described[44]. Both monolayer cell tissues and pellets were digested with 1 mg/ml proteinase K in 0.1M ammonium acetate at 50°C for 16 hours. Digested samples were mixed with DMMB dye (pH 1.5) at a ratio of 1:20, and the sGAG content of the samples were determined by comparing the ratio of 525 nm to 595 nm readings to the standard curve derived from shark chondroitin sulfate. Measured sGAG content of each sample was normalized by its DNA content using Hoechst 33258 dye (Sigma) as previously described[45].

2.2.4 Gene expression Analysis

Total RNA of each sample was extracted using TRI Reagent® RT (Molecular Research Center). For pellet culture, five pellets were combined and homogenized in the same reagent using the Micro Tube Homogenizer. Equal amounts of extracted RNA were reverse-transcribed into cDNA using High-Capacity cDNA Reverse Transcription Kit (Life Technologies). Synthesized cDNA was amplified using Fast SYBR® Green Master Mix (Life Technologies) on Applied Biosystems® 7500 Fast platform. The mean cycle threshold of the housekeeping genes ($\overline{Ct}_{hk}$) *Hprt* and *Ppia*[46] were used to calculate the fold change in transcript levels compared to day 0 samples using the $\Delta\Delta Ct$ method. Relative expression levels were calculated as $x = 2^{-\Delta\Delta Ct}$, in which $\Delta\Delta Ct = \Delta E - \Delta C$, $\Delta E = Ct_{exp} - \overline{Ct}_{hk}$ at the time-point of interest, and $\Delta C = Ct_{exp} - \overline{Ct}_{hk}$ at day 0. The forward and reverse primer sequences are listed in Table 2-1.

Table 2-1. The sequences of primers used

Gene		Primer Sequences (5'→3')		Primer Sequences (5'→3')
Acan	Forward	CGCCACTTTCATGACCGAGA	Reverse	CAAATTGCAGAGAGTGTCCGT
Adamts4	Forward	ATGGCCTCAATCCATCCCAG	Reverse	AAGCAGGGTTGGAATCTTTGC
Adamts5	Forward	GGAGCGAGGCCATTTACAAC	Reverse	CGTAGACAAGGTAGCCCACTTT
Col2a1	Forward	ACGAGGCAGACAGTACCTTG	Reverse	AGTAGTCTCCGCTCTTCCACT
Col10a1	Forward	CCAAACGCCCACAGGCATAA	Reverse	TGCCTTGTTCTCCTCTTACTGG
Hprt	Forward	CTGGTGAAAAGGACCTCTCGAA	Reverse	CTGAAGTACTCATTATAGTCAAGGGCAT
Ppia	Forward	CGCGTCTCCTTCGAGCTGTTTG	Reverse	TGTAAAGTCACCACCCTGGCACAT
Mmp13	Forward	GGAGCCCTGATGTTTCCCAT	Reverse	GTCTTCATCGCCTGGACCATA

2.2.5 Histological Analysis

Monolayer cultures were washed twice with PBS and fixed in 70% ethanol at room temperature for one hour. Proteoglycan accumulation in monolayer tissues was evaluated by staining the sectioned tissue with 3% Alcian blue dye (Poly Scientific) at 4℃ for 16 hours. Stained tissues were washed three times with PBS and imaged using bright field microscopy.

2.2.6 Western Blot Analysis

Cultured cells were lyzed in RIPA Lysis and Extraction Buffer (Thermo Scientific) supplemented with protease inhibitor cocktail (Sigma), rotated at 4 °C for one hour, and centrifuged at 12,000*g* for 10 minutes to remove cellular debris. Total protein content within each sample was determined with the Pierce BCA Protein Assay Kit (Pierce). Protein (5-15 μg) was separated on a 10% NuPAGE Bis-Tris Protein Gel and then transferred to a polyvinylidene difluoride membranes (Millipore). Membranes were blocked with Tris-buffered saline-Tween 20 (TBS-T, 0.1% Tween 20) and 5% BSA for 1 h at room temperature. Following blocking, membranes were incubated in TBS-T, 0.1% Tween 20 and 5% BSA overnight at 4 °C with rabbit anti-Runx2 antibody (Cell Signaling Technology, D1H7, 1:2000) and rabbit anti-β-actin antibody (Abcam, 119716, 1:5000). Positive staining was visualized using the LiCor C-DiGit chemiluminescence and quantified using the LiCor Image Studio.

2.2.7 Statistical Analysis

Statistical analysis was performed using GraphPad Prism software. All comparisons over multiple time points were analyzed by two-way ANOVA with Tukey's multiple comparison method. Comparisons in experiment with a single time point were analyzed by one-way ANOVA followed by Sidak correction. Significant difference is indicated by * P<0.05, ** P<0.01, ***P<0.001, ****P<0.0001. All error bars indicate the standard error of the mean (s.e.m.).

2.3 Results

2.3.1 RUNX2 Expression in the Monolayer ATDC5 Chondrogenic Model

We first characterized the different phases of chondrocyte development in the ATDC5 cells in monolayer cultures. At confluence, ATDC5 cells were chondrogenically induced by the supplementation of ITS+ and AA2P to the growth medium. After 24 hours, secondary proliferation post contact-inhibition occurred in response to the addition of ITS+, reflected by 1.8-fold increase in the total amount of DNA in each culture (**Figure 2-1a**). Proliferation of the cells plateaued at day 5, where it was 2.9 times higher than that of day 0. Cartilaginous nodules began to appear on day 7, as indicated by the positive staining of Alcian blue dye (**Figure 2-1b**). These Alcian blue-positive areas continued to grow within the monolayer from day 7 to day 21, accompanied by the darker staining within each nodule at the later time points. The accumulation of sGAG-rich matrix was further quantified using DMMB assay (**Figure 2-1c**). Upregulation of *Acan* and *Col2a1* gene expression coincided with the initial appearance of the cartilaginous nodules, further confirming early chondrogenesis. Both peaked at day 10 (**Figure 2-1d**). RUNX2 expression was transiently downregulated after the initial exposure to the chondrogenic stimuli, shown by the minimal detection from western blotting (**Figure 2-1e**). However, differentiating cells started to express RUNX2 protein again at day 7 and continued to upregulate it until day 21. The mRNA level of *Col10a1* started to elevate at day 10 and reached to the maximum level at day 21.

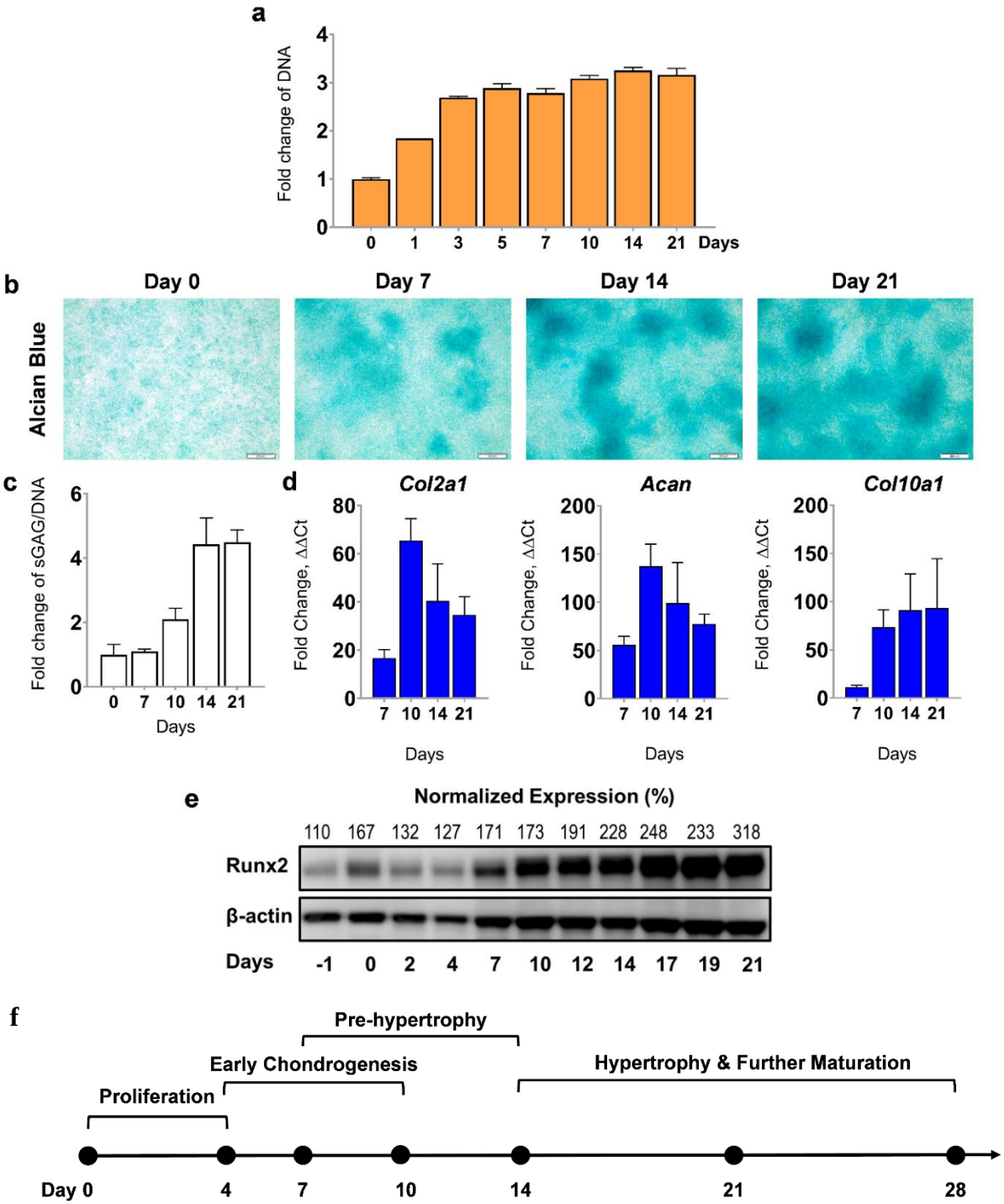

Figure 2-1. Early and late chondrogenesis in monolayer ATDC5 culture. (a) Fold change (relative to day 0) in DNA content over 21 days of differentiation (n=3). (b) Alcian blue staining at day 0, 7, 14, and 21 to show accumulation of sGAG-rich matrix (4× magnification). (c) Fold change (relative to day 0) in sGAG accumulation normalized to DNA content (n≥8, three independent experiments). (d) Quantification of mRNA expression (relative to day 0 and the housekeeping genes *Hprt* and *Ppia*) of early (*Acan* and *Col2a1*) and late (*Col10a1*) chondrogenic markers (n≥5, two independent experiments). (e) Quantified RUNX2 protein expression (%, relative to β-actin) over

21 days of differentiation. All data represented as mean ± s.e.m. (f) the time-course of chondrocyte maturation in monolayer cultures of ATDC5 cells.

2.3.2 Constitutively Silencing RUNX2 Inhibits Chondrogenesis

In cultures treated with Dox from day 0, RUNX2 protein was depleted in cells expressing inducible sh*Runx2* by day 7 (**Figure 2-2a**). There was also no significant proliferation in these cultures from day 0 (**Figure 2-2b**). There was also no detectable amounts of matrix accumulation or expression of mRNA for *Acan* and *Col2a1* by day 14, while the scramble controls had successfully formed many Alcian blue-positive nodules **(Figure 2-2c-e)**. In contrast, in the absence of Dox, the formation of the sGAG-rich nodules and upregulation of early chondrogenic markers were observed in both inducible sh*Runx2* and scramble cultures.

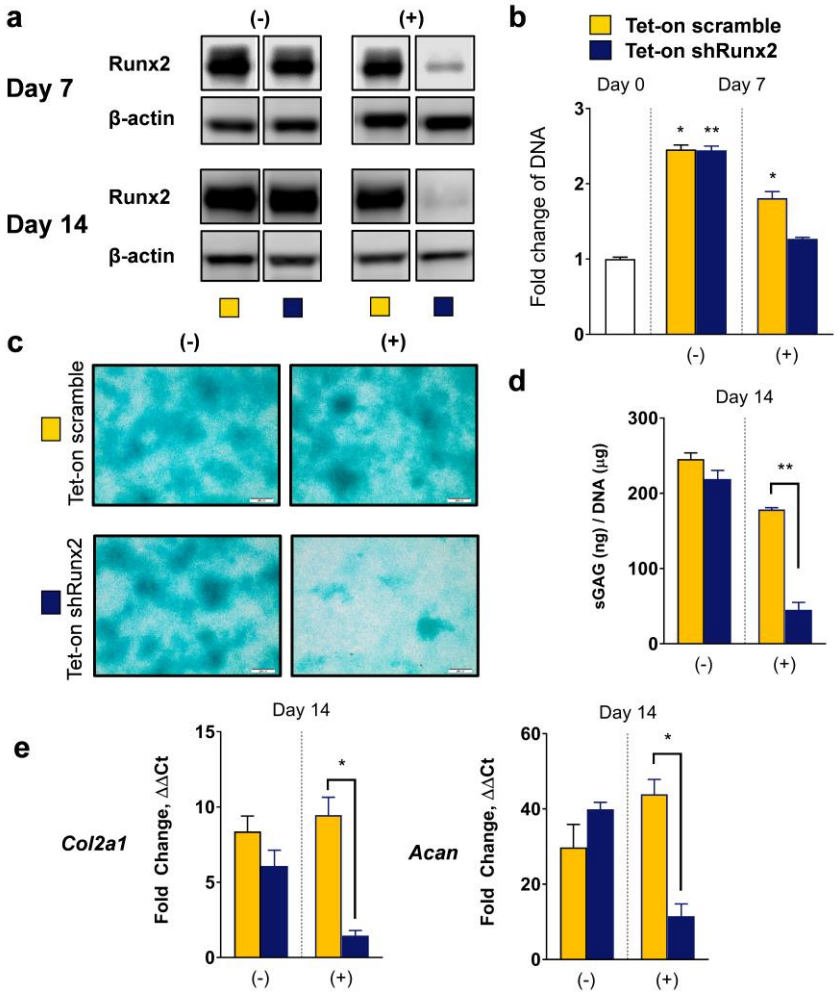

Figure 2-2. Effects of constitutively active RUNX2 silencing on early chondrogenesis. ATDC5 cells expressing Tet-on sh*Runx2*/scramble differentiated in the absence (-) or presence (+) of 0.5 µg/ml doxycycline for 14 days. (a)

Western blot analysis of RUNX2 and β-actin at day 7 and 14. (b) Fold change (relative to day 0) in DNA content at day 7 (different groups at day 7 were compared against day 0). (c) Alcian blue staining, (d) sGAG accumulation normalized to DNA content, (e) quantification of mRNA expression (relative to *Hprt* and *Ppia*) of *Acan* and *Col2a1* at day 14. Polyclonal populations were established by combining selected cells from two independent transduction experiments (two viral batches, n=3). All data represented as mean ± s.e.m. Significant difference is indicated by * P<0.05 and ** P<0.01 by two-way ANOVA with Tukey's multiple comparison method.

2.3.3 Delayed RUNX2 Silencing Enhances Matrix Accumulation During Chondrogenesis

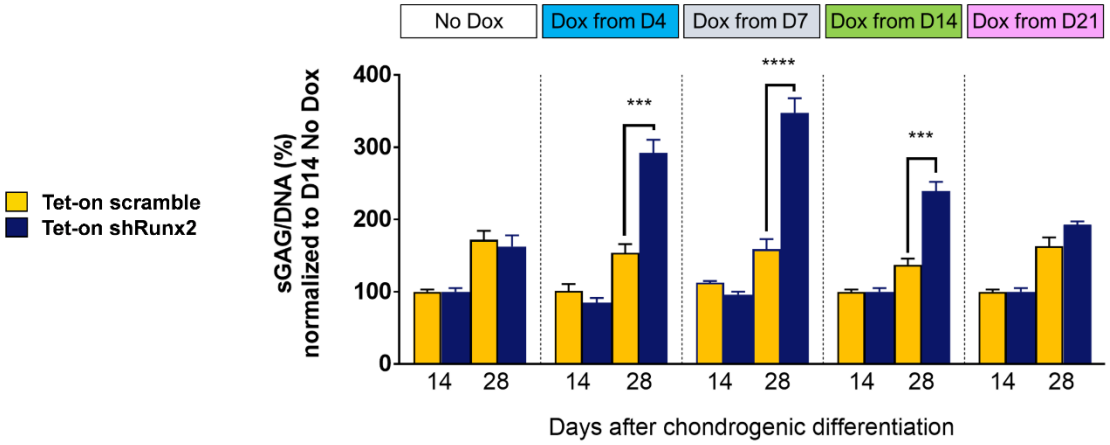

Figure 2-3. Effects of RUNX2 silencing at different maturation stages of chondrogenesis. Fold change (%, relative to D14 No Dox controls) in sGAG accumulation normalized to DNA content at day 14 and 28. Data represented as mean ± s.e.m. Polyclonal populations were established by combining selected cells from two independent transduction experiments (two viral batches, n=3). Significant difference between Tet-on sh*Runx2* and scramble groups at each time point is indicated by ***P<0.001 and ****P<0.0001 by two-way ANOVA with Tukey's multiple comparison method.

To determine if the RUNX2 silencing-induced suppression of matrix accumulation continued after pre-chondrogenic proliferation, Dox treatment was started at the onset of specific maturation stages (days 4, 7, 14, or 21; **Figure 2-1f**) and continued through day 28. When RUNX2 was inhibited just after the initial phase of proliferation (day 4), cells expressing Tet-on sh*Runx2* accumulated 1.9 times higher amount of matrix by day 28 when compared to that of the scramble controls. A similar positive effect on matrix accumulation was also observed when inhibition was initiated at the start of RUNX2 protein upregulation (day 7) and maximum *Col10a1* gene expression (day 14), resulting in a 2.19- and a 1.75-fold increase by day 28, respectively (**Figure 2-3**).

Although the addition of Dox from day 7 decreased the level of RUNX2 protein in Tet-on sh*Runx2* cells, complete depletion did not occur in response to the concentration of Dox that was

used (**Figure 2-4a**). At both day 14 and 28, the downregulated protein expression of RUNX2 in the sh*Runx2* cells correlated with lower mRNA levels of *Col10a1* compared to the scramble controls (**Figure 2-4b**). Interestingly, Dox treatment from day 7 also seemed to result in significant upregulation of *Acan* and *Col2a1* genes in the scramble cells at day 14 when compared to the non-treated scramble controls. However, the addition of Dox did not change expression levels of these two early chondrogenic markers in sh*Runx2* cells.

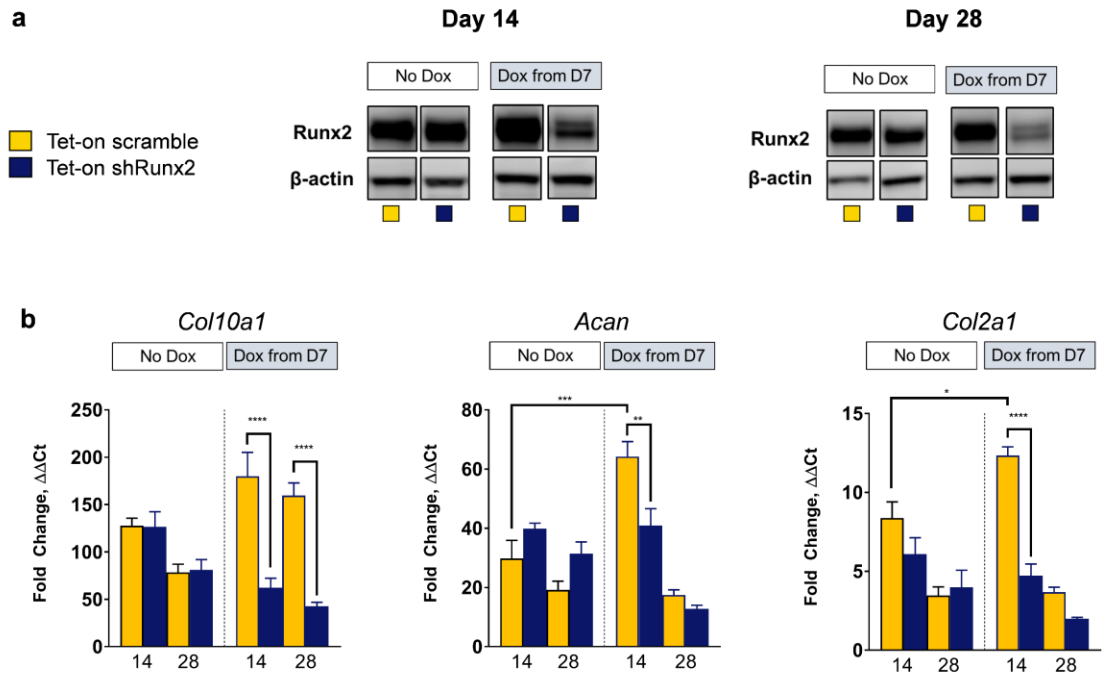

Figure 2-4. Effects of 7-day delayed RUNX2 silencing on chondrogenesis. Dox (0.5 µg/ml) was supplemented from day 7 during the differentiation of ATDC5 cells expressing Tet-on sh*Runx2*/scramble until day 28. (a) Western blot analysis of RUNX2 and β-actin at day 14 and 28. (b) Quantification of mRNA expression (relative to *Hprt* and *Ppia*) of *Col10a1*, *Acan* and *Col2a1* at day 14 and 28. Polyclonal populations were established by combining selected cells from two independent transduction experiments (two viral batches, n=3). All data represented as mean ± s.e.m. Significant difference is indicated by * P<0.05, ** P<0.01, ***P<0.001, ****P<0.0001 by two-way ANOVA with Tukey's multiple comparison method.

2.3.4 Delayed RUNX2 Silencing Suppresses *Mmp13* Transcription During Hypertrophy

To further examine the effects of delayed RUNX2 suppression on the gene expression of matrix-degrading enzymes, we also measured the mRNA levels of *Mmp13*, *Adamts4* (aggrecanase-1), and *Adamts5* (aggrecanase-2) in 4-, 7-, and 14-day delayed silencing groups after hypertrophy occurred (day 21 and 28). Dox treatment from day 7 and 14 of Tet-on sh*Runx2* cells significantly

lowered mRNA levels of *Mmp13* at both day 21 and 28 while their corresponding scramble controls exhibited little change (**Figure 2-5a**). Although Dox treatment from day 4 also downregulated *Mmp13* in sh*Runx2* cells, a similar decrease was observed in scramble cultures by day 14. In contrast to *Mmp13*, *Adamts4* expression was not affected by Dox induction throughout the culture period (**Figure 2-5b**). Interestingly, addition of Dox seemed to broadly increase the mRNA levels of *Adamts5* in both sh*Runx2* and scramble cells compared to non-treated ones (statistical significance was found in all treated groups, not labeled). However, the only significant difference was observed between sh*Runx2* and scramble cultures at day 28 in the 4-day delayed Dox condition (**Figure 2-5c**). Together, these results suggest RUNX2 silencing reduces the transcription of *Mmp13* but not *Adamts4* or *Adamts5* during chondrocyte hypertrophy.

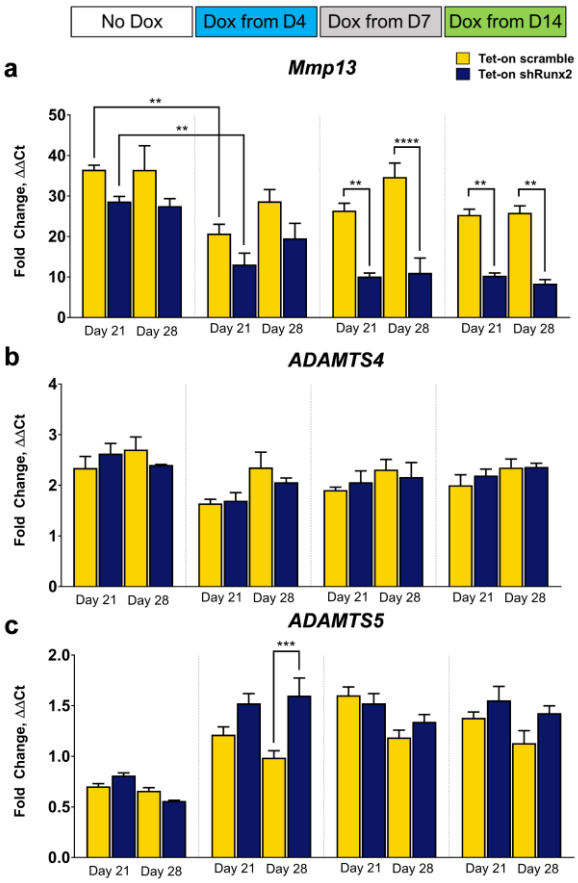

Figure 2-5. Effects of delayed RUNX2 silencing on gene expression of matrix degrading enzymes. Quantification of mRNA expression (relative to *Hprt* and *Ppia*) of (a) *Mmp13*, (b) *Adamts4*, and (c) *Adamts5* at day 21 and 28. Polyclonal populations were established by combining selected cells from two independent transduction experiments

(two viral batches, n=3). All data represented as mean ± s.e.m. Significant difference is indicated by * P<0.05, ** P<0.01, ***P<0.001, ****P<0.0001 by two-way ANOVA with Tukey's multiple comparison method.

2.4 Discussion & Conclusion

In this chapter, we demonstrate that the loss of RUNX2 function during the chondrogenesis of mesenchymal progenitors can elicit distinct cellular responses at different stages of differentiation. Using a 2D ATDC5 model with inducible sh*Runx2* expression, we show that RNAi of *Runx2* in the undifferentiated cells inhibits mesenchymal proliferation and differentiation into chondrocytes. However, induced expression of shRunx2 after the pre-chondrogenic proliferation phase or early chondrogenesis enhances the accumulation of cartilaginous matrix. We also observed that RUNX2 silencing decreases the transcription of *Mmp13* but does not affect the gene expression of *Adamts4* or *Adamts5* during hypertrophy. In addition, RUNX2 silencing during early chondrogenesis and pre-hypertrophy may also moderately downregulate the gene expression of *Acan* and *Col2a1*. Thus, maximizing the accumulation of cartilaginous matrix via RNAi of *Runx2* requires balancing the inhibition of degradation and repression of production by optimizing the timing and dosing of sh*Runx2* expression.

Here, our results suggest that RNAi of *Runx2* in undifferentiated progenitor cells inhibits the proliferation required for *in vitro* chondrogenesis. Unlike the well-established role of RUNX2 in driving chondrocyte maturation, its involvement in early events of chondrogenesis remains unclear. Progenitor cells within the prechondrogenic condensation first proliferate before committing to chondrogenic differentiation[47–49]. *Runx2* expression has been detected within these condensations[37–39]. Recently, Dexheimer *et al.* showed that this transient phase of proliferation is required for *in vitro* chondrogenesis of human MSCs after cells are condensed into a micromass pellet[50]. In our study, when chondrogenesis is induced in confluent monolayer ATDC5 cultures, the differentiation initiates with a similar phase of proliferation that overrides the contact inhibition during the first 4 days, which does not occur under the RNAi of *Runx2*. In accordance with our

observations, Akiyama *et al.* also showed that introduction of the dominant negative form of RUNX2 in ATDC5 cells inhibits the cellular condensation and subsequent chondrogenic differentiation[51]. Similar suppression of chondrogenesis is also observed when *Zfp521*, an inhibitor of RUNX2, is overexpressed in ADTC5 cells[52]. However, it is worth noting that Runx2$^{-/-}$ mice do form cartilaginous skeleton[53,54], suggesting that the *in vivo* cartilage formation involves different signaling pathways from those required for *in vitro* chondrogenesis. Nonetheless, constitutively active RNAi of *Runx2* is not suitable for MSC-based cartilage tissue engineering.

Our results also show that delayed RUNX2 silencing in chondroprogenitors after the pre-chondrogenic proliferation phase does not interfere with their further progression to early chondrogenesis; instead it increases the amount of matrix accumulated by these differentiated chondrocytes, supporting our original hypothesis. As chondrogenesis proceeds, the role of RUNX2 changes[55]. After pre-chondrogenic proliferation *in vivo*, Nkx3.2-mediated repression of *Runx2* promotes early chondrogenesis by activating *Sox9*[56]. These findings are analogous to our observation of the downregulation of RUNX2 after chondrogenic induction in ATDC5 cells. They also likely explain why loss of RUNX2 function after day 4 no longer blocks chondrogenesis in ATDC5 cells. As in growth plate chondrocytes[57], the low protein expression of RUNX2 is not permanent in the ATDC5 model. Quickly following the upregulation of *Col2a1* and *Acan*, protein expression of RUNX2 elevated and drove differentiated chondrocytes to the pre-hypertrophic and then hypertrophic phenotypes. As expected, induced RUNX2 silencing at this stage of chondrocyte maturation decreased mRNA levels of both *Col10a1* and *Mmp13*. MMP13 can degrade both aggrecan[16] and type II collagen[17] and downregulation of *Mmp13* due to the loss of RUNX2 function has been reported to reduce the breakdown of these structural molecules in Runx2

deficient mice[58]. This is consistent with our observation that RUNX2 silencing leads to an increased level of matrix accumulation after control groups undergo hypertrophy.

Importantly, results from this chapter indicate that RNAi of *Runx2* in chondrocytes that are transitioning to the pre-hypertrophic phenotype maximizes the accumulation of matrix since it is a net function of production and turnover. While RUNX2 silencing is desirable for reducing MMP13-mediated matrix degradation, we also noticed that it seems to downregulate the gene expression of *Acan* and *Col2a1* at varying levels. While the relationship RUNX2 activity and transcription of *Acan* and *Col2a1* remains to be clarified, RUNX2, together with RUNX1, has been shown to induce the expression of *Sox5* and *Sox6*, which further control the induction of *Col2a1*[59]. Additionally, RUNX2 is a common target of TGF-β1 and BMP-2, both of which are frequently used to induce chondrogenesis of MSCs[60]. These studies, together with our results, suggest that Runx2 activity may also contribute to the production of aggrecan and type II collagen. Although we cannot easily decouple the regulation of early chondrogenic markers and matrix-degrading enzymes by RUNX2, the different expression profiles of early and late chondrogenic markers allow us to optimize the temporal activation of sh*Runx2* expression to maximize the accumulation of matrix during chondrogenesis. Identifying such an optimal time is critical because the premature loss of RUNX2 function reduces the production of aggrecan and type II collagen while the belated silencing permits uncontrolled matrix degradation.

Although exogenous cues can be used to control the temporal induction of RNAi as well as levels of RUNX2 suppression, the application potential of this type of RUNX2 silencing is limited for several reasons. First, the continuous suppression of RUNX2 translation would require sustained delivery of doxycycline during the entire life cycle of the implanted cells. Second, the outcome of ubiquitous RUNX2 silencing among a heterogeneous population of stem

cells/chondrocytes could be suboptimal. In addition, long-term use of doxycycline or other inducers might cause cytotoxicity, especially when high levels of RUNX2 silencing is needed. These limitations create a need to develop a method that could target the RNAi of *Runx2* exclusively in chondrocytes that are maturing to hypertrophy. Ideally, it should also be able to provide self-regulated levels of silencing based on the states of the cells. Finally, observations from this chapter resulted only from a 2D chondrogenic environment, which might omit important cellular response that can only be observed in a three-dimensional microenvironment.

2.5 Reference

1. Viswananthan, S., Wolfstadt, J., Chahal, J. & Gomez-Aristizabal, A. *Osteoarthritis: Pathogenesis, Diagnosis, Available Treatments, Drug Safety, Regenerative and Precision Medicine*. (Springer Switzerland, 2015). doi:10.1007/978-3-319-19560-5_12
2. Du, G. *et al.* Abnormal Mechanical Loading Induces Cartilage Degeneration by Accelerating Meniscus Hypertrophy and Mineralization After ACL Injuries In Vivo. *Am. J. Sports Med.* **44,** 652–63 (2016).
3. Natoli, R. M. & Athanasiou, K. A. Traumatic loading of articular cartilage: Mechanical and biological responses and post-injury treatment. *Biorheology* **46,** 451–85 (2009).
4. Milentijevic, D., Rubel, I. F., Liew, A. S. L., Helfet, D. L. & Torzilli, P. A. An in vivo rabbit model for cartilage trauma: a preliminary study of the influence of impact stress magnitude on chondrocyte death and matrix damage. *J. Orthop. Trauma* **19,** 466–73 (2005).
5. Tibesku, C. O. *et al.* Hyaline cartilage degenerates after autologous osteochondral transplantation. *J. Orthop. Res.* **22,** 1210–1214 (2004).
6. Kreuz, P. C. *et al.* Results after microfracture of full-thickness chondral defects in different compartments in the knee. *Osteoarthr. Cartil.* **14,** 1119–1125 (2006).
7. Schnabel, M. *et al.* Dedifferentiation-associated changes in morphology and gene expression in primary human articular chondrocytes in cell culture. *Osteoarthr. Cartil.* **10,** 62–70 (2002).
8. Studer, D. *et al.* Human chondroprogenitors in alginate-collagen hybrid scaffolds produce stable cartilage *in vivo*. *J. Tissue Eng. Regen. Med.* **11,** 3014–3026 (2017).
9. Horas, U. MD; Pelinkovic, D. MD; Herr, G. DSc; Aigner, T. MD; Schnettler, R. M. Autologous Chondrocyte Implantation and Osteochondral Cylinder Transplantation in Cartilage Repair of the Knee Joint : A Prospective, Comparative Trial. *J. Bone Jt. Surg.* **85,** 185–192 (2003).
10. Sudo, K. *et al.* Mesenchymal Progenitors Able to Differentiate into Osteogenic, Chondrogenic, and/or Adipogenic Cells In Vitro Are Present in Most Primary Fibroblast-

Like Cell Populations. *Stem Cells* **25,** 1610–1617 (2007).

11. Pittenger, M. F. *et al.* Multilineage potential of adult human mesenchymal stem cells. *Science* **284,** 143–7 (1999).

12. Scotti, C. *et al.* Recapitulation of endochondral bone formation using human adult mesenchymal stem cells as a paradigm for developmental engineering. *Proc. Natl. Acad. Sci. U. S. A.* **107,** 7251–6 (2010).

13. Farrell, E. *et al.* In-vivo generation of bone via endochondral ossification by in-vitro chondrogenic priming of adult human and rat mesenchymal stem cells. *BMC Musculoskelet. Disord.* **12,** 31 (2011).

14. Farrell, M. J. *et al.* Functional properties of bone marrow-derived MSC-based engineered cartilage are unstable with very long-term in vitro culture. *J. Biomech.* **47,** 2173–82 (2014).

15. Mueller, M. B. & Tuan, R. S. Functional characterization of hypertrophy in chondrogenesis of human mesenchymal stem cells. *Arthritis Rheum.* **58,** 1377–88 (2008).

16. Fosang, A. J., Last, K., Knäuper, V., Murphy, G. & Neame, P. J. Degradation of cartilage aggrecan by collagenase-3 (MMP-13). *FEBS Lett.* **380,** 17–20 (1996).

17. Mitchell, P. G. *et al.* Cloning, expression, and type II collagenolytic activity of matrix metalloproteinase-13 from human osteoarthritic cartilage. *J. Clin. Invest.* **97,** 761–768 (1996).

18. Zheng, Q. *et al.* Type X collagen gene regulation by Runx2 contributes directly to its hypertrophic chondrocyte-specific expression in vivo. *J. Cell Biol.* **162,** 833–42 (2003).

19. Li, F. *et al.* Runx2 Contributes to Murine Col10a1 Gene Regulation Through Direct Interaction With Its Cis-Enhancer. doi:10.1002/jbmr.504

20. Wang, X. *et al.* Regulation of MMP-13 expression by RUNX2 and FGF2 in osteoarthritic cartilage. *Osteoarthr. Cartil.* **12,** 963–73 (2004).

21. Nishimura, R. *et al.* Osterix regulates calcification and degradation of chondrogenic matrices through matrix metalloproteinase 13 (MMP13) expression in association with transcription factor Runx2 during endochondral ossification. *J. Biol. Chem.* **287,** 33179–90 (2012).

22. Yoshida, C. A. *et al.* Runx2 and Runx3 are essential for chondrocyte maturation, and Runx2 regulates limb growth through induction of Indian hedgehog. *Genes Dev.* **18,** 952–63 (2004).

23. Zelzer, E. *et al.* Tissue specific regulation of VEGF expression during bone development requires Cbfa1/Runx2. *Mech. Dev.* **106,** 97–106 (2001).

24. Sun, X., Wei, L., Chen, Q. & Terek, R. M. HDAC4 represses vascular endothelial growth factor expression in chondrosarcoma by modulating RUNX2 activity. *J. Biol. Chem.* **284,** 21881–90 (2009).

25. Johnstone, B., Hering, T. M., Caplan, a I., Goldberg, V. M. & Yoo, J. U. In vitro chondrogenesis of bone marrow-derived mesenchymal progenitor cells. *Exp. Cell Res.* **238,** 265–72 (1998).

26. Bian, L. *et al.* Enhanced MSC chondrogenesis following delivery of TGF-β3 from alginate microspheres within hyaluronic acid hydrogels in vitro and in vivo. *Biomaterials* **32,** 6425–34 (2011).

27. Worster, A. A. *et al.* Chondrocytic differentiation of mesenchymal stem cells sequentially exposed to transforming growth factor-β1 in monolayer and insulin-like growth factor-I in a three-dimensional matrix. *J. Orthop. Res.* **19,** 738–749 (2001).

28. Schmitt, B. *et al.* BMP2 initiates chondrogenic lineage development of adult human mesenchymal stem cells in high-density culture. *Differentiation* **71,** 567–577 (2003).

29. Sekiya, I., Colter, D. C. & Prockop, D. J. BMP-6 Enhances Chondrogenesis in a Subpopulation of Human Marrow Stromal Cells. *Biochem. Biophys. Res. Commun.* **284,** 411–418 (2001).

30. Longobardi, L. *et al.* Effect of IGF-I in the Chondrogenesis of Bone Marrow Mesenchymal Stem Cells in the Presence or Absence of TGF- □ Signaling. **21,** 626–636 (2006).

31. Lee, K., Silva, E. A. & Mooney, D. J. Growth factor delivery-based tissue engineering: general approaches and a review of recent developments. *J. R. Soc. Interface* **8,** 153–70 (2011).

32. Matsunobu, T. *et al.* Critical roles of the TGF-β type I receptor ALK5 in perichondrial formation and function, cartilage integrity, and osteoblast differentiation during growth plate development. *Dev. Biol.* **332,** 325–338 (2009).

33. van den Bosch, M. H. *et al.* Canonical Wnt signaling skews TGF-β signaling in chondrocytes towards signaling via ALK1 and Smad 1/5/8. *Cell. Signal.* **26,** 951–958 (2014).

34. Fischer, J., Dickhut, A., Rickert, M. & Richter, W. Human articular chondrocytes secrete parathyroid hormone-related protein and inhibit hypertrophy of mesenchymal stem cells in coculture during chondrogenesis. *Arthritis Rheum.* **62,** 2696–2706 (2010).

35. Li, T.-F. *et al.* Parathyroid hormone-related peptide (PTHrP) inhibits Runx2 expression through the PKA signaling pathway. *Exp. Cell Res.* **299,** 128–136 (2004).

36. Weiss, S., Hennig, T., Bock, R., Steck, E. & Richter, W. Impact of growth factors and PTHrP on early and late chondrogenic differentiation of human mesenchymal stem cells. *J. Cell. Physiol.* **223,** n/a-n/a (2009).

37. Inada, M. *et al.* Maturational disturbance of chondrocytes inCbfa1-deficient mice. *Dev. Dyn.* **214,** 279–290 (1999).

38. Kim, I. S., Otto, F., Zabel, B. & Mundlos, S. Regulation of chondrocyte differentiation by Cbfa1. *Mech. Dev.* **80,** 159–70 (1999).

39. Stricker, S., Fundele, R., Vortkamp, A. & Mundlos, S. Role of Runx Genes in Chondrocyte Differentiation. *Dev. Biol.* **245,** 95–108 (2002).

40. Atsumi, T., Miwa, Y., Kimata, K. & Ikawa, Y. A chondrogenic cell line derived from a differentiating culture of AT805 teratocarcinoma cells. *Cell Differ. Dev.* **30,** 109–16 (1990).

41. Shukunami, C. *et al.* Chondrogenic differentiation of clonal mouse embryonic cell line ATDC5 in vitro: differentiation-dependent gene expression of parathyroid hormone (PTH)/PTH-related peptide receptor. *J. Cell Biol.* **133,** 457–68 (1996).

42. Shukunami, C. *et al.* Cellular hypertrophy and calcification of embryonal carcinoma-derived chondrogenic cell line ATDC5 in vitro. *J. Bone Miner. Res.* **12,** 1174–88 (1997).

43. Meerbrey, K. L. *et al.* The pINDUCER lentiviral toolkit for inducible RNA interference in vitro and in vivo. *Proc. Natl. Acad. Sci. U. S. A.* **108,** 3665–70 (2011).

44. Carrion, B. *et al.* The Synergistic Effects of Matrix Stiffness and Composition on the Response of Chondroprogenitor Cells in a 3D Precondensation Microenvironment. *Adv. Healthc. Mater*. (2016). doi:10.1002/adhm.201501017

45. Kim, Y. J., Sah, R. L., Doong, J. Y. & Grodzinsky, A. J. Fluorometric assay of DNA in cartilage explants using Hoechst 33258. *Anal. Biochem.* **174,** 168–76 (1988).

46. Zhai, Z., Yao, Y., Wang, Y., Ohgishi, M. & Fukui, T. Importance of Suitable Reference Gene Selection for Quantitative RT-PCR during ATDC5 Cells Chondrocyte Differentiation. *PLoS One* **8,** e64786 (2013).

47. Murtaugh, L. C., Chyung, J. H. & Lassar, A. B. Sonic hedgehog promotes somitic chondrogenesis by altering the cellular response to BMP signaling. *Genes Dev.* **13,** 225–37 (1999).

48. Murtaugh, L. C., Zeng, L., Chyung, J. H. & Lassar, A. B. The chick transcriptional repressor Nkx3.2 acts downstream of Shh to promote BMP-dependent axial chondrogenesis. *Dev. Cell* **1,** 411–22 (2001).

49. Marcelle, C., Ahlgren, S. & Bronner-Fraser, M. In Vivo Regulation of Somite Differentiation and Proliferation by Sonic Hedgehog. *Dev. Biol.* **214,** 277–287 (1999).

50. Dexheimer, V., Frank, S. & Richter, W. Proliferation as a requirement for in vitro chondrogenesis of human mesenchymal stem cells. *Stem Cells Dev.* **21,** 2160–9 (2012).

51. Akiyama, H. *et al.* Positive and negative regulation of chondrogenesis by splice variants of PEBP2?A/CBF?1 in clonal mouse EC cells, ATDC5. *J. Cell. Physiol.* **181,** 169–178 (1999).

52. Correa, D. *et al.* Zfp521 is a target gene and key effector of parathyroid hormone-related peptide signaling in growth plate chondrocytes. *Dev. Cell* **19,** 533–46 (2010).

53. Komori, T. *et al.* Targeted disruption of Cbfa1 results in a complete lack of bone formation owing to maturational arrest of osteoblasts. *Cell* **89,** 755–64 (1997).

54. Otto, F. *et al.* Cbfa1, a candidate gene for cleidocranial dysplasia syndrome, is essential for osteoblast differentiation and bone development. *Cell* **89,** 765–771 (1997).

55. Komori, T. Runx2, A multifunctional transcription factor in skeletal development. *J. Cell. Biochem.* **87,** 1–8 (2002).

56. Lengner, C. J. *et al.* Nkx3.2-mediated repression of Runx2 promotes chondrogenic differentiation. *J. Biol. Chem.* **280,** 15872–9 (2005).

57. Tchetina, E., Mwale, F. & Poole, A. R. Distinct phases of coordinated early and late gene expression in growth plate chondrocytes in relationship to cell proliferation, matrix assembly, remodeling, and cell differentiation. *J. Bone Miner. Res.* **18,** 844–51 (2003).

58. Liao, L. *et al.* Deletion of Runx2 in Articular Chondrocytes Decelerates the Progression of DMM-Induced Osteoarthritis in Adult Mice. *Sci. Rep.* **7,** 2371 (2017).

59. Kimura, A. *et al.* Runx1 and Runx2 cooperate during sternal morphogenesis. *Development* **137,** 1159–1167 (2010).

60. Lee, K. S. *et al.* Runx2 is a common target of transforming growth factor beta1 and bone morphogenetic protein 2, and cooperation between Runx2 and Smad5 induces osteoblast-specific gene expression in the pluripotent mesenchymal precursor cell line C2C12. *Mol. Cell. Biol.* **20,** 8783–92 (2000).

Chapter 3 Phosphate Regulates Chondrogenesis in a Biphasic and Maturation-dependent Manner

This chapter was published in *Differentiation* in 2017 [95]

3.1 Introduction

Understanding the factors regulating chondrogenesis and endochondral ossification is important to treating developmental disorders and the cartilaginous diseases, as well as improving stem cell-based cartilage tissue regeneration. Dysfunction in chondrocyte proliferation can lead to developmental issues, such as achondroplasia[1] and hypochondroplasia[2]. Hypertrophic differentiation of chondrocytes, a process that occurs normally during endochondral ossification, is associated with pathogenic changes in osteoarthritic articular cartilage[3–5]. Mesenchymal stem cells (MSCs) also express hypertrophic markers after chondrogenic induction *in vitro*[6,7] and *in vivo*[8], hindering their clinical application for cartilage tissue regeneration.

One potent factor that mediates cell fate in chondrocytic cells is inorganic phosphate (Pi). Studies in ATDC5[9–11], primary growth plate[12], and limb bud cells[13] have established that Pi in the range of 2-4mM upregulates collagen type X expression and apoptosis in mature chondrocytes, thus, inducing terminal differentiation. The role of Pi as a signaling molecule has also been demonstrated in several other cell types[14–18], including osteochondral progenitor cells in which it induces osteogenic differentiation[14,15]. Furthermore, many of these cell-mediated activities are regulated by other exogenous cues, such as growth factors[19–21] and matrix composition[13].

The response to Pi is orchestrated by the activity of phosphatases, such as alkaline phosphatase (ALP)[22–24], the availability of pyrophosphate (PPi)[25,26], and activity of sodium-

dependent phosphate transporters in skeletal[19,27,28] and non-skeletal systems[29,30]. ALP cleaves PPi to release Pi[31], and ALP expression in the growth plate progressively increases from being hardly detectable in the proliferative zone to higher in the maturing zone, and highest in the hypertrophic zones[32]. Deficiency of ALP activity causes hypophosphatasia, which is a skeletal disease associated with diminished or absent hypertrophic zones in the growth plate[33]. The expression profile of sodium-dependent phosphate cotransporter 1 (PiT-1) has been found to be variable during endochondral ossification. *In vitro*, expression levels were found to be highest during the early stages of chondrogenesis in the CFK2 chondroprogenitor cell line[34] and during the proliferative and the early phase of hypertrophy in ATDC5 cells[28,35]. *In vivo*, the expression profile of PiT-1 has been variable depending on species[36]. The effects of Pi during terminal differentiation require the activity of PiT-1[19,27,28,37], as inhibition of its activity negates Pi induced apoptosis during terminal differentiation[37].

Although ALP activity is highly upregulated in hypertrophic and terminally differentiated chondrocytes during endochondral ossification[32], Pi is present in the resting and proliferative zones of the growth plate[38]. However, few studies have investigated whether chondrogenic differentiation or early events in the endochondral ossification pathway are regulated by Pi. Kimata *et al*. demonstrated that Pi treatment upregulated cell proliferation through ERK1/2 mediated cyclin D1 expression in the ATDC5 cell line and primary chondrocytes[28]. Wang *et al*. also showed that transient Pi treatment upregulated collagen type II gene expression[34]. Taken together with the previously reported expression profile of PiT-1 and activity of ALP, these studies suggest that Pi plays a direct regulatory role in early chondrogenic differentiation and proliferation during endochondral ossification.

To elucidate the role of phosphate in early chondrogenic events, we used ATDC5 cells in 2D and 3D cultures. This cell line, established by Atsumi *et al*. from the mouse teratocarcinoma cells AT805, recapitulate the phases of endochondral ossification, from chondrogenic commitment to hypertrophic differentiation, with the addition of insulin[39–41]. In these cells, chondrogenic maturation and matrix mineralization occur on an accelerated timescale if given an exogenous source of phosphate[10,11]. Since ALP activity has also been shown to change as chondrocytes differentiate and mature[32,42], we used β-glycerophosphate (βGP) as our phosphate source to ensure cells control the release of phosphate. Although 10mM βGP is considered a supraphysiologic concentration of organic phosphate for *in vitro* studies[43], it was found in this study that the maximum Pi concentration in the media using this level of βGP is 4mM, the concentration employed in many previous mechanistic studies[9,28,34]. So that the Ca × Pi never reaches levels that lead to dystrophic precipitation of $CaPO_4$, calcium concentration was maintained at 1.3mM[30,44]. Using this media formulation, we found that the response of chondroprogenitor cells was regulated by Pi availability on a per cell basis (Pi abundance). Specifically, moderate Pi abundance upregulates markers of chondrogenesis whereas high abundance levels inhibit chondrogenesis and stimulate rapid matrix mineralization. We also show that this biphasic response to Pi concentration is mediated by ALP activity and cellular uptake of Pi and is dependent on the maturation stage of chondrocytes. Finally, delaying the addition of exogenous phosphate to ATDC5 cells in 3D cultures upregulates the expression of hypertrophic markers and accelerates terminal differentiation without dystrophic mineral formation, demonstrating that this culture system may serve as a rapid and physiologic model of endochondral ossification.

3.2 Methods

3.2.1 Cell culture

ATDC5 cells (Sigma) were maintained in DMEM/F12 (Life Technologies) supplemented with 5% FBS (Life Technologies) and 1% Antibiotic-Antimycotic (Life Technologies). Chondrogenesis of ATDC5 cells was induced with chondrogenic differentiation medium (ITS+) consisting of the growth medium supplemented with 1% ITS+ Premix (Corning) and 50 µg/ml ascorbate acid-2-phosphate (Sigma). Co-treatment medium (ITS+/βGP) consists of ITS+ medium supplemented with 10 mM β-glycerophosphate (Sigma). Non-chondrogenic mineralizing medium (βGP) consists of growth medium supplemented with 10mM βGP. Calcium concentration was maintained at 1.3mM.

3.2.2 Monolayer (2D) culture

Four days prior to chondrogenic induction, cells were seeded at the density of 6000 cells/cm^2 in multiple well plates. When cells reached 100% confluence (D0), differentiation was initiated by replacing the growth medium with differentiation medium. Cultures were fed with 2ml medium every other day and maintained for 21 days.

3.2.3 Pellet (3D) culture

Four days prior to chondrogenic induction, cells were seeded at the density of 6000 cells/cm^2. When cells reached 100% confluence (D0), they were trypsinized and centrifuged into pellets containing 2.5×10^5 cells in round-bottomed polypropylene 96-well-plate. Cultures were fed with 200µl medium every other day. Pellet cultures were maintained for 21 days with differentiation medium. In delayed treatment, pellets were switched to ITS+/βGP medium after 7 or 14 days in ITS+ medium.

3.2.4 Biochemical analysis

Cartilage-specific matrix production was measured by the 1,9-dimethylmethylene blue (DMMB) assay as previously described [45]. Both monolayer cell tissues and pellets were digested with 1 mg/ml proteinase K in 0.1M ammonium acetate at 50°C for 16 hours. Digested samples

were mixed with DMMB dye (pH 1.5) at a ratio of 1:20, and the GAG content of the samples were determined by comparing the ratio of 525 nm to 595 nm readings to the standard curve derived from shark chondroitin sulfate. Measured GAG content of each sample was normalized by its DNA content using Hoechst 33258 dye (Sigma) as previously described [46]. To measure mineral content of each sample, insoluble residues from the proteinase K digestion were collected and hydrolyzed by with 10% (w/w) acetic acid for 48 hours at 40°C. Hydrolyzed solution was added to Arsenazo III dye (Pointe Scientific) at ratio of 1:15, and the absorbance was read at 650 and 500 nm. The mineral content was calculated by comparing the ratio of these two absorbance readings to a standard curve created from calcium chloride.

3.2.5 Gene expression

Total RNA of each sample was extracted using TRI Reagent® RT (Molecular Research Center). For pellet culture, five pellets were combined and homogenized in the same reagent using the Micro Tube Homogenizer. Equal amounts of extracted RNA were reverse-transcribed into cDNA using High-Capacity cDNA Reverse Transcription Kit (Life Technologies). Synthesized cDNA was amplified using SYBR® Green PCR Master Mix (Life Technologies) on Applied Biosystems® 7500 Fast platform. The mean cycle threshold of the housekeeping genes ($\overline{Ct}_{hk}$) *Hprt* and *Ppia*[47] were used to calculate the fold change in transcript levels compared to day 0 samples using the $\Delta\Delta Ct$ method. Relative expression levels were calculated as $x = 2^{-\Delta\Delta Ct}$, in which $\Delta\Delta Ct = \Delta E - \Delta C$, $\Delta E = Ct_{exp} - \overline{Ct}_{hk}$ at the time-point of interest, and $\Delta C = Ct_{exp} - \overline{Ct}_{hk}$ at day 0. The forward and reverse primer sequences are listed in **Table 3-1**.

Table 3-2. The sequences of primers used

Gene		Primer Sequences (5'→3')		Primer Sequences (5'→3')
Acan	Forward	CGCCACTTTCATGACCGAGA	Reverse	CAAATTGCAGAGAGTGTCCGT
Col2a1	Forward	ACGAGGCAGACAGTACCTTG	Reverse	AGTAGTCTCCGCTCTTCCACT
Col10a1	Forward	CCAAACGCCCACAGGCATAA	Reverse	TGCCTTGTTCTCCTCTTACTGG
Hprt	Forward	CTGGTGAAAAGGACCTCTCGAA	Reverse	CTGAAGTACTCATTATAGTCAAGGGCAT
Ppia	Forward	CGCGTCTCCTTCGAGCTGTTTG	Reverse	TGTAAAGTCACCACCCTGGCACAT
Sox9	Forward	CGGAACAGACTCACATCTCTCC	Reverse	GCTTGCACGTCGGTTTTGG
Runx2	Forward	CCACGGCCCTCCCTGAACTCT	Reverse	ACTGGCGGGGTGTAGGTAAAGGTG
Ctnnb1	Forward	CACAGCTCCTTCCCTGAGTG	Reverse	CTGCCCGTCAATATCAGCTACT
Axin2	Forward	AAGCCCCATAGTGCCCAAAG	Reverse	GGGTCCTGGGTAAATGGGTG
Slc20a1	Forward	GGAACGGCTTGATAGATGTGG	Reverse	GCAGAACCAAACATAGCACTGAC
Slc20a2	Forward	CCGTCCAGTGGCTTCACTAT	Reverse	AGTCACGAACCAGGCAACAA
Osteopontin	Forward	AGCAAGAAACTCTTCCAAGCAA	Reverse	GTGAGATTCGTCAGATTCATCCG
Osteocalcin	Forward	GCCCTGAGTCTGACAAAGGTA	Reverse	GGTGATGGCCAAGACTAAGG

3.2.6 Histological analysis

Monolayer cultures were washed with PBS, and fixed in 70% ethanol at 4℃ for 16 hours. Differentiated pellets were washed with PBS, and fixed in 5% buffered formalin at 4℃ for 16 hours. Fixed pellets were washed with 70% ethanol, embedded in paraffin wax, and then 7 μm sections were taken. Proteoglycan accumulation in monolayer tissues and pellets was evaluated by staining the sectioned tissue with 3% Alcian blue dye (Poly Scientific), and calcium deposition was visualized by staining with 2% Alizarin red S dye (pH 4.3).

3.2.7 Alkaline Phosphatase Activity Analysis

Alkaline phosphatase activity was measured by the QuantiChrom™ Alkaline Phosphatase Assay Kit (BioAssay Systems). Both monolayer cell tissues and pellets were washed with PBS, then lyzed in 0.2% Triton-100 solution for 30 minutes at room temperature. Upon addition of lysis buffer, pellet samples were ground with a pestle to break apart the tissue. Alkaline phosphatase activity was determined by taking the ratio of the difference between 405 nm readings taken immediately after adding the assay buffer (t=0) and after 4 minutes on a plate reader to the difference between the 405 nm readings of the calibrator (Tartrazine) and deionized water using the equation from the manufacturer's protocol.

3.2.8 Phosphate Concentration Analysis

Concentration of phosphate in the media was determined using the QuantiChrom™ Phosphate Assay Kit (BioAssay Systems). Media from each test condition was harvested and diluted 1:20 with water prior to the addition of assay reagent. Phosphate concentration was determined by reading optical density at 620 nm, followed by calculation using equations given in the manufacturer's protocol.

3.2.9 Statistical analysis

Statistical analysis was performed using GraphPad Prism software. All comparisons over multiple time points were analyzed by two-way ANOVA with Tukey's multiple comparison method. Comparisons in experiment at a single time point were analyzed by one-way ANOVA followed by Sidak correction. Significant difference is indicated by * $P<0.05$, ** $P<0.01$, ***$P<0.001$, ****$P<0.0001$. All error bars indicate the standard error of the mean (s.e.m.).

3.3 Results

3.3.1 The influence of βGP supplementation on early chondrogenesis in 2D and 3D cultures

To better understand the individual and synergistic effects of βGP on early chondrogenesis, we monitored the gene expression of early chondrogenic markers, *Acan* and *Col2a1* gene expression as well as the amount of cartilaginous matrix produced by ATDC5 cells in both high density monolayer (2D) and pellet (3D) cultures. Both culture types were treated with ITS+, βGP, or ITS+/βGP for 14 days. Notably, the expression of genes and matrix components were 2-10 times higher in 3D cultures compared to 2D. Nonetheless, both 2D and 3D cultures exhibited a similar trend of chondrogenic gene expression and matrix accumulation when they were treated with ITS+ or βGP individually. Chondrogenesis and proliferation (not shown) of chondrogenic cells occurs within the first 7 days of culture in ITS+ medium in 2D and 3D. Upregulation of *Acan* and *Col2a1* gene expression (Fig 3-1a) and production of sGAG-rich matrix (Fig 3-1b & 1d) in

both monolayer and pellet cultures treated with ITS+ confirmed early chondrogenesis. In the absence of ITS+, cells cultured in medium supplemented with 10mM βGP did not express chondrogenic markers in either culture type (Fig 3-1a, b & d) and induced rapid mineralization of the matrix (Fig 3-1c & e). The response to combined ITS+/βGP treatment, however, was dissimilar in the two systems. In monolayer culture, cells differentiated with ITS+/βGP showed significantly higher mRNA levels of *Acan* and *Col2a1* (Fig 3-1a) as well as a 1.6-fold increase in accumulation of an sGAG-rich matrix (Fig 3-1b & 1d) compared the ITS+ alone group. Mineral also formed in these cultures, but did not appear to be associated with nodules of chondrogenic cells. Conversely, the addition of βGP to ITS+ treated pellet cultures suppressed expression of *Acan* and *Col2a1* genes and matrix accumulation and stimulated mineralization.

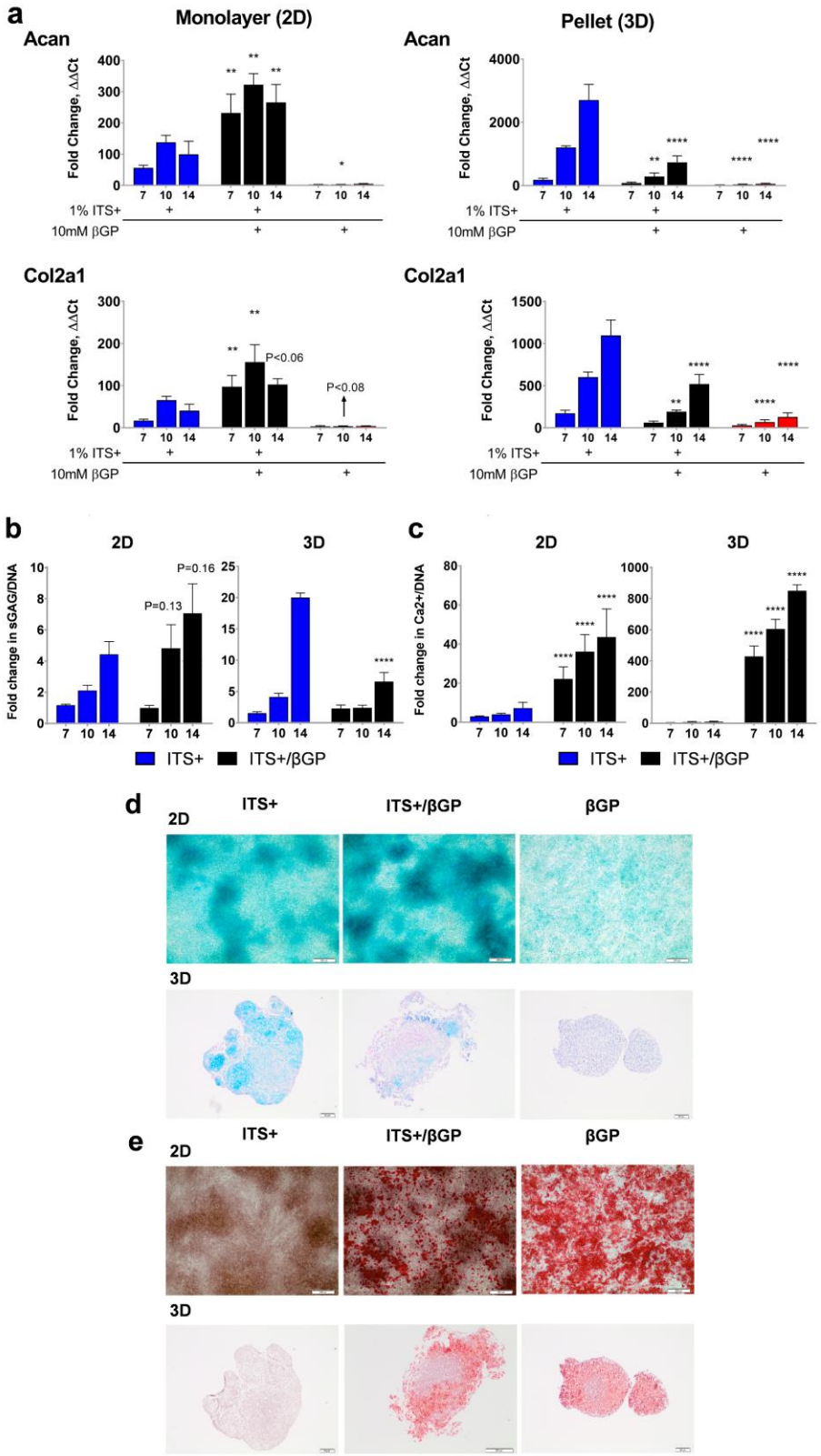

Figure 3-1. Differential effects of ITS+/βGP co-treatment on early chondrogenesis of ATDC5 cells in 2D and 3D cultures. (a) Quantification of mRNA expression (relative to day 0 and the housekeeping genes *Hprt* and *Ppia*) of early chondrogenic markers (*Acan* and *Col2a1*) in monolayer (2D) and pellet (3D) cultures over 14 days of

differentiation. Fold change (relative to day 0) in sGAG accumulation (b) and calcium deposition (c) normalized to DNA content over 14 days of differentiation in 2D and 3D cultures treated with ITS+ or ITS+/βGP. (d) Alcian blue staining of 2D and 3D cultures at day 14 to show accumulation of sGAG-rich matrix. 3D cultures stained also with nuclear fast red counterstain to show cell structure. (e) Alizarin Red staining of 2D and 3D cultures at day 14 to show mineral content in each sample. Data represented as mean ± s.e.m. Significant difference from the ITS+ group at the same time point ($n \geq 8$) is indicated by * $P<0.05$, ** $P<0.01$, ***$P<0.001$, ****$P<0.0001$ by two-way ANOVA with Tukey's multiple comparison method. NS, not significant.

3.3.2 The culture-dependent effect of ITS+/βGP on early chondrogenesis is regulated by ALP activity and Pi abundance.

To determine if the effects of βGP supplementation on ATDC5 cells is controlled by cell-mediated regulation of Pi availability, we measured the ALP activity of the cells and subsequent Pi concentration in the media of both systems during early chondrogenesis (days 1, 3, 5, and 7). The ALP activity of cells in monolayer cultures (Fig 3-2a) induced with ITS+ alone or ITS+/βGP increased steadily over the first 7 days. In comparison, cells treated with βGP only had a higher level of ALP activity, which peaked at day 3 and was maintained until day 5. By day 7, ALP activity was similar in all 2D culture conditions. In contrast to 2D cultures, ALP activity was highest in cells on day 1 in 3D–ITS+ cultures and then rapidly decreased as differentiation proceeded during the first week. When pellets were treated with βGP or co-treated with ITS+/βGP, ALP activity was maintained at this high level through day 3 and then decreased to levels similar to the 3D–ITS+ control group (Fig 3-2d).

The basal concentration of Pi in the medium of 2D and 3D ITS+-treated cultures was 1mM (the concentration in DMEM/F12). With βGP treatment, Pi concentration in the medium increased to 4mM on average in 2D cultures from days 3-7 (Fig 3-2b) regardless of ALP activity. Slightly lower Pi levels (~3.6mM on average) were found in 3D cultures treated with βGP or ITS+/βGP (Fig 3-2e).

We further estimated the Pi availability on a per cell basis by normalizing the total Pi content in the medium by total DNA content (Fig 3-2c & f), which we are defining as Pi abundance. Three levels of Pi abundance were observed and were found to be dependent on culture condition

(2D vs. 3D) and ITS+ and/or βGP supplementation: low abundance (Pi/DNA < 10 ng/µg) was found in 2D–ITS+ cultures; moderate abundance (Pi/DNA=25.3 – 32.3 ng/µg) was found in 2D–ITS+/βGP and 3D–ITS+ cultures; and high abundance (Pi/DNA > 60 ng/µg) was detected in culture conditions with the highest-level ALP activity—2D–βGP, 3D–ITS+/βGP, and 3D–βGP. As was shown in Fig. 1, groups exposed to moderate Pi abundance levels had enhanced expression of *Acan* and *Col2a1* as well as increased sGAG accumulation (Fig 3-1b & 1d) whereas high Pi abundance suppressed these markers in 3D cultures. Thus, high Pi abundance correlates with inhibition of early chondrogenesis while moderate Pi abundance correlates with enhanced chondrogenic differentiation.

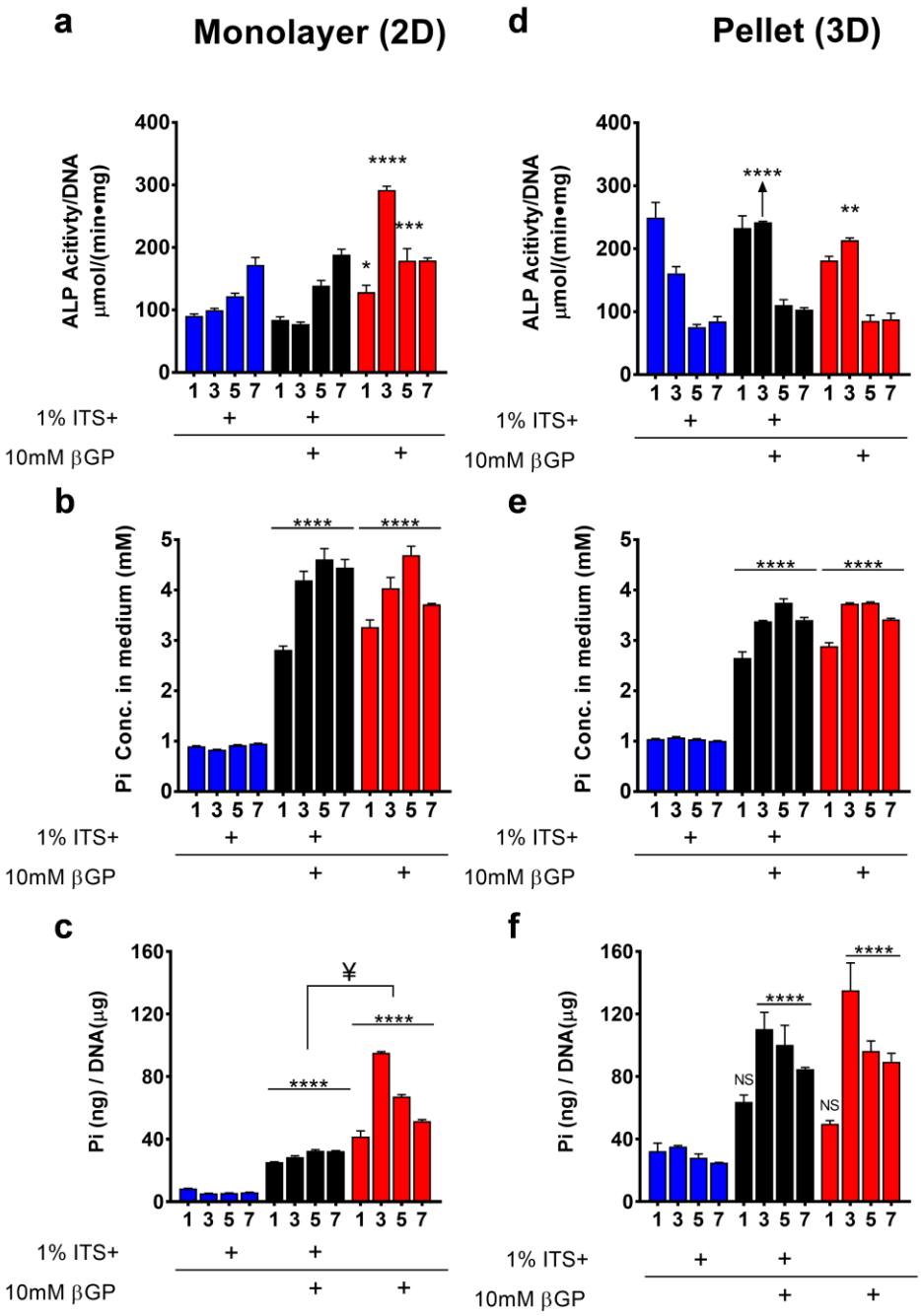

Figure 3-2. The culture-dependent effect of ITS+/βGP on early chondrogenesis is regulated by ALP activity and Pi abundance. (a & d) Normalized ALP activity, (b & e) Pi concentration (mM) present in the medium, and (c & f) Pi availability on a per cell basis during the first seven days of differentiation in 2D and 3D cultures treated with ITS+, ITS+/βGP, or βGP (n=3). Data represented as mean ± s.e.m. Significant difference from the ITS+ group at the same time point is indicated by * P<0.05, ** P<0.01, ***P<0.001, ****P<0.0001 by two-way ANOVA corrected with Tukey's multiple comparison method. NS, not significant. ¥ indicates significance difference between ITS+/ βGP and βGP conditions at the same time point (P<0.0001).

To explore the possible pathways that could be involved in mediating the response to available levels of Pi to the cells, we examined the gene expression of mediators of chondrogenesis

(*Sox9*), chondrocyte hypertrophy (*Runx2*), and a known inhibitor of chondrogenesis, β-catenin (*Ctnnb1*) as well as their gene targets (*Col2a1*, *Col10a1*, and *Axin2*, respectively) before, during, and after the change in Pi abundance at day 1, day 3, and day 7. Although Pi abundance increased in response to additional βGP supplementation starting at day 3, there were not significant discrepancies in gene expression between groups with different Pi levels until day 7. The increase in Pi abundance from low to moderate (comparing 2D ITS+ to 2D ITS+/βGP) correlated with higher mRNA levels of *Sox9* and its gene target *Col2a1*, as well as *Col10a1*. However, no significant difference in the expression of *Runx2*, *Ctnnb1*, or *Axin2* was observed (Fig 3-3a). The shift from moderate to high Pi abundance (comparison of 3D–ITS+ to 3D–ITS+/βGP) resulted in elevated *Col10a1* gene expression with no associated change in the expression levels of *Runx2*. High Pi abundance also reduced the level of *Col2a1* gene expression and increased the gene expression of *Ctnnb1* and its target *Axin2* (Fig 3-3b).

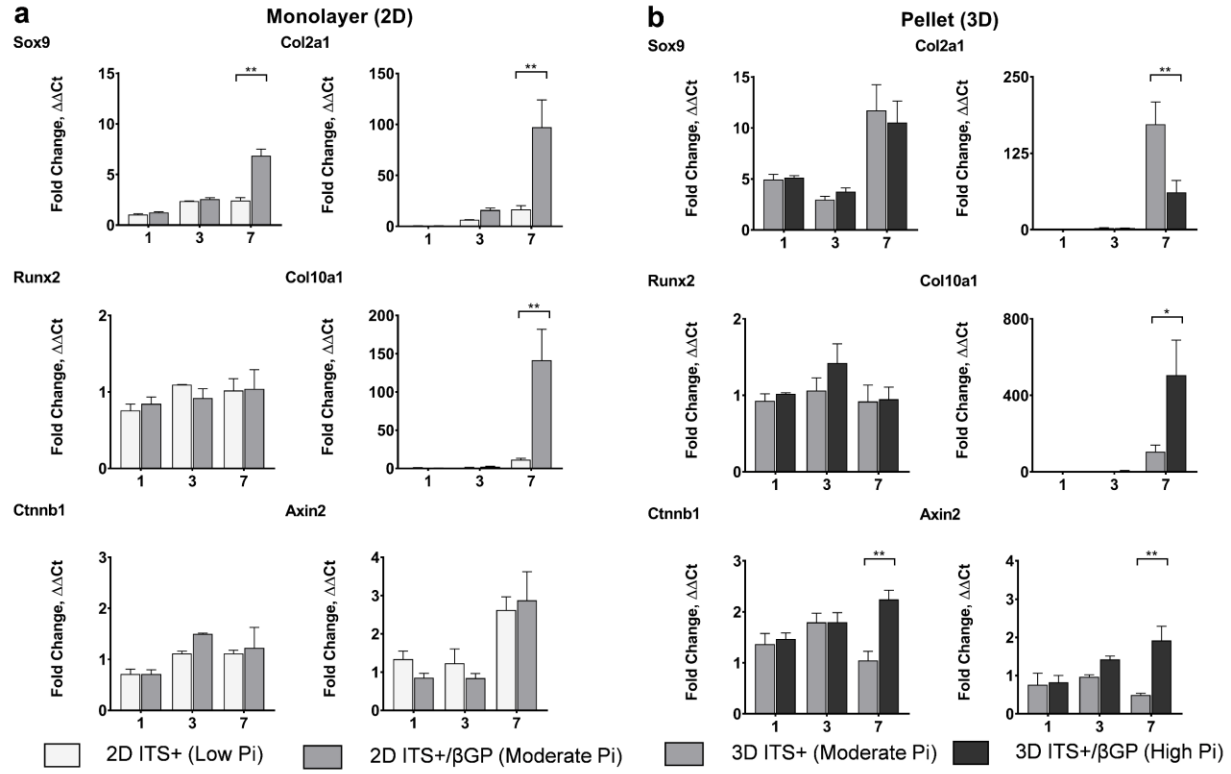

Figure 3-3. Gene expression reveals possible pathways involved in the biphasic regulation of Pi. Quantification of mRNA expression (relative to day 0 and Hprt and Ppia) of genes and downstream effectors associated with early chondrogenesis and hypertrophy in 2D (a) and 3D (b) cultures treated with ITS+ and ITS+/βGP during the first seven days of differentiation. Data represented as mean ± s.e.m. Significant difference from the ITS+ group at the same time point is indicated by * P<0.05, ** P<0.01, ***P<0.001, ****P<0.0001 by two-way ANOVA with Tukey's multiple comparisons. NS, not significant. n≥3.

3.3.3 Inhibition of ALP Activity restores early chondrogenesis in 3D

The next step was to examine if the activity of ALP and Pi uptake by ATDC5 cells played a role in the βGP-induced inhibition of early chondrogenesis in 3D cultures. ALP activity and Pi uptake were individually inhibited using levamisole and PFA, respectively. In 3D–ITS+/βGP cultures, levamisole treatment reduced the Pi abundance to Pi/DNA=48.4 ng/µg after day 3 (Fig 3-4a). This is a level slightly higher than the moderate range, but the difference was not significant. ALP inhibition in the ITS+/βGP group enhanced markers of early chondrogenesis compared to 3D–ITS+ cultures (moderate Pi abundance). There was a slight increase in *Col2a1* gene expression over ITS+ controls (Fig. 3-1b; not significant) and significantly higher sGAG expression (Fig 3-4c & d). Furthermore, levamisole treatment reduced expression of the phosphoprotein osteopontin (OPN), a marker sensitive to phosphate treatment[48]. Without the addition of βGP, levamisole treatment had no effect on chondrogenesis (data not shown). Pi abundance was reduced with treatment of PFA, but remained in the high range (Pi/DNA>64.3 ng/µg; Fig 3-4a). Accordingly, PFA treated pellets were noticeably smaller than other conditions. In these pellets, Col*2a1* expression and matrix deposition were inhibited (Fig 3-4b & c). Taken together with the response of the cells exposed to moderate Pi abundance in 2D cultures, the response of ATDC5 cells to both inhibitors in 3D indicates that phosphate uptake is required for early chondrogenesis and that a moderate level of phosphate will enhance matrix production of chondrocytes.

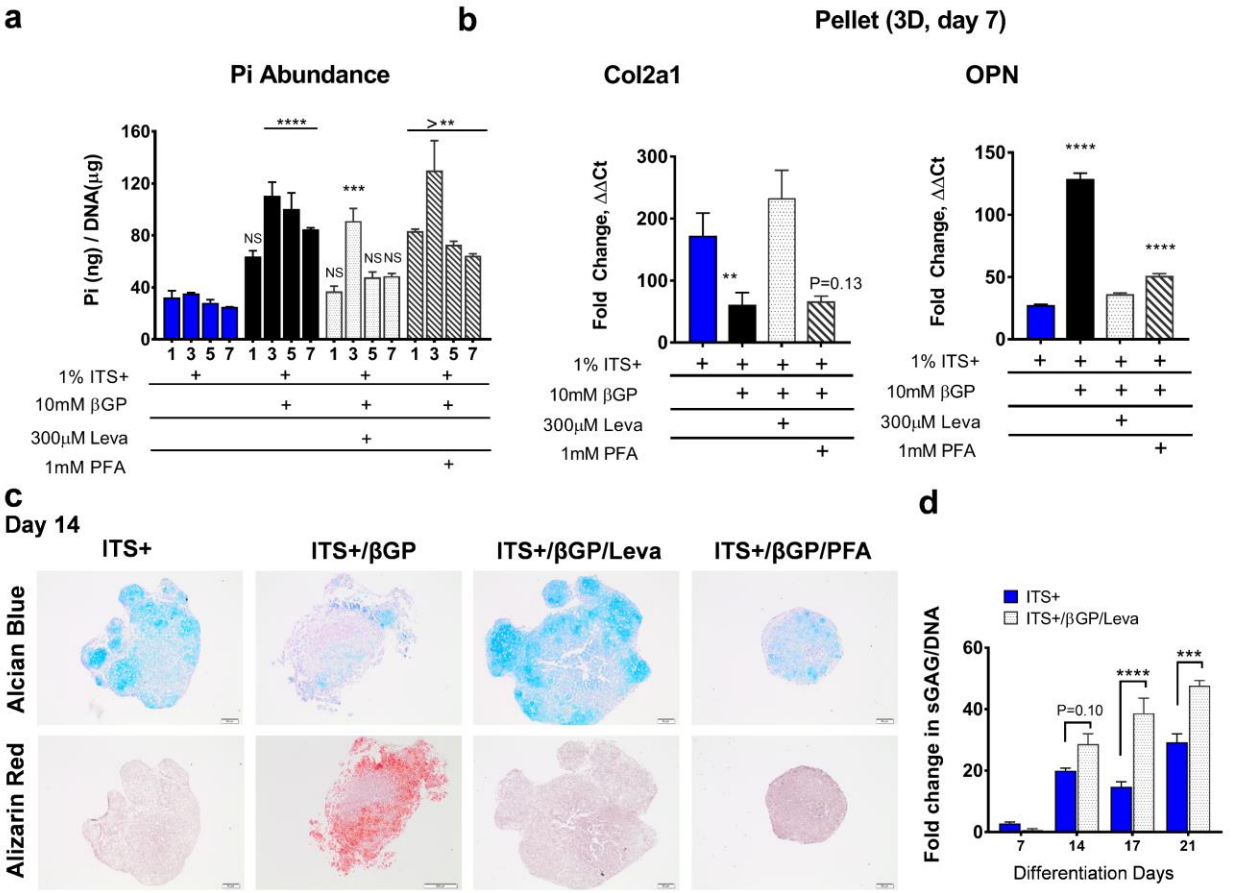

Figure 3-4. Inhibition of ALP Activity or Pi uptake restored early chondrogenesis in 3D. (a) Pi availability on a per cell basis in 3D culture treated with ITS+, ITS+/βGP, ITS+/βGP/levamisole, or ITS+/βGP/PFA during the first seven days of differentiation. (b) Quantification of mRNA expression (relative to day 0 and *Hprt* and *Ppia*) of the chondrogenic marker *Col2a1* and phosphate uptake marker *OPN* at day 7 of differentiation. (c) Alcian blue and alizarin red staining of 3D cultures treated with ITS+, ITS+/βGP, ITS+/βGP/levamisole, or ITS+/ βGP/PFA at day 14 of differentiation. Pellets stained with Alcian blue were also stained with nuclear fast red counterstain to show cell structure. (d) Fold change in sGAG accumulation normalized to DNA content (relative to day 0) over 21 days of differentiation in 3D cultures treated with ITS+ or ITS+/βGP/levamisole. Data represented as mean ± s.e.m. Significant difference from the ITS+ group at the same time point is indicated by * P<0.05, ** P<0.01, ***P<0.001, ****P<0.0001 by one-way or two-way ANOVA with Tukey's multiple comparisons. NS, not significant. n≥3.

3.3.4 Delayed βGP supplementation expedites late chondrogenesis in 3D cultures

To determine if the biphasic response to βGP continues after early chondrogenesis, βGP treatment was delayed for 7 or 14 days in pellet cultures. While Pi abundance was significantly increased in both delayed groups once βGP was added, the level remains in the moderate range (Pi/DNA<42 ng/μg; Fig 3-5a). The expression of *Acan* or *Col2a1* genes on days 14 and 21 of culture was comparable to or slightly higher than the ITS+ group (not significant; Fig 3-5c). Accordingly, the βGP-induced inhibition of sGAG production was not observed as demonstrated

by histological staining (Fig 3-5b) and quantification of sGAG production (Fig 3-5d). Instead, sGAG accumulation was increased in the 7-day delayed group 1 week after the addition of βGP. By day 21 of culture, sGAG levels in both delayed groups were equivalent to the ITS+ group.

Col10a1 gene expression was upregulated by day 21 in the 7-day delayed group over cultures treated with ITS+ alone or ITS+/βGP from day 0 (Fig 3-5c). Calcium accumulation was the same 7 days after βGP addition in both delayed groups, which was 13.5% of the amount accumulated when βGP was added from day 0 (Fig 3-5e). Notably, calcium deposition in the delayed group did not occur linearly as observed in cultures with βGP from day 0. Thus, moderate Pi abundance induces hypertrophy and mineralization in ATDC5 cells without altering their chondrogenic response.

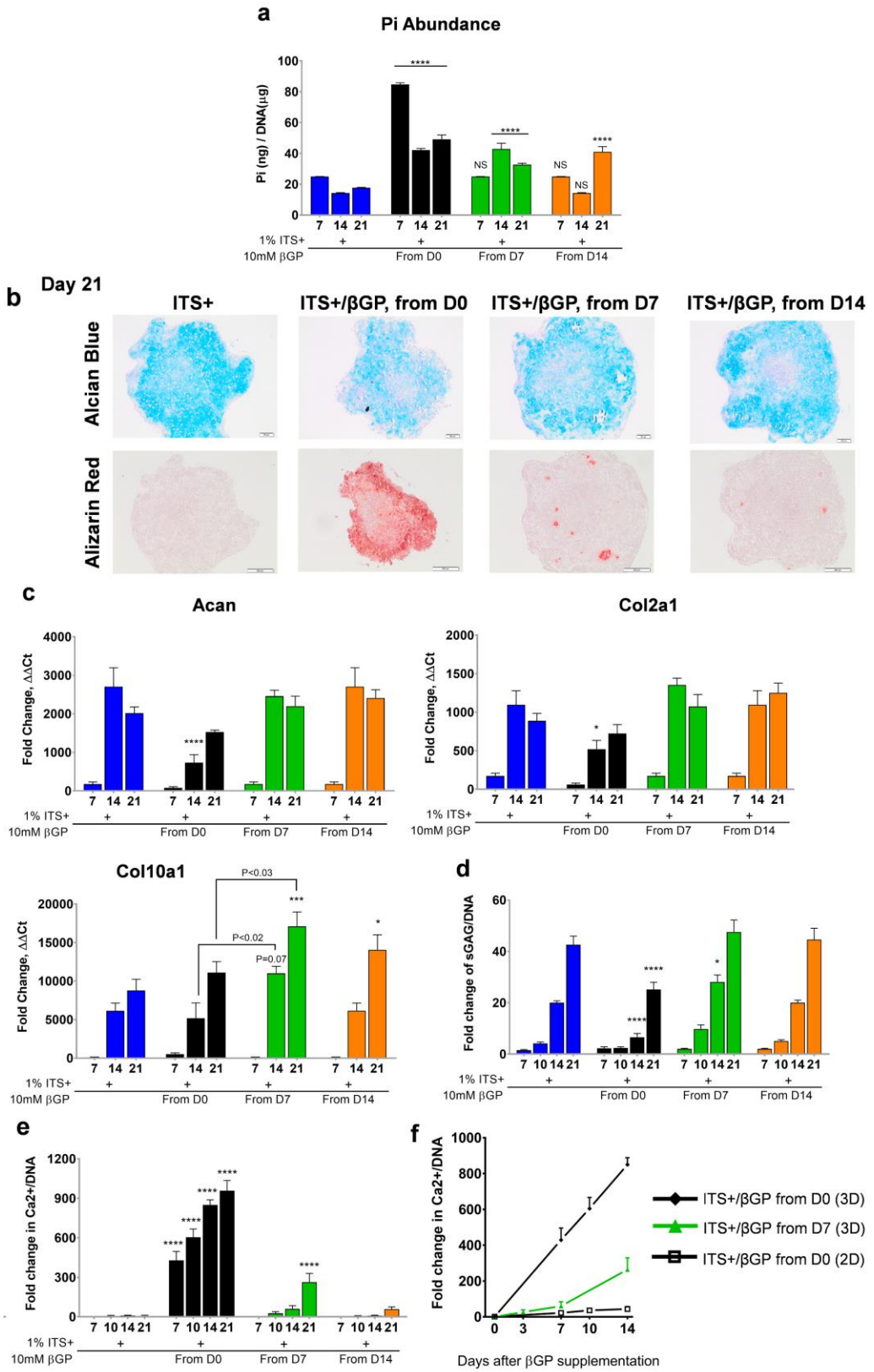

Figure 3-5. Delayed βGP supplement expedites late chondrogenesis. (a) Pi availability on a per cell basis in 3D culture treated with ITS+, and ITS+/βGP supplemented from day 0, day 7, day 14 during 21 days of differentiation. (b) Alcian blue and alizarin red staining of delayed 3D cultures at day 21. Fold changes in mRNA expression (relative

to day 0 and the housekeeping genes Hprt and Ppia) of early and late chondrogenic markers (*Acan*, *Col2a1*, and *Col10a1*) (c), normalized sGAG accumulation (d), and normalized calcium deposition (e) in delayed 3D cultures over 21 days of differentiation. (f) Comparison of fold changes in normalized calcium deposition between 7-day delayed and no delay 2D and 3D cultures after βGP supplementation. Data represented as mean ± s.e.m. Significant difference between ITS+ and other conditions at the same time point is indicated by * P<0.05, ** P<0.01, ***P<0.001, ****P<0.0001 by two-way ANOVA with Tukey's multiple comparison method. NS, not significant. n≥4.

3.4 Discussion & Conclusion

Here we demonstrate that the availability of Pi on a per cell basis and the maturation point of chondroprogenitor cells both determine their response to phosphate during endochondral ossification. Using the measure of Pi abundance, we show that there is a biphasic response to phosphate during early chondrogenesis – moderate levels enhance chondrogenesis and matrix production whereas, if the differentiating chondrocytes are exposed to high levels during early endochondral ossification, chondrogenesis is inhibited and rapid calcification ensues. The observed discrepancy in Pi abundance between 2D and 3D systems also highlights the culture-dependent ALP activity in response to βGP. It was possible to reduce Pi abundance to moderate levels by partially inhibiting ALP activity, which reversed βGP-induced suppression of chondrogenesis. Similar to 2D cultures, moderate Pi abundance increased expression of chondrogenic markers and deposition of sGAG-rich matrix in 3D cultures. After early chondrogenesis (7-10 days), the response to βGP delivery by these cells is no longer biphasic and hypertrophy makers are upregulated. Thus, the cell response to Pi is maturation-dependent.

We show that it is important to evaluate the effect of Pi on chondrogenesis by examining its availability on a per cell level. Emerging evidence has shown that Pi can function as a signaling molecule to regulate cellular functions and differentiation of MSCs[14], osteoblasts[15], and chondrocytes[9,49]. In both osteoblasts and chondrocytes, the signaling function of Pi was shown to be mediated by phosphate influx through sodium-dependent phosphate transporters[14,34]. In culture, the volume of medium and number of cells present, in addition to the concentration of Pi, would affect the Pi influx among individual cells. Taking these factors into consideration, the availability

of Pi on a per cell level is significantly different in two scenarios reported here. First, 2D and 3D culture have different ratios of medium volume to the number of cells in individual wells, resulting in culture-dependent discrepancy in Pi abundance. Second, significant proliferation occurs during the chondrogenic differentiation in both systems, changing the cell number in the culture. Thus, Pi abundance decreases as differentiation proceeds, which, as we have shown, alters cellular response. Thus, these factors should be accounted for in studies of the effects of exogenous phosphate on cell function.

The literature indicates that Pi both negatively and positively regulates early chondrogenesis[28,34,50–56]. Our results strongly suggest a biphasic model that may explain these discrepancies. For instance, recent studies that have shown that the Wnt/β-catenin pathway prevents MSCs chondrogenesis[50,51], possibly promoted by A2b adenosine receptor activity that is mediated by cellular phosphate uptake through PiT-1[52 53–55]. In accordance with these studies, we observed increased gene expression of *Ctnnb1* (β-catenin) and its target gene, *Axin2,* as well as decreased Sox9 activity, extrapolated from decreased expression of *Col2a1*, in the high Pi culture, which suggests that high Pi abundance inhibits early chondrogenesis through upregulation of β-catenin activity. The measured increase in Sox9 expression and activity in response to moderate Pi conditions in our studies agrees with the results of Wang et al., which reported upregulation of PiT-1 and Col2a1 gene and protein expression in response to short-term Pi treatment (24hr) in differentiating CFK2 cells[34]. Additionally, Kimata et al. demonstrated that 4mM Pi enhanced proliferation in early stages of chondrogenic differentiation of ATDC5 cells and primary chondroprogenitors through phosphorylation of ERK1/2[28], a pathway also involved in the upregulation of aggrecan expression[56]. To our knowledge, most literature on the signaling function of phosphate reports Pi level in the form of medium concentration. Therefore, it is difficult to

correlate previous results with the biphasic effect observed here without calculating the numbers of cells used in those studies. Future studies that monitor Pi abundance may resolve the biphasic response observed here and in the literature.

Delaying βGP supplementation in pellet culture until after the progression of early chondrogenesis prevented exposing the cells to high Pi abundance during this stage, as cells rapidly reduced their ALP activity after differentiation was initiated. This model may better reflect *in vivo* conditions, as ALP activity is detected in bone marrow chondroprogenitor cells but not in resting or proliferative chondrocytes in growth plate[32]. The moderate increase in the Pi abundance in the delayed model also led to a mineral deposition profile that resembles the physiological mineralization of cartilage matrix[57,58], unlike the linear mineral formation observed in non-delayed group. This may be due to the presence of matrix deposited during early chondrogenesis. For example, aggrecan, a high molecular weight proteoglycan, has been reported to inhibit the growth mineral crystals[59–61]. Degradation and reorganization of collagen are also important for correct mineral formation in bone[62,63]. Therefore, this model may be used to further evaluate the role of matrix accrual and modification on the response of chondroprogenitor cells to phosphate and cartilage mineralization during endochondral ossification as well as diseases, such as osteoarthritis.

Some limitations of this study need to be considered. Our analyses are based on extracellular Pi concentration in the medium, which may not directly reflect Pi uptake by the cells. It would be interesting to measure the phosphate influx into the cells to further clarify the role of Pi in regulating early chondrogenesis. Moreover, the ATDC5 cell line used in this study is derived from embryonic teratocarcinoma. While the response of this cell line has been verified in primary cells in many studies[28,64,65], additional experiments designed to investigate the role of Pi in primary chondrocytes and stem cells will help validate our findings. Furthermore, we have neglected the

contribution of other regulatory proteins, such as glycoprotein-1 (PC-1) and ankylosis protein (ANK) and phosphatases such as phosphatase orphan 1 (PHOSPHO1), that have been shown to mediate the balance of PPi/Pi in mineralizing cultures. Future studies will determine the role of these factors in mediating the biphasic response of ATDC5 cells to Pi.

3.5 Reference

1. Pannier, S. *et al.* Delayed bone age due to a dual effect of FGFR3 mutation in Achondroplasia. *Bone* **47,** 905–915 (2010).
2. Krejci, P. *et al.* Analysis of STAT1 Activation by Six FGFR3 Mutants Associated with Skeletal Dysplasia Undermines Dominant Role of STAT1 in FGFR3 Signaling in Cartilage. *PLoS One* **3,** e3961 (2008).
3. Von Der Mark, K. *et al.* Type x collagen synthesis in human osteoarthritic cartilage. indication of chondrocyte hypertrophy. *Arthritis Rheum.* **35,** 806–811 (1992).
4. Johnson, K. A., van Etten, D., Nanda, N., Graham, R. M. & Terkeltaub, R. A. Distinct transglutaminase 2-independent and transglutaminase 2-dependent pathways mediate articular chondrocyte hypertrophy. *J. Biol. Chem.* **278,** 18824–32 (2003).
5. Thouverey, C., Bechkoff, G., Pikula, S. & Buchet, R. Inorganic pyrophosphate as a regulator of hydroxyapatite or calcium pyrophosphate dihydrate mineral deposition by matrix vesicles. *Osteoarthr. Cartil.* **17,** 64–72 (2009).
6. Farrell, M. J. *et al.* Functional properties of bone marrow-derived MSC-based engineered cartilage are unstable with very long-term in vitro culture. *J. Biomech.* **47,** 2173–82 (2014).
7. Mauck, R. L., Yuan, X. & Tuan, R. S. Chondrogenic differentiation and functional maturation of bovine mesenchymal stem cells in long-term agarose culture. *Osteoarthr. Cartil.* **14,** 179–189 (2006).
8. Pelttari, K. *et al.* Premature induction of hypertrophy during in vitro chondrogenesis of human mesenchymal stem cells correlates with calcification and vascular invasion after ectopic transplantation in SCID mice. *Arthritis Rheum.* **54,** 3254–3266 (2006).
9. Magne, D. *et al.* Phosphate is a specific signal for ATDC5 chondrocyte maturation and apoptosis-associated mineralization: possible implication of apoptosis in the regulation of endochondral ossification. *J. Bone Miner. Res.* **18,** 1430–42 (2003).
10. Altaf, F. M., Hering, T. M., Kazmi, N. H., Yoo, J. U. & Johnstone, B. Ascorbate-enhanced chondrogenesis of ATDC5 cells. *Eur. Cell. Mater.* **12,** 64-9-70 (2006).
11. Newton, P. T. *et al.* Chondrogenic ATDC5 cells: an optimised model for rapid and physiological matrix mineralisation. *Int. J. Mol. Med.* **30,** 1187–93 (2012).
12. Kim, H. J., Delaney, J. D. & Kirsch, T. The role of pyrophosphate/phosphate homeostasis in terminal differentiation and apoptosis of growth plate chondrocytes. *Bone* **47,** 657–665

(2010).

13. Boskey, A. L., Stiner, D., Binderman, I. & Doty, S. B. Effects of proteoglycan modification on mineral formation in a differentiating chick limb-bud mesenchymal cell culture system. *J. Cell. Biochem.* **64,** 632–643 (1997).

14. Shih, Y.-R. V *et al.* Calcium phosphate-bearing matrices induce osteogenic differentiation of stem cells through adenosine signaling. *Proc. Natl. Acad. Sci. U. S. A.* **111,** 990–5 (2014).

15. Beck, G. Inorganic phosphate regulates multiple genes during osteoblast differentiation, including Nrf2. *Exp. Cell Res.* **288,** 288–300 (2003).

16. Rangrez, A. Y. *et al.* Inorganic Phosphate Accelerates the Migration of Vascular Smooth Muscle Cells: Evidence for the Involvement of miR-223. *PLoS One* **7,** e47807 (2012).

17. Chang, S.-H. *et al.* Elevated Inorganic Phosphate Stimulates Akt-ERK1/2-Mnk1 Signaling in Human Lung Cells. *Am. J. Respir. Cell Mol. Biol.* **35,** 528–539 (2006).

18. Spina, A. *et al.* Inorganic Phosphate as a Novel Signaling Molecule with Antiproliferative Action in MDA-MB-231 Breast Cancer Cells. *Biores. Open Access* **2,** 47–54 (2013).

19. Cecil, D. L., Rose, D. M., Terkeltaub, R. & Liu-Bryan, R. Role of interleukin-8 in PiT-1 expression and CXCR1-mediated inorganic phosphate uptake in chondrocytes. *Arthritis Rheum.* **52,** 144–54 (2005).

20. Watanabe, H., de Caestecker, M. P. & Yamada, Y. Transcriptional cross-talk between Smad, ERK1/2, and p38 mitogen-activated protein kinase pathways regulates transforming growth factor-beta-induced aggrecan gene expression in chondrogenic ATDC5 cells. *J. Biol. Chem.* **276,** 14466–73 (2001).

21. Palmer, G., Guicheux, J., Bonjour, J. P. & Caverzasio, J. Transforming growth factor-beta stimulates inorganic phosphate transport and expression of the type III phosphate transporter Glvr-1 in chondrogenic ATDC5 cells. *Endocrinology* **141,** 2236–43 (2000).

22. Bellows, C. G., Aubin, J. E. & Heersche, J. N. M. Initiation and progression of mineralization of bone nodules formed in vitro: the role of alkaline phopsphatase and organic phopshate. *Bone Miner.* **14,** 27–40 (1991).

23. Mikami, Y. *et al.* Alkaline phosphatase determines polyphosphate-induced mineralization in a cell-type independent manner. *J. Bone Miner. Metab.* **34,** 627–637 (2016).

24. An, J. *et al.* Tartrate-Resistant Acid Phosphatase Deficiency in the Predisposition to Systemic Lupus Erythematosus. *Arthritis Rheumatol.* **69,** 131–142 (2017).

25. Tenenbaum, H. C. Levamisole and inorganic pyrophosphate inhibit beta-glycerophosphate induced mineralization of bone formed in vitro. *Bone Miner.* **3,** 13–26 (1987).

26. Addison, W. N., Azari, F., Sørensen, E. S., Kaartinen, M. T. & McKee, M. D. Pyrophosphate inhibits mineralization of osteoblast cultures by binding to mineral, up-regulating osteopontin, and inhibiting alkaline phosphatase activity. *J. Biol. Chem.* **282,** 15872–83 (2007).

27. Suzuki, A. *et al.* Enhanced expression of the inorganic phosphate transporter Pit-1 is

involved in BMP-2-induced matrix mineralization in osteoblast-like cells. *J. Bone Miner. Res.* **21,** 674–83 (2006).

28. Kimata, M. *et al.* Signaling of extracellular inorganic phosphate up-regulates cyclin D1 expression in proliferating chondrocytes via the Na+/Pi cotransporter Pit-1 and Raf/MEK/ERK pathway. *Bone* **47,** 938–947 (2010).

29. Li, X., Yang, H.-Y. & Giachelli, C. M. Role of the sodium-dependent phosphate cotransporter, Pit-1, in vascular smooth muscle cell calcification. *Circ. Res.* **98,** 905–12 (2006).

30. Yang, H., Curinga, G. & Giachelli, C. M. Elevated extracellular calcium levels induce smooth muscle cell matrix mineralization in vitro. *Kidney Int.* **66,** 2293–9 (2004).

31. Murshed, M., Harmey, D., Millán, J. L., McKee, M. D. & Karsenty, G. Unique coexpression in osteoblasts of broadly expressed genes accounts for the spatial restriction of ECM mineralization to bone. *Genes Dev.* **19,** 1093–104 (2005).

32. Miao, D. & Scutt, A. Histochemical Localization of Alkaline Phosphatase Activity in Decalcified Bone and Cartilage. *J. Histochem. Cytochem.* **50,** 333–340 (2002).

33. Fedde, K. N. *et al.* Alkaline Phosphatase Knock-Out Mice Recapitulate the Metabolic and Skeletal Defects of Infantile Hypophosphatasia. *J. Bone Miner. Res.* **14,** 2015–2026 (1999).

34. Wang, D. *et al.* Alterations in the sensing and transport of phosphate and calcium by differentiating chondrocytes. *J. Biol. Chem.* **276,** 33995–4005 (2001).

35. Guicheux, J. *et al.* A novel in vitro culture system for analysis of functional role of phosphate transport in endochondral ossification. *Bone* **27,** 69–74 (2000).

36. Palmer, G., Zhao, J., Bonjour, J., Hofstetter, W. & Caverzasio, J. In vivo expression of transcripts encoding the glvr-1 phosphate transporter/retrovirus receptor during bone development. *Bone* **24,** 1–7 (1999).

37. Mansfield, K., Teixeira, C. ., Adams, C. . & Shapiro, I. . Phosphate ions mediate chondrocyte apoptosis through a plasma membrane transporter mechanism. *Bone* **28,** 1–8 (2001).

38. Kakuta, S., Golub, E. E. & Shapiro, I. M. Morphochemical analysis of phosphorus pools in calcifying cartilage. *Calcif. Tissue Int.* **37,** 293–299 (1985).

39. Atsumi, T., Miwa, Y., Kimata, K. & Ikawa, Y. A chondrogenic cell line derived from a differentiating culture of AT805 teratocarcinoma cells. *Cell Differ. Dev.* **30,** 109–16 (1990).

40. Shukunami, C. *et al.* Chondrogenic differentiation of clonal mouse embryonic cell line ATDC5 in vitro: differentiation-dependent gene expression of parathyroid hormone (PTH)/PTH-related peptide receptor. *J. Cell Biol.* **133,** 457–68 (1996).

41. Shukunami, C. *et al.* Cellular hypertrophy and calcification of embryonal carcinoma-derived chondrogenic cell line ATDC5 in vitro. *J. Bone Miner. Res.* **12,** 1174–88 (1997).

42. SAKANO, S. *et al.* Collagen and Alkaline Phosphatase Gene Expression During Bone Morphogenetic Protein (BMP)-Induced Cartilage and Bone Differentiation. *Clin. Orthop.*

Relat. Res. **292,** (1993).

43. Bonewald, L. F. *et al.* Von Kossa Staining Alone Is Not Sufficient to Confirm that Mineralization In Vitro Represents Bone Formation. *Calcif. Tissue Int.* **72,** 537–547 (2003).

44. Hunter, G. K. & Bader, S. M. A mathematical modelling study of epiphyseal cartilage calcification. *J. Theor. Biol.* **138,** 195–211 (1989).

45. Carrion, B. *et al.* The Synergistic Effects of Matrix Stiffness and Composition on the Response of Chondroprogenitor Cells in a 3D Precondensation Microenvironment. *Adv. Healthc. Mater.* (2016). doi:10.1002/adhm.201501017

46. Kim, Y. J., Sah, R. L., Doong, J. Y. & Grodzinsky, A. J. Fluorometric assay of DNA in cartilage explants using Hoechst 33258. *Anal. Biochem.* **174,** 168–76 (1988).

47. Zhai, Z., Yao, Y., Wang, Y., Ohgishi, M. & Fukui, T. Importance of Suitable Reference Gene Selection for Quantitative RT-PCR during ATDC5 Cells Chondrocyte Differentiation. *PLoS One* **8,** e64786 (2013).

48. Beck, G. R., Zerler, B. & Moran, E. Phosphate is a specific signal for induction of osteopontin gene expression. *Proc. Natl. Acad. Sci. U. S. A.* **97,** 8352–7 (2000).

49. Fujita, T. *et al.* Phosphate stimulates differentiation and mineralization of the chondroprogenitor clone ATDC5. *Jpn. J. Pharmacol.* **85,** 278–81 (2001).

50. Hill, T. P., Später, D., Taketo, M. M., Birchmeier, W. & Hartmann, C. Canonical Wnt/beta-catenin signaling prevents osteoblasts from differentiating into chondrocytes. *Dev. Cell* **8,** 727–38 (2005).

51. Day, T. F., Guo, X., Garrett-Beal, L. & Yang, Y. Wnt/beta-catenin signaling in mesenchymal progenitors controls osteoblast and chondrocyte differentiation during vertebrate skeletogenesis. *Dev. Cell* **8,** 739–50 (2005).

52. Shih, Y.-R. V *et al.* Calcium phosphate-bearing matrices induce osteogenic differentiation of stem cells through adenosine signaling. *Proc. Natl. Acad. Sci. U. S. A.* **111,** 990–5 (2014).

53. D'Alimonte, I. *et al.* Adenosine A1 receptor stimulation enhances osteogenic differentiation of human dental pulp-derived mesenchymal stem cells via WNT signaling. *Stem Cell Res.* **11,** 611–24 (2013).

54. Costa, M. A. *et al.* On the role of subtype selective adenosine receptor agonists during proliferation and osteogenic differentiation of human primary bone marrow stromal cells. *J. Cell. Physiol.* **226,** 1353–66 (2011).

55. He, W., Mazumder, A., Wilder, T. & Cronstein, B. N. Adenosine regulates bone metabolism via A1, A2A, and A2B receptors in bone marrow cells from normal humans and patients with multiple myeloma. *FASEB J.* **27,** 3446–54 (2013).

56. Watanabe, H., de Caestecker, M. P. & Yamada, Y. Transcriptional cross-talk between Smad, ERK1/2, and p38 mitogen-activated protein kinase pathways regulates transforming growth factor-beta-induced aggrecan gene expression in chondrogenic ATDC5 cells. *J. Biol. Chem.* **276,** 14466–73 (2001).

57. Boskey, A. L., Doty, S. B. & Binderman, I. Adenosine 5'-triphosphate promotes mineralization in differentiating chick limb-bud mesenchymal cell cultures. *Microsc. Res. Tech.* **28,** 492–504 (1994).

58. Boskey, A. L. *et al.* Modulation of extracellular matrix protein phosphorylation alters mineralization in differentiating chick limb-bud mesenchymal cell micromass cultures. *Bone* **42,** 1061–1071 (2008).

59. Cuervo, L. A., Pita, J. C. & Howell, D. S. Inhibition of calcium phosphate mineral growth by proteoglycan aggregate fractions in a synthetic lymph. *Calcif. Tissue Res.* **13,** 1–10 (1973).

60. Chen, C.-C., Boskey, A. L. & Rosenberg, L. C. The inhibitory effect of cartilage proteoglycans on hydroxyapatite growth. *Calcif. Tissue Int.* **36,** 285–290 (1984).

61. Chen, C.-C. & Boskey, A. L. Mechanisms of proteoglycan inhibition of hydroxyapatite growth. *Calcif. Tissue Int.* **37,** 395–400 (1985).

62. Silva, M. J. *et al.* Decreased collagen organization and content are associated with reduced strength of demineralized and intact bone in the SAMP6 mouse. *J. Bone Miner. Res.* **21,** 78–88 (2006).

63. Nudelman, F. *et al.* The role of collagen in bone apatite formation in the presence of hydroxyapatite nucleation inhibitors. *Nat. Mater.* **9,** 1004–9 (2010).

64. Santoro, A. *et al.* Choosing the right chondrocyte cell line: Focus on nitric oxide. *J. Orthop. Res.* **33,** 1784–1788 (2015).

65. Fukai, A. *et al.* Akt1 in murine chondrocytes controls cartilage calcification during endochondral ossification under physiologic and pathologic conditions. *Arthritis Rheum.* **62,** 826–836 (2010).

Chapter 4 Self-regulatory RUNX2 Silencing Gene Circuits Improve MSC-based Cartilage Regeneration

4.1 Introduction

Mesenchymal stem cell (MSC)-based cartilage tissue engineering has great potential to repair cartilage damage. The chondrogenic potential of these highly proliferative stem cells has been well proven[1,2,3]. Compared to isolating autologous chondrocytes from patients' already injured cartilage, harvesting MSCs, usually from the iliac crests, is less invasive and less prone to donor site morbidity. However, chondrocytes differentiated from MSCs (MdChs) only maintain a transient articular phenotype before further differentiating to the hypertrophic phenotype, recapitulating aspects of the maturation program of chondrocytes during endochondral ossification[4,5]. At the hypertrophic stage, chondrocytes stop producing and start degrading the structural matrix macromolecules aggrecan and type II collagen, compromising the mechanical integrity of the overall tissue. The inferior mechanical properties of tissues derived from MdChs pose major concerns for articular cartilage repair[6].

Many molecular and biophysical cues stimulate chondrocyte hypertrophy, such as IHH[7], TGF-β[8], Wnt/β-catenin[9], Smad[10], and calcium[11]. Each of these pathways promote chondrocyte maturation via Runx2 activity [9,12,13]. Using a doxycycline-inducible lentiviral system, we demonstrated that RNAi of Runx2 in differentiating chondrocytes can effectively suppress markers of hypertrophy and enhance matrix accumulation by targeting RUNX2-activated degradation from MMP13 in chapter 2. However, we also found that loss of RUNX2 function in undifferentiated

progenitor cells blocks *in vitro* chondrogenesis. To target the timing of RUNX2 suppression and to maintain suppression of basal RUNX2 levels in long-term applications (e.g. after the implantation of engineered tissues into a focal defect), tissue-specific promoters can be used to direct RUNX2 silencing to exclusively target maturing chondrocytes after chondrogenesis occurred in MdChs. Therefore, maturation-associated matrix degradation due to RUNX2 activity can be inhibited while undifferentiated stem cells can continue to develop into matrix-producing chondrocytes, maximizing the overall accumulation of articular cartilage-specific structural macromolecules.

Tissue-specific promoters only represent a small portion of mammalian promoters[14]; however, they are essential to the function of a physiological system consisting of different types of cells. For example, more than 400 distinct types of cells arise from a single fertilized egg during human development[15]. Although they all carry the identical genetic information, each cell type expresses a signature profile of activated genes under the control of tissue-specific promoters[16], contributing to a certain phenotype. In mammalian cells, gene promoters can be separated into two classes: "broad" and "sharp"[17], and tissue-specific ones often belong to the "sharp" category because of their well-defined, narrow transcription start sites (usually less than a few nucleotides)[18,19]. Such a focused pattern of transcription start sites likely require transcription to be initiated by particular transcription factors, contributing to the tissue-specific gene expression. Applications of tissue-specific promoters in biomedical research typically follow the discovery of a cell type-specific marker, such as osteoblast/osteocalcin[20], pancreatic β cell/insulin [21], hepatocytes/Albumin-α-Fetoprotein[22], cardiomyocytes/myosin heavy chain[23], mammary epithelial cells/milk whey acidic protein[24], articular chondrocytes/aggrecan[25], etc. Frequently, the promoters of these marker genes are used to create conditional knock-out mouse

models to avoid premature deaths from a global disruption of essential genes[26,27,28]. With an increasing number of tissue-specific promoters become available, hundreds of different genes have been knocked out in various cell types. (e.gs., chondrocytes [29], pancreatic β cells[30], suprabasal urothelial cells[31], hepatocytes[32], cardiomyocytes[33], and mammary epithelial cells[34]).

Tissue-specific promoters can also help target the early and late chondrogenic phenotypes. When mesenchymal progenitors first differentiate into chondrocytes, they express a high level of *Col2a1* gene[35]. Using the *Col2a1* promoter, chondrocyte-specific knockout of *Vegf* [36], *Fosl2* [37], *Trsp* [38], *Pten* [39], *Nf1* [40], *Smo* [41], and *Ext1*[42] mice have been created to study the roles of these protein in chondrogenesis. Among chondrocytes that are not programmed to become articular chondrocytes, they soon transition to the pre-hypertrophic and hypertrophic phenotype, accompanied by the upregulated gene expression of type X collagen[43]. Because of the its unique specificity to chondrocyte hypertrophy, the promoter of *Col10a1* have been extensively characterized and used to generate transgenic mice models [44,45]. Recently, Gebhard *et al*. showed that the expression of *Col10a1* in murine chondrocytes is controlled by its promoter up to 4.6 kb upstream of the transcription start site[46]. Zheng *et al*. further identified a 150-bp cis-enhancer within the distal region (-4.4kb to -3.8 kb) that directly contributes to the specific expression of *Col10a1* in hypertrophic chondrocytes via Runx2 binding[47]. Therefore, the *Col10a1* promoter can be used to initiate *in vitro* transcription confined to pre-hypertrophic or hypertrophic chondrocytes.

We hypothesize that a *Col10a1*-like promoter can initiate RUNX2 silencing exclusively in maturing chondrocytes without interfering with early chondrogenesis of MSCs. Since larger size vectors often reduce the efficiency of viral packaging, truncated versions (<1kb) of the endogenous tissue-specific promoters are often created to drive transgene expression or RNAi in certain cell types. To minimize the size of the RUNX2 silencing gene circuit, we designed a synthetic *cis*

promoter which consists of a single or multiple copies of the 150-bp *cis*-enhancers immediately upstream of the basal promoter of *Col10a1* to recapitulate the hypertrophy-specific activity of the endogenous *Col10a1* promoter. Using these *cis* promoters to drive miRNA-based sh*Runx2* (referred as *cis*-sh*Runx2* gene circuits), we show that these gene circuits can enhance the accumulation of matrix by MSC-derived chondrocytes via tunable negative-feedback regulation of intracellular RUNX2 activity.

4.2 Methods

4.2.1 Synthesis of *cis* Promoter

Single copies of *Col10a1* basal promoter (-220 to 110 bp) and *cis*-enhancer (-4296 to -4147 bp) were synthesized by IDT technology. Two PCR amplification reactions of *cis*-enhancer were performed using primers 5'-AAAAATTCAAAATTTTATCGATCACGAGACTAGCCTC-CTGTTTCACG and 5'-AACAGGAGGCGGATCTAACAGATTGTAGAATCAGAGTA or using primers 5'-CAATCTGTTAGATCCGCCTCCTGTTTCACG and 5'-AACAGGAGGCGG-ATCTAACAGATTGTAGAATCAGAGTA. *Col10a1* basal promoter was PCR amplified using primers 5'- ATTCTACAATCTGTTGAATTCTCATGCAC and 5'-CGGGCCCGCGGTACC GTCGACTGCAGAATT. These PCR products from three amplification reactions were assembled into pLenti-CMVtight-eGFP-Puro that was digested with BstBI and PspXI using Gibson Assembly Kit. Successfully cloned plasmid containing 1*cis*, 2*cis*, and 3*cis* promoters were confirmed by Sanger sequencing: 1*cis*-eGFP-Puro, 2*cis*-eGFP-Puro, and 3*cis*-eGFP-Puro.

4.2.2 Synthesis of *cis*-sh*Runx2* Gene Circuit and Viral Production

1*cis*-Luc-sh*Runx2* was made by first digesting Tet-on-Luc-sh*Runx2* with NheI and AgeI to remove the Tet-on (TRE2) promoter. 1*cis* promoter was PCR amplified from 1*cis*-eGFP-Puro using primers 5'-GTTCTAGGCTAGCTTAAAGGATTTTATCGATCACGAGACT and 5'-

GGTGGCGACCGGTAGGCTGGTACCGAGCTCGAATTCTCCA, and then digested with NheI and AgeI. Digested 1*cis* promoter was ligated to Tet-on-Luc-sh*Runx2* vector. To remove luciferase from 1*cis*-Luc-sh*Runx2*, mir30-sh*Runx2* was PCR amplified using primers 5'-GATCCAGCCTACCGGTAAGCCTTGTTAAGTGCTCGC and 5'-CTAAAGTAGCCCCTT-GAATTCCGAGGCAGTAGGCA. The PCR product was digested with EcoRI and AgeI, and then ligated to 1*cis*-Luc-sh*Runx2* that was also digested with EcoRI and AgeI. Similarly, 2*cis*-Luc-sh*Runx2*, 2*cis*-sh*Runx2*, 3*cis*-Luc-sh*Runx2*, 3*cis*-sh*Runx2* and their corresponding scramble vectors were synthesized as described above. Correct cloning was confirmed by Sanger sequencing at UM Sequencing core, and lentiviral supernatant of the correct plasmid vectors was produced at UM Vector Core.

4.2.3 Chondrogenic Cell Cultures

ATDC5 cells (Sigma) were maintained in DMEM/F12 (Life Technologies) supplemented with 5% FBS (Life Technologies) and 1% Antibiotic-Antimycotic (Life Technologies). Chondrogenesis of ATDC5 cells was induced with chondrogenic differentiation medium consisting of the growth medium supplemented with 1% ITS+ Premix (Corning) and 50 µg/ml ascorbate acid-2-phosphate (Sigma).

Four days prior to chondrogenic induction of ATDC5 in monolayer (2D) culture, cells were seeded at a density of 10,000 cells/cm^2 in multiple well plates. When cells reached 100% confluence (D0), chondrogenesis was initiated by replacing the growth medium with differentiation medium. Cultures were fed with fresh medium every other day and maintained up to 28 days.

Four days prior to chondrogenic induction in pellet (3D) culture, cells were seeded at a density of 10,000 cells/cm^2. When cells reached 100% confluence (D0), they were trypsinized and

centrifuged into pellets containing 2.5×10^5 cells in round-bottomed polypropylene 96-well-plate. Chondrogenesis was initiated by replacing the growth medium with differentiation medium and maintained for 35 days.

C57BL/6 Mouse Mesenchymal Stem Cells (Cyagen) were maintained according to manufacturer's instruction. Chondrogenesis of mMSCs was induced with chondrogenic differentiation medium consisting of DMEM(high-glucose) supplemented with 0.1 μM dexamethasone, 50 μg/mL ascorbate 2-phosphate, 40 μg/mL L-proline, 100 μg/mL sodium pyruvate, 1% ITS+, 50 ng/mL BMP-2, and 10 ng/mL TGF-β3. When cells reached 85% confluence (D0), they were trypsinized and centrifuged into pellets containing 2.0×10^5 cells in round-bottomed polypropylene 96-well-plate. Chondrogenesis was initiated by replacing the growth medium with differentiation medium and maintained for 56 days.

4.2.4 Luciferase Assay

Luciferase activity of ATDC5 cultures in multiple wells was measured daily. D-luciferin stock was added to the culture medium at a final concentration of 150 μg/mL and gently mixed. Luciferin-added cultures were incubated at 37°C for 30 minutes before measured using SYNERGY H1 microplate reader (BioTek). Each plate was measured three times to minimize reading machine errors. Measured cultures were fed with fresh differentiation medium afterward.

4.2.5 Biochemical Analysis

Cartilage-specific matrix production was measured by the 1,9-dimethylmethylene blue (DMMB) assay as previously described [48]. Both monolayer cell tissues and pellets were digested with 1 mg/ml proteinase K in 0.1M ammonium acetate at 50°C for 16 hours. Digested samples were mixed with DMMB dye (pH 1.5) at a ratio of 1:20, and the sGAG content of the samples were determined by comparing the ratio of 525 nm to 595 nm readings to the standard curve

derived from shark chondroitin sulfate. Measured sGAG content of each sample was normalized by its DNA content using Hoechst 33258 dye (Sigma) as previously described [49].

4.2.6 Gene expression Analysis

Total RNA of each sample was extracted using TRI Reagent® RT (Molecular Research Center). For pellet culture, five pellets were combined and homogenized in the same reagent using the Micro Tube Homogenizer. Equal amounts of extracted RNA were reverse-transcribed into cDNA using High-Capacity cDNA Reverse Transcription Kit (Life Technologies). Synthesized cDNA was amplified using Fast SYBR® Green Master Mix (Life Technologies) on Applied Biosystems® 7500 Fast platform. The mean cycle threshold of the housekeeping genes ($\overline{Ct}_{hk}$) *Hprt* and *Ppia*[50] were used to calculate the fold change in transcript levels compared to day 0 samples using the $\Delta\Delta Ct$ method. Relative expression levels were calculated as $x = 2^{-\Delta\Delta Ct}$, in which $\Delta\Delta Ct = \Delta E - \Delta C$, $\Delta E = Ct_{exp} - \overline{Ct}_{hk}$ at the time-point of interest, and $\Delta C = Ct_{exp} - \overline{Ct}_{hk}$ at day 0. The forward and reverse primer sequences are listed in **Table 4-1**.

Table 4-1. The sequences of primers used

Gene		Primer Sequences (5'→3')		Primer Sequences (5'→3')
Acan	Forward	CGCCACTTTCATGACCGAGA	Reverse	CAAATTGCAGAGAGTGTCCGT
Col2a1	Forward	ACGAGGCAGACAGTACCTTG	Reverse	AGTAGTCTCCGCTCTTCCACT
Col10a1	Forward	CCAAACGCCCACAGGCATAA	Reverse	TGCCTTGTTCTCCTCTTACTGG
Hprt	Forward	CTGGTGAAAAGGACCTCTCGAA	Reverse	CTGAAGTACTCATTATAGTCAAGGGCAT
Ppia	Forward	CGCGTCTCCTTCGAGCTGTTTG	Reverse	TGTAAAGTCACCACCCTGGCACAT
Mmp13	Forward	GGAGCCCTGATGTTTCCCAT	Reverse	GTCTTCATCGCCTGGACCATA

4.2.7 Histological Analysis

Differentiated pellets were washed with PBS and fixed in 5% buffered formalin at 4℃ for 16 hours. Fixed pellets were washed with 70% ethanol, embedded in paraffin wax, and then 7 μm sections were taken. Proteoglycan accumulation in monolayer tissues and pellets was evaluated by staining the sectioned tissue with 3% Alcian blue dye (Poly Scientific).

4.2.8 Immunohistochemical Analysis

Samples were prepared for immunohistochemical (IHC) staining by fixation in 5% formalin. Samples were then embedded in paraffin wax and cut into 7 μm sections. Slides were deparaffinized in xylene and rehydrated through decreasing concentrations of ethanol (100%, 95%, 70%). Antigen retrieval was performed BD Retrievagen A Solution System for 20 minutes at 85 °C Blocking of slides was done in 1% BSA and 10% goat serum in PBS for 2 hours at room temperature. After blocking, slides were incubated overnight at 4 °C in the following antibodies: RUNX2 (Abcam, 23981) and COL10A1 (ABclonal, A6889) are used for overnight primary incubation at 4 °C. HRP-conjugated secondary antibody goat anti-rabbit (Abcam, ab97080). Slides were developed using DAB Substrate Kit (Abcam, 64238) with hematoxylin counterstaining before imaging.

4.2.9 Statistical Analysis

Statistical analysis was performed using GraphPad Prism software. All comparisons over multiple time points were analyzed by two-way ANOVA with Tukey's multiple comparison method. Comparisons in experiment with a single time point were analyzed by one-way ANOVA followed by Sidak correction. Significant difference is indicated by * $P<0.05$, ** $P<0.01$, ***$P<0.001$, ****$P<0.0001$. All error bars indicate the standard error of the mean (s.e.m.).

4.3 Results

4.3.1 Synthetic *Col10a1*-like Promoters

We hypothesized that a synthetic promoter consisting of the core promoter sequence of *Col10a1* and RUNX2 binding sites can recapitulate a specificity to hypertrophic chondrocytes. To test this hypothesis, we incorporated a truncated *Col10a1* basal promoter downstream of the 150bp *cis*-enhancer to drive the expression of luciferase and eGFP (**Figure 4-1**). Polyclonal ATDC5 populations that stably express the luciferase reporter construct were chondrogenically induced

and cultured for 21 days in monolayer. Luciferase activity in these differentiating cells was initially expressed at a minimal level until day 6, then rapidly upregulated to, and maintained at an elevated level after day 10 (**Figure 4-2b**). Such an activity profile of the 1*cis* promoter resembles the gene expression of *Col10a1* (**Figure 4-2a**).

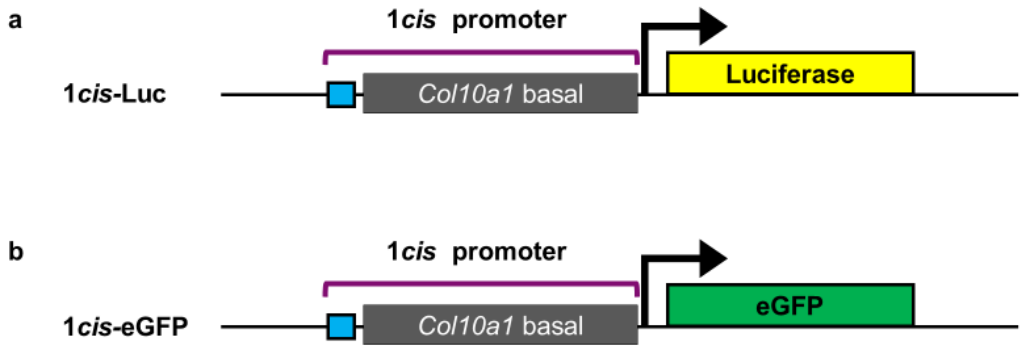

Figure 4-1. Reporter constructs of 1*cis* promoter. (a) Diagram of 1*cis*-Luc. 1*cis*-Luc encodes the firefly luciferase under the control of the synthetic 1*cis* promoter and a constitutive cassette (puromycin N-acetyltransferase, not shown). (b) Diagram of 1*cis*-eGFP. 1*cis*-eGFP encodes the enhanced green fluorescent protein under the control of the synthetic 1*cis* promoter and a constitutive cassette (puromycin N-acetyltransferase, not shown).

To confirm that the 1*cis* promoter is exclusively activated in cells undergoing chondrogenesis, we transduced the cells with the eGFP reporter construct and induced chondrogenesis in these cells. By day 7, eGFP fluorescence was only seen in cartilaginous nodules. Little eGFP fluorescence was observed in cells that were not chondrogenically induced nor ones that had not yet formed cartilaginous nodules (**Figure 4-2c**). At day 14, we harvested these cells for Western blot analysis, which showed that eGFP protein was solely expressed in cells that were exposed to chondrogenic stimuli (**Figure 4-2d**). Taken together, these data illustrate that 1*cis* promoter has a similar phenotype-specificity to endogenous *Col10a1* promoter, and its transcriptional activity is limited to differentiated ATDC5 cells and upregulated as these cells transition to the hypertrophic phenotype.

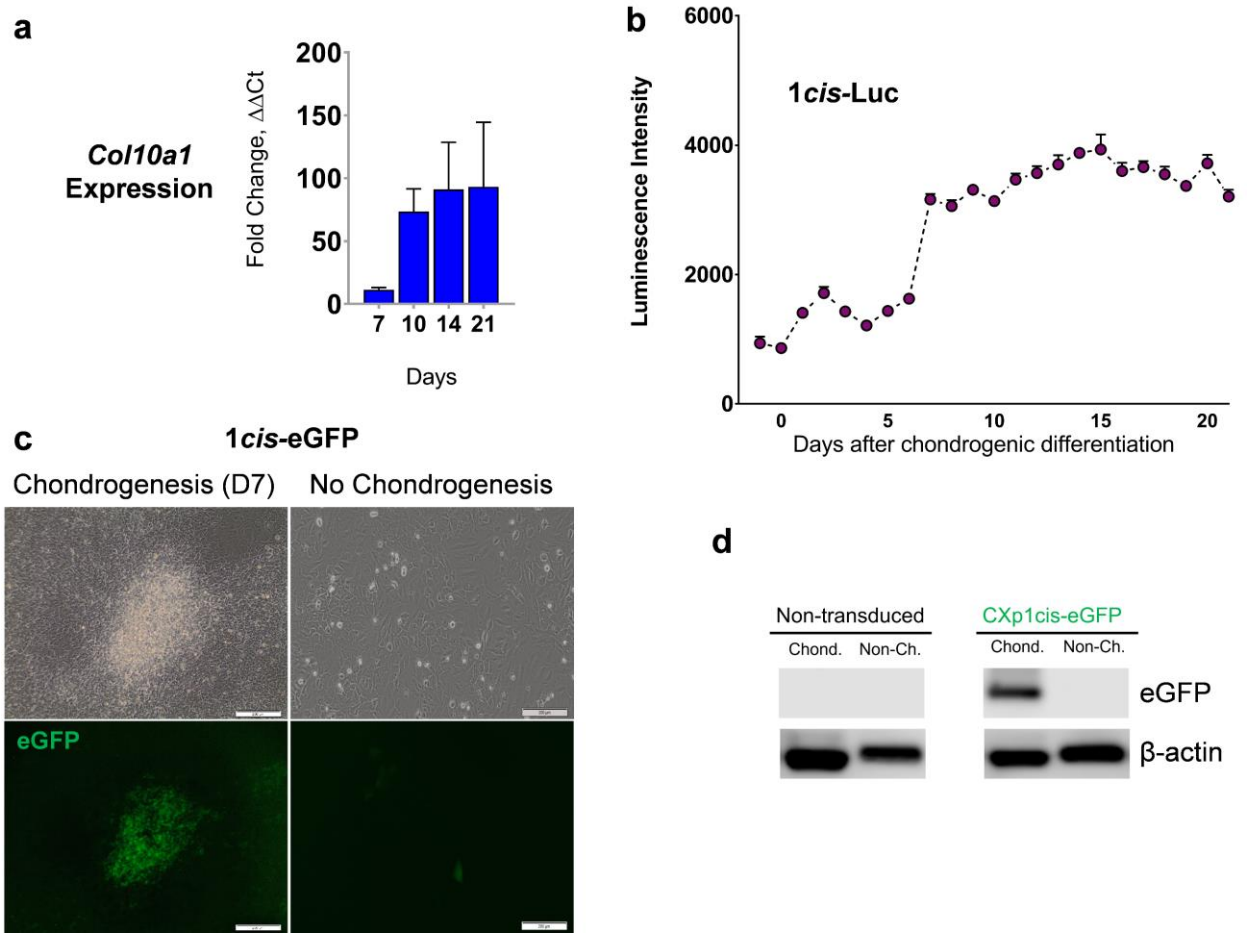

Figure 4-2. Synthetic 1*cis* promoter resembles endogenous *Col10a1* promoter. (a). Quantification of mRNA expression (relative to day 0 and the housekeeping genes *Hprt* and *Ppia*) of *Col10a1* in non-transduced ATDC5 monolayer cultures over 21 days of chondrogenic differentiation (two independent experiments, n≥5). (b) Total luciferase activity from ATDC5 cultures expressing 1*cis*-Luc over 21 days of differentiation (two independent experiments, n=6). (c) Bright field and fluorescent imaging of ATDC5 cells transduced with 1*cis*-eGFP before and after 7-day chondrogenic differentiation. (d) eGFP and β-actin (internal control) levels in non-transduced ATDC5 and ones transduced with 1*cis*-eGFP were determined after 14-day chondrogenic differentiation were determined by Western blot.

4.3.2 Activity of RUNX2 Suppressing Gene Circuits

To determine whether the 1*cis* promoter could be used to provide self-regulated RNAi of RUNX2 in pre-hypertrophic ATDC5 cells, we created a lentiviral vector that co-expresses the luciferase cDNA and sh*Runx2* sequence under the control of the engineered promoter and established polyclonal ATDC5 cell populations stably expressing such a vector (**Figure 4-3a**). As chondrogenesis occurred, the luciferase activity, as a surrogate measurement of the promoter activation, was expressed at a minimal level in cells expressing 1*cis*-sh*Runx2* during the first 6

days, similar to that in cells transduced with 1*cis*-scramble vector. From day 7, 1*cis*-sh*Runx2* cultures exhibited a significantly lower level of luciferase activity than the scramble controls (**Figure 4-4a**). While the total activity from both groups fluctuated throughout further differentiation, a relative decrease of 18.1±5.1% activity was reached and stabilized under the control of the 1*cis*-sh*Runx2* vector, indicating a lower level of RUNX2 activity in cells expressing this gene circuit (**Figure 4-4b**).

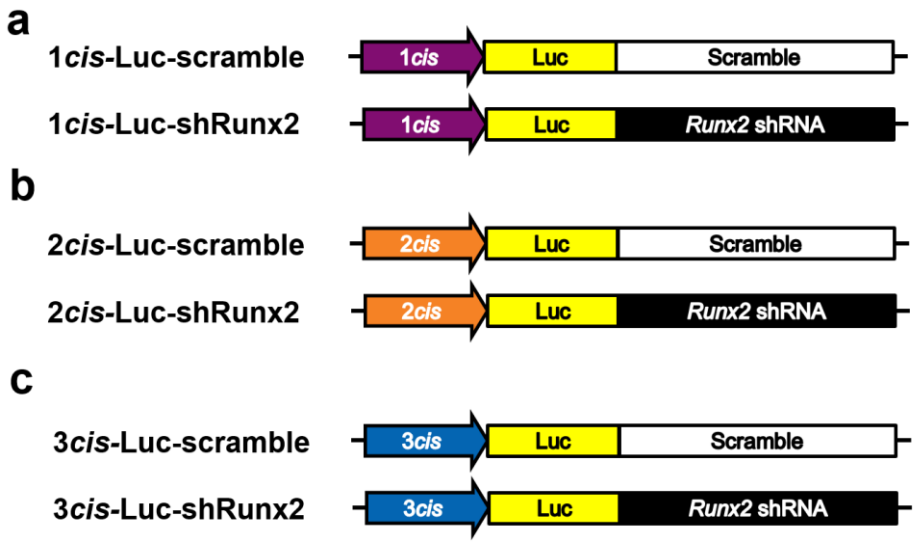

Figure 4-3. Design of *cis*-sh*Runx2* gene circuits and their corresponding scramble vectors. (a) Diagrams of 1*cis*-Luc-sh*Runx2* and 1*cis*-Luc-scramble. 1*cis*-Luc-sh*Runx2*/scramble encode the firefly luciferase immediately upstream of the miRNA-based sh*Runx2* or scramble sequences under the control of 1*cis* promoter and a constitutive cassette (puromycin N-acetyltransferase, not shown). Diagrams of (b) 2*cis*- and (c) 3*cis*-Luc-sh*Runx2* gene circuits and their scramble vectors.

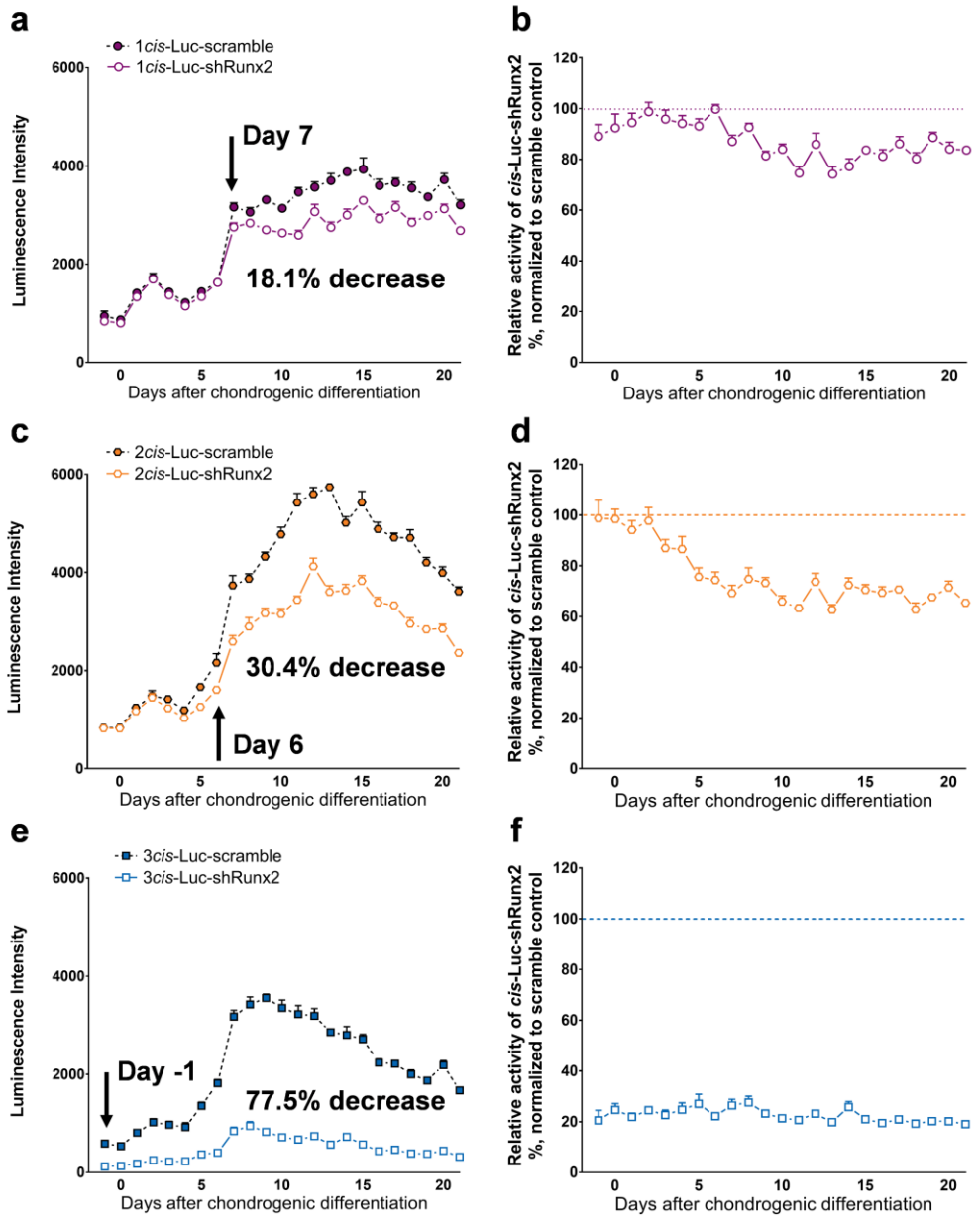

Figure 4-4. Activity of cis-sh*Runx2* gene circuits in monolayer ATDC5 model. Total luciferase activity of cultures expressing (a) 1*cis*-Luc-sh*Runx2*/scramble, (c) 2*cis*-Luc-sh*Runx2*/scramble, and (e) 3*cis*-Luc-sh*Runx2*/scramble during 21-day chondrogenic differentiation. Relative activity of (b) 1*cis*-, (d) 2*cis*-, and (f) 3*cis*-Luc-shRunx2 were calculated by normalizing to activity of corresponding scramble controls at each time point. Data represented as mean ± s.e.m. Significant difference between groups at each time point (n=6 from two independent transduction experiments) is calculated by two-way ANOVA with Tukey's multiple comparison method.

We similarly synthesized 2*cis*-sh*Runx2* and 3*cis*-sh*Runx2* gene circuits and their corresponding scramble control vectors (**Figure 4-3b&c**). During the first five days of chondrogenic differentiation, gene circuits containing the 2*cis* promoter exhibited the same level

of minimal activity as 1*cis*. However, starting from day 6, gene circuit activity increased 56.8% over 1*cis* circuits (**Figure 4-4c**). The stronger 2*cis* promoter drove the total gene circuit activity in 2*cis*-sh*Runx2* cultures to equilibrate at a level that was 30.4±4.2% lower than the scramble controls (**Figure 4-4d**). The addition of a third *cis*-enhancer did not further increase the total gene circuit activity (**Figure 4-4e**). Nonetheless, cells expressing 3*cis*-sh*Runx2* exhibited a more prominent reduction (77.5±2.6%) in gene circuit activity when compared to the scramble controls throughout chondrogenic differentiation (**Figure 4-4f**). Collectively, this data demonstrates the ability of these gene circuits to negatively regulate the expression of RUNX2 during chondrogenic differentiation as well as the tunable silencing efficacy via adjusting the number of *cis*-enhancers incorporated into the *Col10a1*-like promoters.

4.3.3 Effects of RUNX2 Suppressing Gene Circuits on Chondrogenesis

To further study how the activity of gene circuits affects chondrogenic differentiation of ATDC5 cells, we examined the gene expression of early and late chondrogenic markers (*Acan*, *Col10a1*, and *Mmp13*) during and after the peak activity of each circuit. Although all three versions (1*cis*, 2*cis*, and 3*cis*) of the RUNX2 silencing circuit lead to less activity of their *Col10a1*-like promoters at both day 14 and 21, significant downregulation of *Col10a1* gene expression (34.4% decrease compared to the scrambled controls) was detected only in the 3*cis*-sh*Runx2* cultures (**Figure 4-5b**). Similar results were obtained for *Mmp13* (**Figure 4-5c**). Interestingly, differentiating cells expressing both 2*cis*- and 3*cis*-RUNX2 silencing circuits also had lower mRNA levels of *Acan*, 19.4% and 33.2% respectively, at day 14 (**Figure 4-5a**). Despite the downregulated *Acan* gene expression, higher amounts of sGAG-rich matrix were accumulated at day 21 and day 28 in cultures of cells expressing 2*cis*-RUNX2 silencing compared to their corresponding scramble controls (**Figure 4-6b**). Although 3*cis*-sh*Runx2* cultures did not

accumulate higher levels of matrix compared to scramble controls at either time point, they are the only group that exhibited no trend of matrix loss from day 21 to day 28 (**Figure 4-6c**).

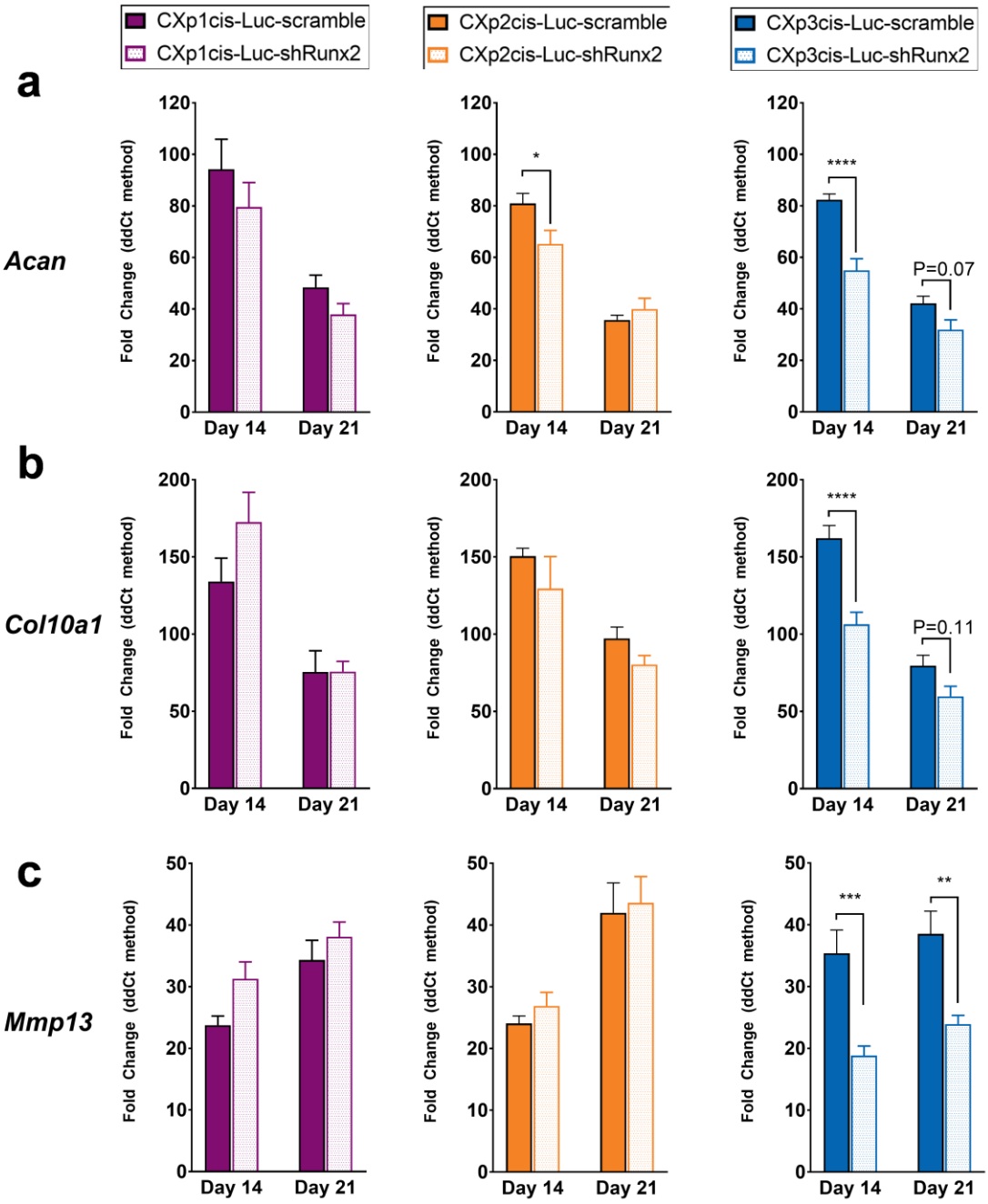

Figure 4-5. Gene expression of early and late chondrogenic markers under the regulation of *cis*-sh*Runx2* gene circuits. Quantification of mRNA expression (relative to day 0 and the housekeeping genes *Hprt* and *Ppia*) of (a) *Acan*, (b) *Col10a1*), and (c) *Mmp13* in monolayer ATDC5 cultures expressing *cis*-sh*Runx2* gene circuits or scramble vectors at day 14 and day 21. Data represented as mean ± s.e.m. Significant difference between groups at each time point (n=4 from two independent transduction experiments) is indicated by * P<0.05, ** P<0.01, ***P<0.001, ****P<0.0001 by two-way ANOVA with Tukey's multiple comparison method.

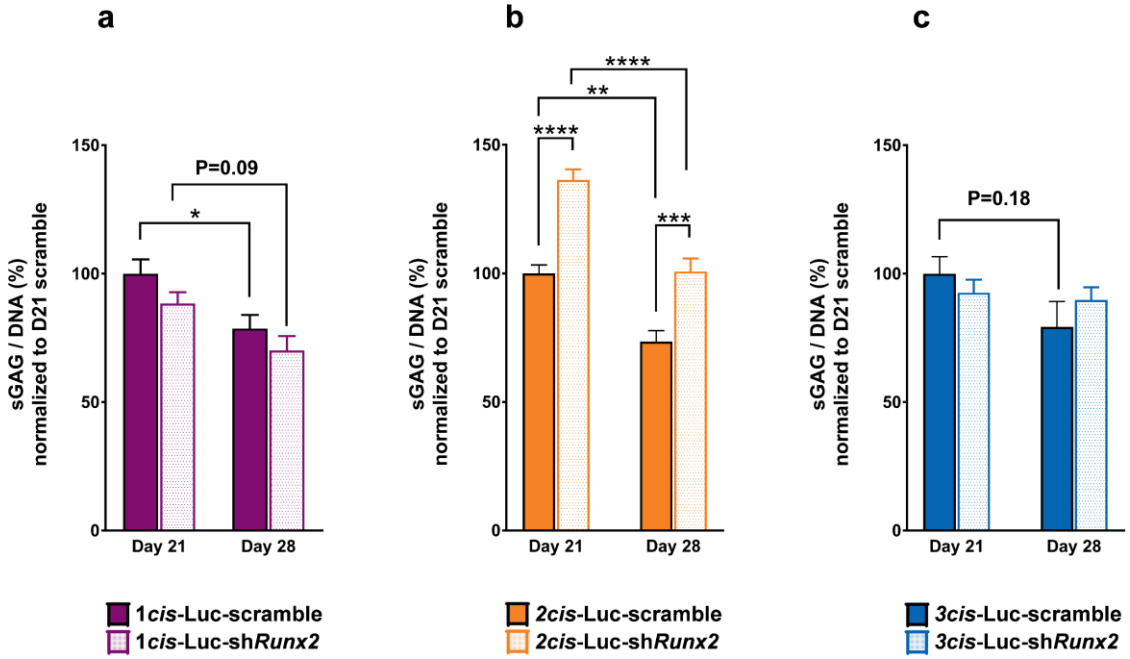

Figure 4-6. Effects of *cis*-sh*Runx2* gene circuits on matrix accumulation. Fold change (%, relative to day 21 scramble controls) in sGAG accumulation by (a) 1*cis*-, (b) 2*cis*-, and (c) 3*cis*-RUNX2 silencing gene circuit at day 21 and 28. Data represented as mean ± s.e.m. Significant difference between groups at each time point (n=6 from two independent transduction experiments) is indicated by * P<0.05, ** P<0.01, ***P<0.001, ****P<0.0001 by two-way ANOVA with Tukey's multiple comparison method.

4.3.4 Activity of RUNX2 Suppressing Gene Circuits in Response to Phosphate

To examine the potential of *cis*-shRunx2 gene circuits to resist upregulation of hypertrophic markers in response to an exogenous cue, we supplemented the differentiation medium with 5mM βGP after ATDC5 cells expressing either 1*cis*- or 3*cis*- shRunx2 were chondrogenically induced for 7 days. In response to βGP, the activity of both the 1*cis* promoter and 1*cis*-shRunx2 gene circuit increased between day 9 and 20, with the maximum increases occurring around day 15 in both cultures (**Figure 4-7a&b**). However, the levels of stimulated activity by βGP differed between the 1*cis*-scramble and 1*cis*-shRunx2 cultures, and cells expressing 1*cis*-shRunx2 exhibited a lower percentage of increase compared to the scramble controls (24.1% vs. 31.1%, **Figure 4-7c**). Similarly, 3*cis*-shRunx2 cultures showed more

resistance to βGP-induced activity increase compared to 3*cis*-scramble controls (27.0% vs. 34.0%, **Figure 4-7d-f**).

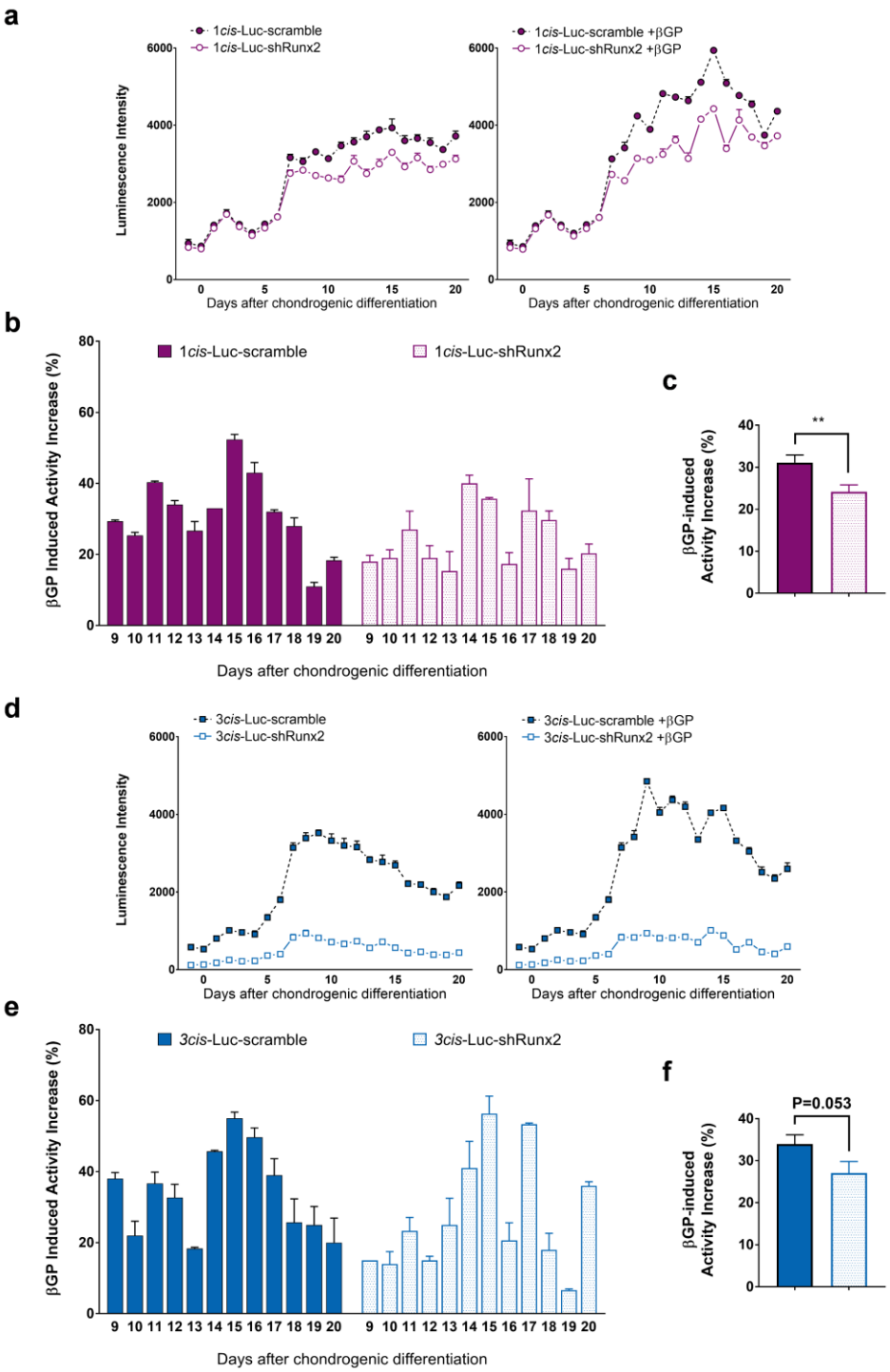

Figure 4-7. Activity of *cis*-sh*Runx2* gene circuits in response to phosphate. (a) Total luciferase activity of cultures expressing 1*cis*-Luc-sh*Runx2*/scramble before and after βGP (5mM) treatment. (b) Relative activity increased (%,

normalized to non-treated cultures at each time point) in response to βGP after day 9. (c) Overall activity increase in 1*cis*-Luc-sh*Runx2*/scramble cultures between day 9 and 20. (d) Total luciferase activity of cultures expressing 3*cis*-Luc-sh*Runx2*/scramble before and after βGP (5mM) treatment. (e) Relative activity increased (%, normalized to non-treated cultures at each time point) in response to βGP after day 9. (f) Overall activity increase in 3*cis*-Luc-sh*Runx2*/scramble cultures between day 9 and 20. Data represented as mean ± s.e.m. Significant difference in (c, n=3) and (f, n=3) is indicated by * $P<0.05$ by unpaired t-test.

4.3.5 Effects of the 3*cis*-sh*Runx2* Gene Circuit on Chondrogenesis in Pellet Cultures

To determine if the strongest RUNX2 silencing gene circuit enhances matrix accumulation by inhibiting the maturation-associated degradation, we monitored the progression of chondrogenesis in ATDC5 cell pellets expressing the 3*cis*-sh*Runx2* circuit (luciferase free) for five weeks. In the 3*cis*-scramble pellets, evident accumulation of sGAG-rich matrix was observed by day 14 in the form of nodules that were stained positive by Alcian blue dye (**Figure 4-8a**). Within these chondrogenic aggregates, little RUNX2 expression was detected by immunohistochemistry. By day 21, a further increase of matrix accumulation occurred, accompanied by the peak expression of RUNX2 (**Figure 4-8b&c**). Following this upregulation, loss of matrix started to become noticeable within certain regions of the chondrogenic aggregates by day 28. By the end of week 5, the majority of tissues formed by 3*cis*-scramble cells was stained negative by Alcian blue dye. In contrast to the elevated level of RUNX2 protein expression at day 21 in the 3*cis*-scramble pellets, the presence of RUNX2 was barely detectable in the 3*cis*-sh*Runx2* pellets (**Figure 4-9b&d**). Despite such a difference, both groups of pellets showed similar morphologies of chondrocytes and levels of Alcian blue and type X collagen staining within their chondrogenic aggregates at this time point (**Figure 4-9a-f**). However, by day 35, a higher amount of matrix was retained in the 3*cis*-sh*Runx2* pellets compared to scramble controls (**Figure 4-9g&h**).

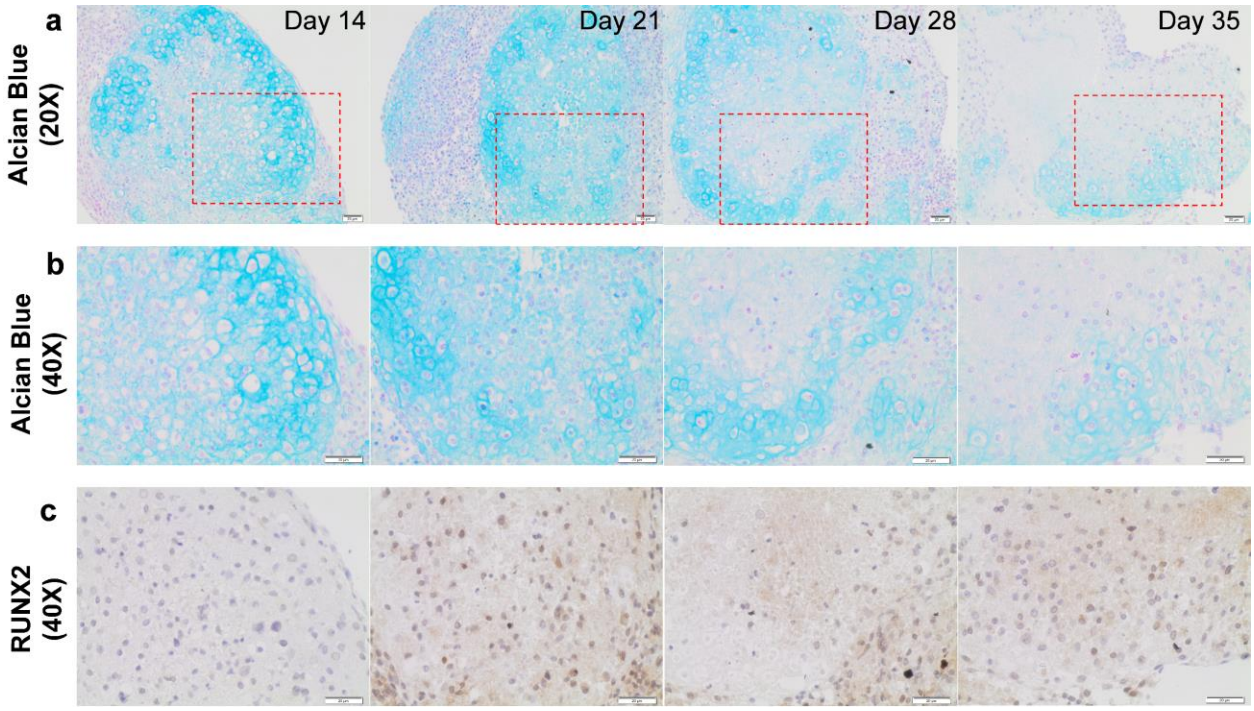

Figure 4-8. Chondrogenesis and maturation in ATDC5 pellets. Alcian blue staining of 3*cis*-scramble pellets at (a) 20× and (b) 40× magnification during five-week chondrogenic differentiation. (c) RUNX2 IHC staining of the chondrogenic regions within the pellets at each time point. Representative images from pellets of three independent transduction experiments.

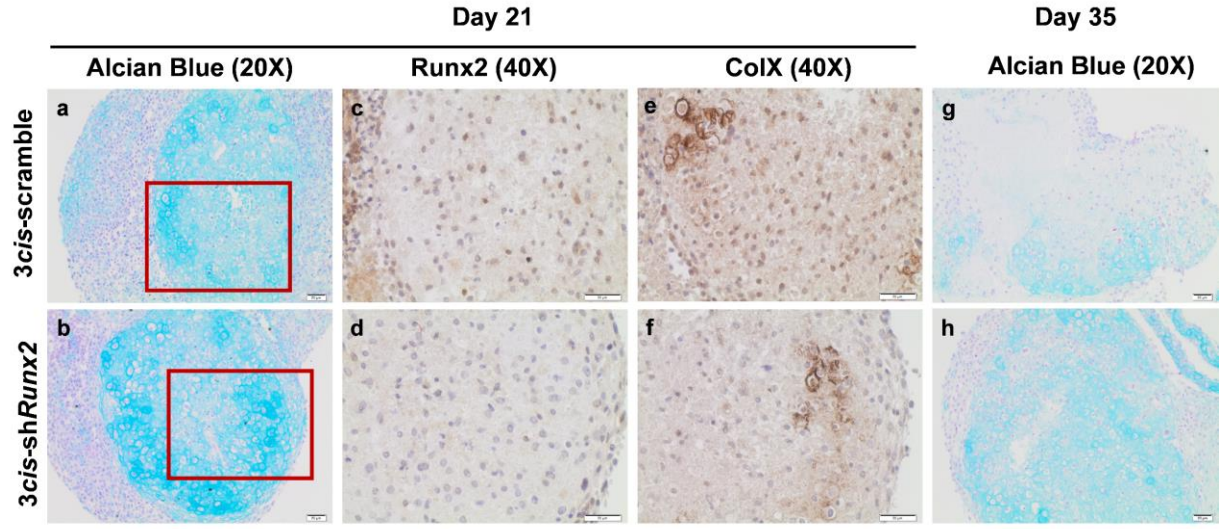

Figure 4-9. Effects of 3*cis*-sh*Runx2* on chondrogenic maturation in 3D ATDC5 model. Alcian blue staining of 3*cis*-sh*Runx2* pellets and 3*cis*-scramble pellets at (a & b) day 21 and (g & h) day 35. (c & d) RUNX2 and (e & f) ColX IHC staining at day 21. Representative images from pellets of three independent transduction experiments were taken at 20× or 40×.

4.3.6 Effects of RUNX2 Suppressing Gene Circuits on Matrix Accumulation in mMSC Pellets

To examine if the activity of RUNX2 silencing gene circuits also improves the accumulation of matrix by MdChs, we created polyclonal murine MSC cell populations that stably express *cis*-Luc-shRunx2 gene circuits and monitored the chondrogenesis of these cells in pellet cultures for eight weeks. In the 3*cis*-Luc-scramble pellets, accumulation of sGAG-rich matrix was observed by day 28 and further increased by day 42 (**Figure 4-10a&b**). Within the following two weeks, a small amount of matrix loss occurred together with the slight enlargement of cells within the chondrogenic regions (**Figure 4-10c**). Compared to their scramble controls, 3*cis*-Luc-shRunx2 pellets deposited less matrix by day 28 but were able to accumulate more by day 42 (**Figure 4-10d&e**). At the end of week 8, 3*cis*-Luc-sh*Runx2* pellets also retained a higher amount of matrix than the scramble controls (**Figure 4-10f**). Similarly, both 1*cis*- and 2*cis*-Luc-sh*Runx2* pellets enhanced matrix accumulation compared to their corresponding scramble controls by the end of culture; however, the difference between 1*cis*- gene circuit and its scramble control were less noticeable compared to their 2*cis*- and 3*cis*- counterparts (**Figure 4-11**).

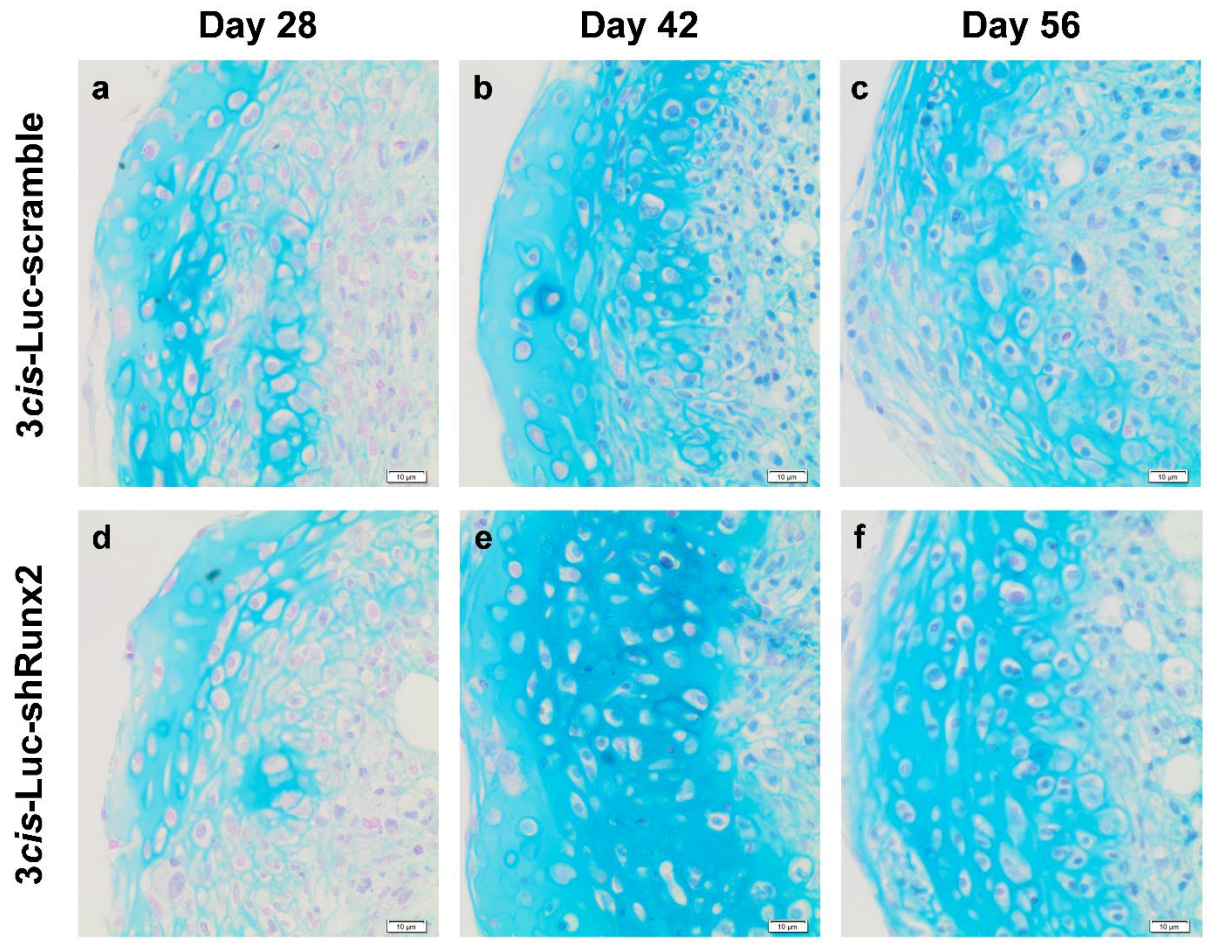

Figure 4-10. Effects of 3*cis*-sh*Runx2* on chondrogenesis in murine MSC pellets. Alcian blue staining of 3*cis*-sh*Runx2* pellets and 3*cis*-scramble pellets at (a & d) day 28, (b & e) day 42, and (c & f) day 56. Representative images from pellets of two independent transduction experiments were taken at 40×.

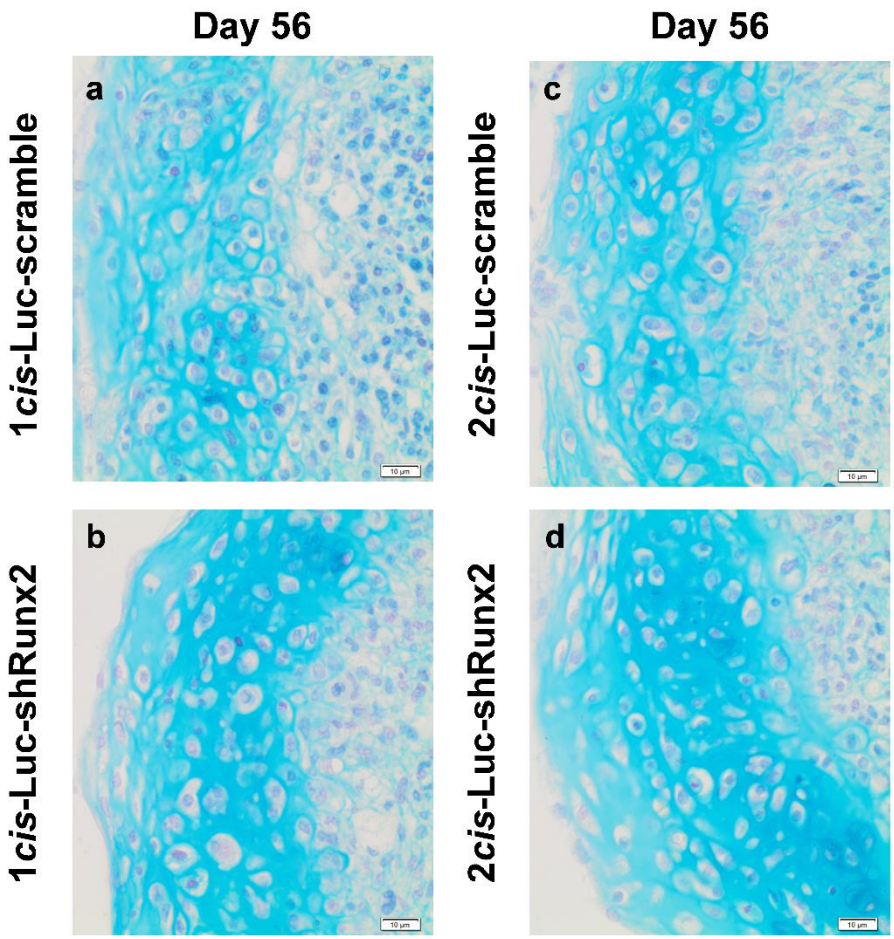

Figure 4-11. Effects of 1*cis*- and 2*cis*-sh*Runx2* on matrix accumulation during murine chondrogenesis. Alcian blue staining of (a & b) 1*cis*-sh*Runx2*/scramble pellets and (c & d) 2*cis*- sh*Runx2*/scramble pellets at day 28. Representative images from pellets of two independent transduction experiments were taken at 40×.

4.4 Discussion & Conclusion

MSCs have great proliferative and chondrogenic potential, making them promising candidates to replace articular chondrocytes for cell-based cartilage repair. Despite these advantages, the long-term effectiveness of MSC-based cartilage regeneration is hampered by the preprogrammed differentiation to chondrocyte hypertrophy and maturation-associated matrix degradation. Here, we demonstrated that the synthetic *Col10a1*-like *cis* promoters can initiate RNAi of *Runx2* in chondrocytes that are transitioning to the pre-hypertrophic phenotype in response to the increasing intracellular RUNX2 activity without interfering with early chondrogenesis of MSCs. The induced

loss of RUNX2 function in turn negatively regulates the activity of the *cis*-sh*Runx2* gene circuit, allowing MSC-derived chondrocytes to resist upregulation of RUNX2 during hypertrophy and maturation-associated matrix degradation. Our findings highlighted three key features of the *cis*-sh*Runx2* gene circuit: 1) the phenotype-specific activation of RNAi, 2) the closed-loop intracellular negative-feedback regulation, and 3) the tunable steady-state level of RUNX2 repression and dynamics.

The *cis*-sh*Runx2* gene circuit relies on its *Col10a1*-like *cis* promoter to induce hypertrophy-specific RUNX2 silencing. The specific expression of *Col10a1* in pre-hypertrophic and hypertrophic chondrocytes requires the binding of RUNX2 in addition to the recruitment of the general transcription factors near the transcription start site[47,51,52], which usually reside within the basal region of mammalian polymerase II promoters. The 330-bp *Col10a1* basal promoter we incorporated contains a highly conserved sequence that precisely describes the transcription start site of *Col10a1* across species[47], providing the DNA template that supports the assembly of the RNA polymerase II transcription initiation complex. Meanwhile, the two putative tandem-repeat within the 150-bp *cis*-enhancer ensures direct binding of RUNX2[47,53]. As a result of the cooperative actions of these two regulatory elements, all three versions of *cis* promoter are sufficient to direct hypertrophy-specific transcription resembling the endogenous *Col10a1* promoter in differentiating chondrocytes. We capitalized on the compact size and phenotype-specificity of the *cis* promoter to target sh*Runx2* expression exclusively in maturing chondrocytes using a lentiviral vector. Therefore, the suppression of early chondrogenesis can be avoided as the loss of RUNX2 function does not occur until MSCs fully differentiate into chondrocytes and transition to pre-hypertrophy. In addition, this approach allows each cell within a heterogenous cell population to downregulate RUNX2 according to its individual maturation clock.

The *cis*-sh*Runx2* gene circuits also establish closed-loop intracellular negative-feedback regulation of RUNX2, allowing differentiating chondrocytes to resist maturation dynamically in response to exogenous cues. The negative feedback motif of *cis*-sh*Runx2* utilizes RUNX2 activity as the central signal. In chondrocytes that are transitioning to hypertrophy, the *cis* promoter (the regulator) initiates the production of sh*Runx2* (the repressor) that downregulates RUNX2 (the signal molecule), which in turn decreases the transcriptional activity of the *cis* promoter (**Figure 4-12**). The negative feedback regulation of chondrocyte maturation also occurs naturally (e.g., PTHrP/IHH feedback loop)[54]. During fetal development, Indian hedgehog (IHH), synthesized by hypertrophic chondrocytes, stimulates maturation and for resting chondrocytes to secrete parathyroid hormone-related protein (PTHrP)[54]. PTHrP, in turn, suppresses IHH production and hypertrophy[55,56]. However, the anti-hypertrophy effect of PTHrP is limited by the range of paracrine signaling as only chondrocytes near the ends of long bones secrete this factor. As a result, chondrocytes residing in the deeper zones will undergo hypertrophy and further terminal differentiation[57]. Free from the dependence on paracrine signaling, *cis*-sh*Runx2* gene circuits allow chondrocytes to resist maturation based their internal tendency to undergo hypertrophy, measured by RUNX2 activity. As a gatekeeper, RUNX2 mediates the signaling of many molecular and biophysical cues to stimulate chondrocyte[9,12,13]. Therefore, by inputting the intracellular RUNX2 activity as the signal for the negative-feedback regulation, cells expressing *cis*-sh*Runx2* can dynamically adjust the level of silencing required to maintain their steady states (levels of RUNX2 suppression) without needing to address the specific pathways underlying hypertrophy stimuli. Such a feature is demonstrated by our observations of the *cis*-sh*Runx2* cultures treated with βGP.

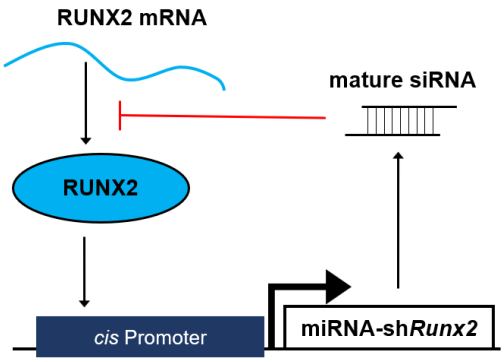

Figure 4-12. cis-sh*Runx2* gene circuit provides negative feedback regulation of RUNX2.

The design of the *cis*-sh*Runx2* gene circuit provides the negative-feedback regulation of RUNX2 with a tunable steady-state (the level of RUNX2 silencing) and dynamics (when to reach steady-state) under the control of *cis*-enhancers. Steady-states and dynamics are two of the most important characteristics of a negative feedback loop[58]. When this motif is used to regulate transcription, a stronger promoter not only allows the system to reach steady-state faster but changes the repression threshold[59]. In the *cis*-sh*Runx2* gene circuit, its steady-state describes the percentage of RUNX2 repression at equilibrium. We observed that increasing the number copies of *cis*-enhancer in the gene circuit progressively enhanced RUNX2 silencing from 18% to nearly 80%. Increasing the number of *cis*-enhancers also led to faster equilibrium of the activity of the gene circuits. Such behaviors likely resulted from the increased responsiveness to RUNX2 as additional binding sites were introduced by extra copies of *cis*-enhancers[47,53]. More importantly, the tunability of the *cis*-sh*Runx2* gene circuit potentially allows us to optimize the matrix accumulation by controlling the dynamics and the level of RUNX2 repression during chondrogenic differentiation. In this study, while 3*cis*-sh*Runx2* exhibited the strongest ability to silence RUNX2, its rapid progression to steady-state also caused silencing in undifferentiated ATDC5 cells and mMSCs. Although the actual level of RUNX2 repression was insufficient to inhibit chondrogenesis, it downregulated the gene expression of *Acan* during the early stages of

chondrogenesis. This likely explains why the increase of matrix accumulation did not occur in ATDC5 3*cis*-sh*Runx2* cultures until after day 21. In contrast, the activity of 2*cis*-sh*Runx2* reached steady-state after chondrocytes were fully differentiated. While this gene circuit caused little interference with the expression of *Acan* during the early phases of chondrocyte development, it only induced 30.4% of RUNX2 repression, potentially limiting its long-term effectiveness in inhibiting matrix degradation. Therefore, future studies that focus on how different *cis*-sh*Runx2* gene circuits affect the matrix turnover and modification are critical to identifying the optimal design for cartilage regeneration.

It is also worth noting that the luciferase reporter played an indispensable role in revealing the three key features of the *cis*-sh*Runx2* gene circuits. Because their phenotype specificity limits the activity of these gene circuits to a small subpopulation of cells among the entire culture, the loss of RUNX2 is difficult to measure using techniques like western blotting. Thanks to the high sensitivity of the luciferase assay, subtle differences among the activity of the gene circuits can be amplified and monitored in real-time. Such an advantage allows us to accurately estimate the level of RUNX2 repression without needing to directly measure the protein expression of RUNX2. Finally, despite its evident enhancing effect on matrix accumulation, the *cis*-sh*Runx2* gene circuit did not completely block the maturation of chondrocyte in either ATDC5 or mMSC cultures. While the incomplete silencing of RUNX2 might have contributed to such observations, it might also suggest that the inhibition of transcription factors besides Runx2 is needed for chondrocytes to fully resist maturation. Using the *cis*-RNAi system developed in this study, future studies can conveniently target single or multiple pro-hypertrophic factors to further improve the matrix accumulation.

4.5 Reference

1. Pittenger, M. F. *et al.* Multilineage potential of adult human mesenchymal stem cells. *Science* **284,** 143–7 (1999).

2. Kurth, T. *et al.* Chondrogenic potential of human synovial mesenchymal stem cells in alginate. *Osteoarthr. Cartil.* **15,** 1178–1189 (2007).

3. Yoo, Jung, Nishimura, Traci, Solchaga, Keita, Caplan, Luis, Goldberg, Arnold, Johnstone, Victor, Cleveland, B. The Chondrogenic Potential of Human Bone-Marrow-Derived Mese... : JBJS. *The Journal of Bone & Joint Surgery* 1745–1757 (1998).

4. Scotti, C. *et al.* Recapitulation of endochondral bone formation using human adult mesenchymal stem cells as a paradigm for developmental engineering. *Proc. Natl. Acad. Sci. U. S. A.* **107,** 7251–6 (2010).

5. Farrell, E. *et al.* In-vivo generation of bone via endochondral ossification by in-vitro chondrogenic priming of adult human and rat mesenchymal stem cells. *BMC Musculoskelet. Disord.* **12,** 31 (2011).

6. Farrell, M. J. *et al.* Functional properties of bone marrow-derived MSC-based engineered cartilage are unstable with very long-term in vitro culture. *J. Biomech.* **47,** 2173–82 (2014).

7. Mak, K. K., Kronenberg, H. M., Chuang, P.-T., Mackem, S. & Yang, Y. Indian hedgehog signals independently of PTHrP to promote chondrocyte hypertrophy. *Development* **135,** 1947–56 (2008).

8. Mueller, M. B. *et al.* Hypertrophy in mesenchymal stem cell chondrogenesis: effect of TGF-beta isoforms and chondrogenic conditioning. *Cells. Tissues. Organs* **192,** 158–66 (2010).

9. Dong, Y.-F., Soung, D. Y., Schwarz, E. M., O'Keefe, R. J. & Drissi, H. Wnt induction of chondrocyte hypertrophy through the Runx2 transcription factor. *J. Cell. Physiol.* **208,** 77–86 (2006).

10. Hellingman, C. A. *et al.* Smad Signaling Determines Chondrogenic Differentiation of Bone-Marrow-Derived Mesenchymal Stem Cells: Inhibition of Smad1/5/8P Prevents Terminal Differentiation and Calcification. *TISSUE Eng. Part A* **17,** (2011).

11. Wang, W., Xu, J. & Kirsch, T. Annexin-mediated Ca2+ influx regulates growth plate chondrocyte maturation and apoptosis. *J. Biol. Chem.* **278,** 3762–9 (2003).

12. Smad-Runx Interactions During Chondrocyte Maturation : JBJS.

13. Yoshida, C. A. *et al.* Runx2 and Runx3 are essential for chondrocyte maturation, and Runx2 regulates limb growth through induction of Indian hedgehog. *Genes Dev.* **18,** 952–63 (2004).

14. Schug, J. *et al.* Promoter features related to tissue specificity as measured by Shannon entropy. *Genome Biol.* **6,** R33 (2005).

15. Vickaryous, M. K. & Hall, B. K. Human cell type diversity, evolution, development, and classification with special reference to cells derived from the neural crest. *Biol. Rev.* **81,** 425 (2006).

16. Xiao, S.-J., Zhang, C., Zou, Q. & Ji, Z.-L. TiSGeD: a database for tissue-specific genes. *Bioinformatics* **26,** 1273–5 (2010).

17. Carninci, P. *et al.* Genome-wide analysis of mammalian promoter architecture and evolution. *Nat. Genet.* **38,** 626–635 (2006).

18. Sandelin, A. *et al.* Mammalian RNA polymerase II core promoters: insights from genome-wide studies. *Nat. Rev. Genet.* **8,** 424–436 (2007).

19. Smallwood, S. A. & Kelsey, G. Genome-wide analysis of DNA methylation in low cell numbers by reduced representation bisulfite sequencing. *Methods Mol. Biol.* **925,** 187–97 (2012).

20. Neugebauer, B. M., Moore, M. A., Broess, M., Gerstenfeld, L. C. & Hauschka, P. V. Characterization of structural sequences in the chicken osteocalcin gene: Expression of osteocalcin by maturing osteoblasts and by hypertrophic chondrocytes in vitro. *J. Bone Miner. Res.* **10,** 157–163 (2009).

21. Ianus, A., Holz, G. G., Theise, N. D. & Hussain, M. A. In vivo derivation of glucose-competent pancreatic endocrine cells from bone marrow without evidence of cell fusion. *J. Clin. Invest.* **111,** 843–50 (2003).

22. Kajiyama, Y., Tian, J. & Locker, J. Characterization of distant enhancers and promoters in the albumin-alpha-fetoprotein locus during active and silenced expression. *J. Biol. Chem.* **281,** 30122–31 (2006).

23. Gulicks, J., Subramaniams, A., Neumanna, J. & Robbinsst, J. Isolation and Characterization of the Mouse Cardiac Myosin Heavy Chain Genes*. **266,** 9180–9185 (1991).

24. Robinson, G. W., McKnight, R. A., Smith, G. H. & Hennighausen, L. Mammary epithelial cells undergo secretory differentiation in cycling virgins but require pregnancy for the establishment of terminal differentiation. *Development* **121,** 2079–2090 (1995).

25. Sive, J. I. *et al.* Expression of chondrocyte markers by cells of normal and degenerate intervertebral discs. *Mol. Pathol.* **55,** 91–7 (2002).

26. Wang, H. *et al.* Knockout of BRD7 results in impaired spermatogenesis and male infertility. *Sci. Rep.* **6,** 21776 (2016).

27. Weimer, J. M. *et al.* Alterations in striatal dopamine catabolism precede loss of substantia nigra neurons in a mouse model of juvenile neuronal ceroid lipofuscinosis. *Brain Res.* **1162,** 98–112 (2007).

28. Meynard, D. *et al.* Lack of the bone morphogenetic protein BMP6 induces massive iron overload. *Nat. Genet.* **41,** 478–481 (2009).

29. Weng, T. *et al.* Genetic inhibition of fibroblast growth factor receptor 1 in knee cartilage attenuates the degeneration of articular cartilage in adult mice. *Arthritis Rheum.* **64,** 3982–92 (2012).

30. Kulkarni, R. N. *et al.* Tissue-Specific Knockout of the Insulin Receptor in Pancreatic β Cells Creates an Insulin Secretory Defect Similar to that in Type 2 Diabetes. *Cell* **96,** 329–339 (1999).

31. Lin, J. H., Zhao, H. & Sun, T. T. A tissue-specific promoter that can drive a foreign gene to

express in the suprabasal urothelial cells of transgenic mice. *Proc. Natl. Acad. Sci. U. S. A.* **92,** 679–83 (1995).

32. Yakar, S. *et al.* Normal growth and development in the absence of hepatic insulin-like growth factor I. *Proc. Natl. Acad. Sci. U. S. A.* **96,** 7324–9 (1999).

33. Li, H. *et al.* Genetic modification of survival in tissue-specific knockout mice with mitochondrial cardiomyopathy. *Proc. Natl. Acad. Sci. U. S. A.* **97,** 3467–72 (2000).

34. Ludwig, T., Fisher, P., Murty, V. & Efstratiadis, A. Development of mammary adenocarcinomas by tissue-specific knockout of Brca2 in mice. *Oncogene* **20,** 3937–3948 (2001).

35. Mackay, A. M. *et al.* Chondrogenic Differentiation of Cultured Human Mesenchymal Stem Cells from Marrow. *Tissue Eng.* **4,** 415–428 (1998).

36. J.J. Haigh, H.P. Gerber, N. Ferrara, E. F. W. Conditional inactivation of VEGF-A in areas of collagen2a1 expression results in embryonic lethality in the heterozygous state. *Development* **127,** 1445–1453 (2000).

37. Florian Karreth, Astrid Hoebertz, Harald Scheuch, Robert Eferl, E. F. W. The AP1 transcription factor Fra2 is required for efficient cartilage development. *Development* **131,** 5717–5725 (2004).

38. Ovchinnikov, D. A., Deng, J. M., Ogunrinu, G. & Behringer, R. R. Col2a1-directed expression of Cre recombinase in differentiating chondrocytes in transgenic mice. *genesis* **26,** 145–146 (2000).

39. Ford-Hutchinson, A. F. *et al.* Inactivation of Pten in Osteo-Chondroprogenitor Cells Leads to Epiphyseal Growth Plate Abnormalities and Skeletal Overgrowth. *J. Bone Miner. Res.* **22,** 1245–1259 (2007).

40. Wang, W. *et al.* Mice lacking Nf1 in osteochondroprogenitor cells display skeletal dysplasia similar to patients with neurofibromatosis type I. *Hum. Mol. Genet.* **20,** 3910–3924 (2011).

41. Hilton, M. J., Tu, X. & Long, F. Tamoxifen-inducible gene deletion reveals a distinct cell type associated with trabecular bone, and direct regulation of PTHrP expression and chondrocyte morphology by Ihh in growth region cartilage. *Dev. Biol.* **308,** 93–105 (2007).

42. Jones, K. B. *et al.* A mouse model of osteochondromagenesis from clonal inactivation of Ext1 in chondrocytes. *Proc. Natl. Acad. Sci. U. S. A.* **107,** 2054–9 (2010).

43. Gu, J. *et al.* Identification and characterization of the novel Col10a1 regulatory mechanism during chondrocyte hypertrophic differentiation. *Cell Death Dis.* **5,** e1469–e1469 (2014).

44. Lu, Y. *et al.* Col10a1-Runx2 transgenic mice with delayed chondrocyte maturation are less susceptible to developing osteoarthritis. *Am. J. Transl. Res.* **6,** 736–45 (2014).

45. Ding, M. *et al.* Targeting Runx2 expression in hypertrophic chondrocytes impairs endochondral ossification during early skeletal development. *J. Cell. Physiol.* **227,** 3446–56 (2012).

46. Gebhard, S. *et al.* A highly conserved enhancer in mammalian type X collagen genes drives

high levels of tissue-specific expression in hypertrophic cartilage in vitro and in vivo. *Matrix Biol.* **23,** 309–322 (2004).

47. Zheng, Q. *et al.* Localization of the cis-enhancer element for mouse type X collagen expression in hypertrophic chondrocytes in vivo. *J. Bone Miner. Res.* **24,** 1022–32 (2009).

48. Carrion, B. *et al.* The Synergistic Effects of Matrix Stiffness and Composition on the Response of Chondroprogenitor Cells in a 3D Precondensation Microenvironment. *Adv. Healthc. Mater.* (2016). doi:10.1002/adhm.201501017

49. Kim, Y. J., Sah, R. L., Doong, J. Y. & Grodzinsky, A. J. Fluorometric assay of DNA in cartilage explants using Hoechst 33258. *Anal. Biochem.* **174,** 168–76 (1988).

50. Zhai, Z., Yao, Y., Wang, Y., Ohgishi, M. & Fukui, T. Importance of Suitable Reference Gene Selection for Quantitative RT-PCR during ATDC5 Cells Chondrocyte Differentiation. *PLoS One* **8,** e64786 (2013).

51. Arnosti, D. N. & Kulkarni, M. M. Transcriptional enhancers: Intelligent enhanceosomes or flexible billboards? *J. Cell. Biochem.* **94,** 890–898 (2005).

52. Harafuji, N., Keys, D. N. & Levine, M. Genome-wide identification of tissue-specific enhancers in the Ciona tadpole. *Proc. Natl. Acad. Sci. U. S. A.* **99,** 6802–5 (2002).

53. Li, F. *et al.* Runx2 Contributes to Murine Col10a1 Gene Regulation Through Direct Interaction With Its Cis-Enhancer. doi:10.1002/jbmr.504

54. Kronenberg, H. M. Developmental regulation of the growth plate. *Nature* **423,** 332–6 (2003).

55. Schipani, E. *et al.* Targeted expression of constitutively active receptors for parathyroid hormone and parathyroid hormone-related peptide delays endochondral bone formation and rescues mice that lack parathyroid hormone-related peptide. *Proc. Natl. Acad. Sci.* **94,** (1997).

56. Weir, E. C. *et al.* Targeted overexpression of parathyroid hormone-related peptide in chondrocytes causes chondrodysplasia and delayed endochondral bone formation. *Proc. Natl. Acad. Sci.* **93,** (1996).

57. Lefebvre, V. & Smits, P. Transcriptional control of chondrocyte fate and differentiation. *Birth Defects Res. Part C Embryo Today Rev.* **75,** 200–212 (2005).

58. Thomas, R., Thieffry, D. & Kaufman, M. Dynamical behaviour of biological regulatory networks—I. Biological role of feedback loops and practical use of the concept of the loop-characteristic state. *Bull. Math. Biol.* **57,** 247–276 (1995).

59. Alon, U. Network motifs: theory and experimental approaches. *Nat. Rev. Genet.* **8,** 450–461 (2007).

Chapter 5 Conclusion and Future Directions

Regenerating articular cartilage from mesenchymal stem cells (MSCs) requires them to adopt and then maintain the stable phenotype of articular chondrocytes. Cartilage differentiation entails a series of well-coordinated signaling stimulation while cartilage homeostasis relies on the balanced anabolic and catabolic activity of chondrocytes which are subject to the actions of numerous biochemical and mechanical cues[1,2]. Conventional approaches based on growth factors and transgene overexpression have showed success in stimulating initial chondrogenesis. However, these methods are less effective in maintaining stable chondrocyte phenotype as fixed growth factor cocktails or forced overexpression of one/two genes cannot provide the versatile responses needed to cope with the constantly changing intracellular and environmental signals.

The concept of the self-regulatory gene circuit proposed in this thesis highlighted the feasibility of introducing an artificial, negative-feedback regulatory pathway into the mammalian cells to target a specific signaling molecule – RUNX2. Therefore, modulated chondrocytes can dynamically counteract various external biochemical or biophysical cues that stimulate RUNX2 activity. Additionally, our design here utilizes synthetic nucleotide elements that resemble the naturally occurring genetic modalities. For example, the *cis* promoters imitate the endogenous Col10a1 promoter; RNAi of *Runx2* via miRNA-based shRNA also mimics the natural microRNA pathways. The similarity between this synthetic signaling cascade and endogenous regulatory machinery not only enhances the compatibility and efficacy of gene circuits but also minimizes

the stress on host cells. Meanwhile, the encouraging results demonstrated in this dissertation have also inspired much future work that could focuses on 1) helping us better understand the existing cis-sh*Runx2* gene circuit, 2) designing new gene circuits that employ novel tissue-specific promoters or target other regulatory pathways.

5.1 Understand and Improve *cis*-sh*Runx2* Gene Circuit

5.1.1 Improve Tunability

In chapter 4, we have discussed the three main features of cis-sh*Runx2:* 1) the phenotype-specific activation of RNAi, 2) the closed-loop intracellular negative-feedback regulation, and 3) the tunable steady-state level of RUNX2 repression and dynamics. Among these, the ability to achieve tunable level of RUNX2 suppression is particularly appealing to us as we could potentially use it to fine-tune the behavior of target cells. However, as we increase the number of *cis* enhancers to increase RUNX2 silencing, loss of RUNX2 function started to occur earlier as well, which could potentially interfere with synthesis of aggrecan and type II collagen. **Therefore, one of the next engineering milestones would be to decouple the dynamics and steady-states of the cis-sh*Runx2* gene circuits.** Specifically, if the levels of RUNX2 suppression could be adjusted without changing when the silencing activity reaches that steady state or vice versa, we could further optimize timing and dosing of RUNX2 silencing to maximize the matrix accumulation. To achieve this goal, tunability can be explored at two different levels of the intergradation of the gene circuit. Obviously, within a single cis-sh*Runx2* unit, different shRNA sequences could be examined to understand their contribution to both steady-state level of RUNX2 repression and silencing dynamics. However, we speculate the range of tunability provided by adjustment at this level is limited as current *cis*-sh*Runx2* gene circuits already employ one of the most potential siRNA sites on the mRNA of *Runx2*[3]. Meanwhile, if the current *cis*-sh*Runx2* expression cassette is treated as a basic unit (one *cis* promoter plus one sh*Runx2*), we could potentially introduce

multiple copies of the same unit or different ones (via a single vector, **Figure 5-1**) to achieve desired RUNX2 expression profile. To preliminarily test this hypothesis, we have transduced ATDC5 cells with the same 1*cis*-sh*Runx2* virus twice and examined if there is any change of activity in the culture. We observed an increased level of RUNX2 suppression with little change of dynamics (**Figure 5-2**). This observation suggests that this approach of tuning circuit activity is effective and can decouple the level of RUNX2 repression and when to reach steady-states.

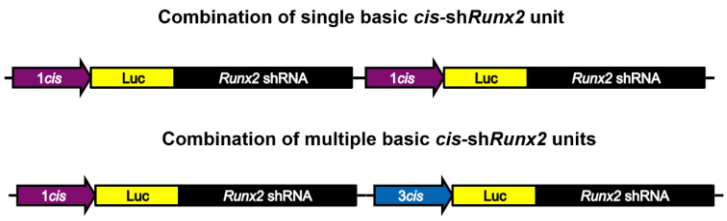

Figure 5-1. Diagram of gene circuits with multiple sh*Runx2* units.

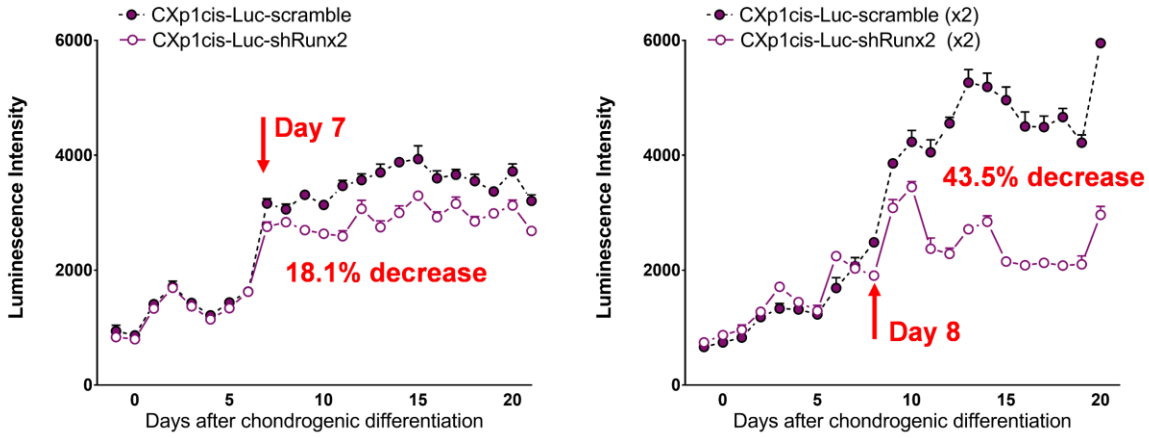

Figure 5-2. Activity between single and double 1*cis*-sh*Runx2* gene circuits. Total luciferase activity of ATDC5 cultures that are transduced with 1*cis*-Luc-sh*Runx2* (a) once and (b) twice.

5.1.2 Investigate Matrix Turnover

In chapters 2 and 4, we independently observed improved matrix accumulation (sGAG) due to RUNX2 silencing. However, a healthy cartilage tissue relies on the balanced anabolic and catabolic activity from the resident chondrocytes. Therefore, understanding the effect of circuit activity on the matrix turnover would provide critical insights for us to choose among the different

versions of *cis*-sh*Runx2*. Specifically, in the future long-term *in vitro* studies, both the retained matrix and degradation fragments of aggrecan and type II collagen should be measured, especially under the simulated inflammatory environments. These results could help us evaluate effects of *cis*-sh*Runx2* gene circuits at different stages of chondrogenic differentiation and use these data to design or fine-tune new gene circuits. In addition, mechanical properties of the final cartilage tissue constructs (gene circuits-modified MSCs encapsulated in scaffolds) developed under the control of different *cis*-sh*Runx2* gene circuits should be measured to examine if the improved phenotype contributes to a superior mechanical strength.

5.2 Design New Gene Circuits

This dissertation also showcased an iterative design process that includes establishment test system, independent validation of vector components, and verification of integrated gene circuits. Taking advantage of this established workflow, we could conveniently explore other target pathways that could be exploited to improve cartilage regeneration. Thanks to the similarity between miRNA-based shRNA and natural microRNA pathways, our gene circuit can be easily converted to induce expression of 1) microRNAs that promote chondrogenesis (e.g., mir410[4]), 2) shRNAs that inhibits other hypertrophy stimulators (e.g., MEF2C[5]), or 3) shRNAs that target matrix-degrading enzymes (e.g., ADAMTS4&5[6]). The list of potential targets has been increasing at rapid pace fueled by our growing knowledge of cartilage development, the invention of genetic tools (e.g., high-throughput sequencing), and computation models. These advances have also promoted our understanding of mammalian tissue-specific promoters and their *cis* regulatory elements. Therefore, we have the potential of designing novel synthetic promoters which not only recapitulate the existing tissue-specificity but also hybrid features that are derived from multiple endogenous promoters. For our application, synthetic murine and human promoters that target

different stages of chondrocyte maturation would be next logical step to expand our library of gene circuits. For example, synthetic promoters that resembling endogenous promoters of *Acan* and *Col2a1* can be used to provide expression of pro-chondrogenic microRNAs prior to the onset of hypertrophy to complement the function of *cis-shRunx2*.

5.3 Challenges Associated with the Clinical Application of Gene Circuit

Despite the promising potentials of gene circuit technology in tissue engineering applications, major hurdles for gene-enhanced cell therapy of cartilage repair include eliminating the risk of oncogene activation, maintaining long-term silencing efficacy, and demonstrating robust clinical superiority and cost-effective against current treatment strategies. Safety concerns associated with the possible activation of oncogene due to the integration of gene vector, especially lentiviral vectors, has been one of the major challenges that hinder the wider application of this type of gene therapy. However, recent advances and positive clinical results in hematopoietic stem cell- and T-cell based gene therapies have been improving the public acceptance as well as attitude from regulatory agencies. More importantly, this attitude shift has also motivated more effort to improve the vector design and reduce insertional mutagenesis from both academic research laboratories and industrial organizations. Specifically, for cartilage tissue engineering, the gene therapy-based repair strategy is faced with a high level of competition from alternative treatments. Since posttraumatic osteoarthritis is not life-threatening, conservative treatments might be preferred until the gene circuit-based cartilage repair methods exhibit significantly superior long-term outcomes, such as restoration of mechanical functions and delayed onset of osteoarthritis. Also, the current pricing of gene therapy treatments is expected to be significantly higher than standard procedures due to the individualized manufacture requirements. Therefore, both

irrefutable evidence of outcome improvements and significant reduction of manufacture cost are also prerequisites for the clinical adoption of gene circuit-based cartilage repair.

5.4 Tissue Engineering Application of Phosphate

In Chapter 3, we also demonstrated the biphasic effect of phosphate on early chondrogenesis. Specifically, moderate Pi abundance enhanced production of aggrecan and type II collagen whereas high Pi abundance inhibited chondrogenic differentiation. For cartilage tissue engineering, the anabolic effect of Pi on matrix synthesis could propose a cost-effective method to improve MSC-based cartilage regeneration. However, application of Pi during chondrogenesis of progenitor cells requires careful calibration as it can easily induce mineralization when supplemented at the wrong concentration. To further investigate the feasibility of using Pi to improve production of aggrecan and type II collagen, we will need to confirm the anabolic effect of Pi in human MSCs. Since the effect of Pi also depends on the maturation state of chondrocytes/MSCs, a systematic characterization of cellular response at various stages of chondrogenesis would be necessary to identify the window of opportunity for Pi-induced matrix production.

5.5 References

1. Goldring, M. B. & Marcu, K. B. Cartilage homeostasis in health and rheumatic diseases. *Arthritis Res. Ther.* **11,** 224 (2009).
2. Houard, X., Goldring, M. B. & Berenbaum, F. Homeostatic Mechanisms in Articular Cartilage and Role of Inflammation in Osteoarthritis. *Curr. Rheumatol. Rep.* **15,** 375 (2013).
3. Lin, L. *et al.* Adenovirus-mediated transfer of siRNA against Runx2/Cbfa1 inhibits the formation of heterotopic ossification in animal model. *Biochem. Biophys. Res. Commun.* **349,** 564–72 (2006).
4. Zhang, Y., Huang, X. & Yuan, Y. MicroRNA-410 promotes chondrogenic differentiation of human bone marrow mesenchymal stem cells through down-regulating Wnt3a. *Am. J. Transl. Res.* **9,** 136–145 (2017).
5. Arnold, M. A. *et al.* MEF2C Transcription Factor Controls Chondrocyte Hypertrophy and Bone Development. *Dev. Cell* **12,** 377–389 (2007).

6. Naito, S. *et al*. Expression of ADAMTS4 (aggrecanase-1) in human osteoarthritic cartilage. *Pathol. Int.* **57,** 703–711 (2007).